UNIVERSITY OF CALIFORNIA SAN DIEGO

Large-Scale Multidisciplinary Design Optimization of the Truss-Braced Wing Concept

A Thesis submitted in partial satisfaction of the
requirements for the degree Master of Science

in

Mechanical and Aerospace Engineering

by

Rajashekar Swaminathan

Committee in charge:

Professor John T.Hwang, Chair
Professor Jiun-Shyan (J.S.) Chen
Professor Oliver T. Schmidt

2024

The Thesis of Rajashekar Swaminathan is approved, and it is acceptable in quality and form for publication on microfilm and electronically.

University of California San Diego

2024

DEDICATION

For my parents, grandmother, my extended family, and my friends.

TABLE OF CONTENTS

LIST OF FIGURES

LIST OF TABLES

ACKNOWLEDGEMENTS

Many people contributed to the successful completion of this thesis. I am deeply appreciative of my co-author, Dr. Darshan Sarojini, whose insights and efforts played a vital role in the development of this thesis. His exceptional mentorship and guidance throughout my degree, and his unwavering patience and support over the past two years have been immensely helpful, and I am profoundly grateful for his constant encouragement.

I would also like to express my heartfelt appreciation to Professor John T. Hwang for his essential support as the chair of my committee. His guidance throughout my research, including our meetings and countless discussions, has been instrumental in shaping this thesis.

Additionally, I wish to acknowledge the support of my friends, both in India and the USA. Their encouragement during challenging times has been instrumental in helping me complete this work. Finally, I would like to thank my family and extended family for their unconditional support throughout my life. Their belief in me has shaped who I am today and will continue to influence who I become in the future.

Chapters 1, 3, 4, in full, are currently being prepared for submission for publication of the material. Darshan Sarojini, and John T.Hwang. The thesis author was the primary investigator and author of this material.

Section 2.1, in part, is currently being prepared for submission for publication of the material. Darshan Sarojini, and John T.Hwang. The thesis author was the primary investigator and author of this material.

ABSTRACT OF THE THESIS

Large-Scale Multidisciplinary Design Optimization of the Truss-Braced Wing Concept

by

Rajashekar Swaminathan

Master of Science in Mechanical and Aerospace Engineering

University of California San Diego, 2024

Professor John T.Hwang, Chair

The Truss-Braced Wing (TBW) concept, with its high aspect ratio, offers a promising route to increased energy efficiency. This thesis demonstrates the application of large-scale Multidisciplinary Design Optimization to the TBW concept, utilizing gradient-based optimization and physics-based models. The first contribution of this thesis is to examine the effect of wing-strut location on the TBW configuration and identify the optimal strut position for its conceptual design using physics-based solvers. It is important to determine the optimal strut placement based on structural sizing, as reducing drag and structural weight while maintaining aerodynamic efficiency is crucial to conceptual aircraft design. Vortex Lattice Methods are employed, considering wave, viscous, and interference drags, with corrections to mitigate wing-

strut interference effects. Structural analysis is based on linear Euler-Bernoulli beam theory, while propulsion analysis uses simplified thrust tables. The second contribution involves applying novel optimization methods to the conceptual design of the TBW configuration. The use of two sub-scale optimization problems followed by a full-scale optimization, a methodology that, to the author's knowledge, has not been previously applied to the TBW configuration is used to minimize fuel consumption across various mission phases while also addressing structural and constraint analyses involving over 140 design variables and 400 constraints. The analysis and optimization are performed using CADDEE (Comprehensive Aircraft high-Dimensional Design Environment), a software library that integrates all discipline models. Results show an 8% reduction in gross weight and a 9% decrease in fuel consumption compared to the initial design, with all major constraints satisfied.

Acronyms

C_D Coefficient of Drag.

C_L Coefficient of Lift.

approx. approximately.

B-Spline Basis Spline.

CADDEE Comprehensive Analysis and high-Dimensional DEsign Environment.

CFD Computational Fluid Dynamics.

CSDL Computational System Design Language.

DoF Degrees of Freedom.

EoM equations of motion.

FFD Free-Form Deformation.

FLOPS FLight OPtimization System.

L/D Lift-to-Drag.

MDO Multidisciplinary Design Optimization.

NASA National Aeronautics and Space Administration.

OML Outer Mold Line.

RANS Reynolds-Averaged Navier-Stokes.

SIFR Solver-Independent Field Representation.

SUGAR Subsonic Ultra Green Aircraft Research.

TBW Truss-Braced Wing.

VLM Vortex Lattice Method.

XDSM design structure matrix.

Chapter 1

Introduction

Air travel has profoundly impacted the world in the 21st century, providing efficient, fast, and safe transportation unmatched by any other mode of long-distance travel. The flexibility in capacity and routing, low infrastructure costs, and freedom from geographic barriers have allowed air travel to connect all corners of the earth rapidly. However, several factors are now converging to threaten the sustainability of air transportation in the coming decades.

The increasing demand for fuel, coupled with diminishing supply, has led to rising and volatile fuel prices. Additionally, the growth of the global economy is straining natural resources, driving up fuel costs while simultaneously increasing travel demand [118, 119, 81]. Consequently, the need for environmentally sustainable aviation is becoming increasingly urgent, with a growing focus on minimizing the ecological footprint of air travel.

In response to escalating aviation demands and heightened environmental concerns, Boeing conducted the Subsonic Ultra Green Aircraft Research (SUGAR) study for National Aeronautics and Space Administration (NASA) in 2009-2010. This study identified and analyzed advanced concepts and technologies for aircraft projected to operate in the 2030-2035 timeframe. The study revealed significant potential improvements in fuel efficiency, emissions, and noise, leading to the development of roadmaps for key technologies. As a result, NASA initiated the ”N+3” subsonic civil transport concept studies, where ”N” is defined as the current standard set by the 737NG [75] vehicle and CFM56 [44] engine technology [109].

This initiative falls under the purview of NASA's Fixed Wing Project within the Fundamental Aeronautics Program. The objectives of the N+3 goals, as delineated in [28], are ambitious and the attainment of these ambitious benchmarks necessitates groundbreaking advancements spanning diverse disciplines, including aerodynamics, propulsion, and structures. Moreover, the successful integration of these innovative technologies into a well-suited vehicle configuration is imperative.

Presently, most large transport aircraft operate within the optimal cruise Lift-to-Drag (L/D) range of 18-20, adhering to the conventional tube-and-wing design. This longstanding configuration has yielded gradual advancements in aerodynamic efficiency throughout the past century [42]. The design's effectiveness is primarily attributed to its ability to balance aerodynamic performance with structural integrity and manufacturability. Recent developments highlight the efficacy of employing lightweight materials, particularly composites, which exhibit a substantial capacity for reducing structural weight and trim drag, consequently enhancing overall energy efficiency. The Boeing 787 transport stands as an exemplar of contemporary air frame design characterized by the strategic incorporation of lightweight structures. Furthermore, the implementation of a high aspect ratio wing design emerges as a promising avenue for achieving additional enhancements in energy efficiency. A higher aspect ratio, which is the ratio of the wingspan to the mean chord, leads to reduced induced drag, making the aircraft more efficient during cruise [2, 24, 110].

Research and development of high aspect ratio wing transport designs has placed a greater emphasis on the studies of aeroelasticity and flutter owing to the increase in the wing flexibility as the wing aspect ratio increases. These studies have sought to develop methods and tools for aeroelasticity by laying the foundation for more modern high aspect ratio wing aircraft such as the Truss-Braced Wing (TBW) [9, 40, 43]. The utilization of truss structures to mitigate the wing root bending moment in ultra-high aspect ratio wings has over a decade of research dedicated to advancing the comprehension of aeroelastic properties and the structural weight implications associated with heightened wing flexibility [66, 29, 114].

The SUGAR Truss-Braced Wing (TBW) aircraft concept, developed by Boeing and funded by NASA, focuses on advanced technologies for improved air transport. Phase I of the project analyzed various configurations including the SUGAR Free, Refined SUGAR, SUGAR Volt, SUGAR Ray, and SUGAR High. The SUGAR High, featuring a high-span strut-braced wing and advanced engine, is a notable design for further development in Phase II.

In Phase II, the focus shifted to the TBW design, which balances reduced weight through structural efficiency with the drag introduced by the truss. This design leverages high aspect ratios and truss structures to minimize wing root bending and enhance aerodynamic performance. The TBW configuration promises significant fuel savings and improved aerodynamic efficiency by reducing drag and promoting laminar flow. However, the braced structures also introduce aerodynamic and structural challenges.

This is why the design process for the TBW involves multidisciplinary optimization Multidisciplinary Design Optimization (MDO) to reconcile aerodynamic and structural needs. In this thesis it we strive to strike a delicate balance between aerodynamic and structural efficiencies, and this is why we use large-scaleMultidisciplinary Design Optimization (MDO) to tack this design challenge.

Previous studies have validated the structural feasibility and performance benefits of the TBW, though they have been limited to lower Mach numbers. To address this, future research must incorporate both aerodynamic and structural modeling across a broader range of Mach numbers and integrate aeroelastic analysis to enhance the overall design. Recent work has focused on coupled aero-structural optimization using various modeling techniques but has not fully explored combined Outer Mold Line (OML) and structural variables or gradient-based optimization methods.

Recent advancements in Multidisciplinary Design Optimization (MDO) have highlighted the effectiveness of gradient-based optimization techniques in refining aircraft designs with numerous variables. For instance, Hwang and Ning utilized the OpenMDAO [39] framework to enhance the range of NASA's X-57 Maxwell electric aircraft, achieving a 12% increase in range

with optimization completed in under ten hours. This success is attributed to the adjoint method, which efficiently handles large numbers of design variables and is crucial for complex aircraft design optimizations [49].

Previous MDO studies have focused on refining wing geometry and configuration to minimize various drag components. While optimal configurations for the number of struts have been established, there has been limited research on the effects of wing-strut positioning, especially in transonic conditions where wing-strut interference becomes significant. Studies by Sarojini et.al [99] and Solano et al. [106] explored the impact of wing-strut location on structural weight but did not include aeroelastic optimizations that account for drag in transonic conditions.

This first contribution of this thesis is to investigate the impact of wing-strut location on the TBW and determine a wing-strut location for the conceptual design of the Truss-Braced Wing (TBW) configuration using physics based solvers. Through a systematic analysis, this research aims to determine an optimal strut placement based on structural sizing, for conceptual aircraft design because of the importance of reducing drag and structural weight while maintaining aerodynamic efficiency, which enhances the novelty of this research. Various wing-strut locations are detailed to determine the configuration with the least wing, strut and jury structural mass. The physics based models in use are a Vortex Lattice Method (VLM) solver for aerodynamics [92], a beam solver for structural analysis [82] and a 1-Dimensional linear model based on the throttle of the TBW configuration.

Furthermore, to perform a conceptual design of the Truss-Braced Wing (TBW), a mission and constraint analysis is crucial. Gur et al. [41] developed a framework for conceptual design of the Truss-Braced Wing (TBW) using FLight OPtimization System (FLOPS) for weight estimation, and semi-empirical methods for aerodynamic analysis. Chakraborty et al. [21] compared the strut-braced Wing configuration against the one-jury TBW configuration and the MDO study by including a mission analysis study for a climb, cruise, and descent mission profile. The study indicated that the one-jury TBW outperformed the strut-braced wing configuration for all span limits in terms of fuel burn. Adding one more jury only offered only marginal

improvements for spans longer than 170 ft(approximately (approx.) 51.816 metres), which suggested that there was no need to investigate more complex truss systems such as three-jury or four-jury TBW. Meadows et. al [74] performed a comparison between a conventional cantilever wing design, a Strut-Braced Wing design, and a one-jury Truss-Braced Wing (TBW) design resulting in a similar conclusion as Chakraborty et. al. While these designs have led to advancements in the design of the Truss-Braced Wing (TBW) there have been very few studies that have done a combined mission and constraint analysis that could further lead to regulations on the stall speed, climb gradient and more.

The second contribution of this thesis is the application of a novel optimization methodology to the conceptual design of the Truss-Braced Wing (TBW) configuration, aimed at minimizing fuel consumption during a mission analysis—including climb, cruise, and descent phases—while also conducting a structural and constraint analysis. This process begins with a sub-scale optimization to identify a wing-strut location, followed by a trim optimization for the selected configuration, which serves as a solid foundation for the full-scale optimization. The novelty of this research lies in the application of two sub-scale optimization problems and one full-scale optimization problem—a methodology that, to the author's knowledge, has not been previously applied to the study of the TBW configuration. Moreover, the application of these large-scale multidisciplinary design optimization (MDO) techniques to the TBW configuration has not been extensively explored in the current literature. By employing a gradient-based approach, this thesis enables rapid exploration of the design space, addressing both nominal and off-nominal mission segments to ensure robust performance across various operational conditions.

Building on the work of Sarojini et al.[98] and Ruh et al.[92], who employed the Comprehensive Analysis and high-Dimensional DEsign Environment (CADDEE) to efficiently address an air-taxi design problem entailing over 100 design variables, achieving resolution within less than thirty minutes using a single processor on a desktop workstation. This study seeks to leverage similar techniques for the TBW design, wherein all the above mentioned analyses are

conducted in Comprehensive Analysis and high-Dimensional DEsign Environment (CADDEE) and physics-based models are written in CSDL. This is because we want the research to apply gradient-based optimization techniques to handle the complex interplay of over 150 design variables, and over 550 constraints related to the TBW, achieving efficient and precise solutions within a constrained computational environment.

In pursuit of these research objectives, I have arrived at the following thesis statement: We utilize a recently developed graph-based modelling approach to apply large scale Multidisciplinary Design Optimization (MDO) to the system level design of the Truss-Braced Wing (TBW) concept.

The subsequent chapters of the thesis are structured as follows: Chapter 2 gives a background on the detailed explanation of the Truss-Braced Wing (TBW) and on various Multidisciplinary Design Optimization (MDO) tools that would be required for this thesis. Chapter 3 delineates the methodology used for the conceptual design of the TBW. This includes the details of the sub-discipline models (structures, aerodynamics, propulsion, and even geometry parametrization) as well as the overall optimization problem formulation. Chapter 4 presents the study's results, and finally chapter 5 furnishes the conclusion, while Chapter 6 outlines potential avenues for future research.

This chapter, in full, is currently being prepared for submission for publication of the material. Darshan Sarojini, and John T.Hwang. The thesis author was the primary investigator and author of this material.

Chapter 2

Background

This chapter presents an overview of related work to the defined research problem. A literature review on how the Truss-Braced Wing (TBW) configuration was settled upon as the design for the future, the drawbacks seen in the configuration and the need to formulate a large-scale Multidisciplinary Design Optimization (MDO) problem to address these problems, are detailed in Section 2.1. Section 2.2 gives a brief overview of Multidisciplinary Design Optimization (MDO) and Computational System Design Language (CSDL) which are the two basic pillars that help us solver our research problem. Furthermore, Section 2.3 discusses the need for a novel framework to analyze the Truss-Braced Wing (TBW) configuration, named Comprehensive Analysis and high-Dimensional DEsign Environment (CADDEE). Additionally, CADDEE's framework is discussed in the same section.

2.1 Literature Review

The SUGAR Truss-Braced Wing (TBW) aircraft concept was developed by Boeing and funded by the NASA Aeronautics Research Mission Directorate (ARMD) Advanced Air Transport Technology (AATT) project, as determined through the NASA Research Announcement (NRA) selection process [10, 11, 13].

In Phase I of the NASA Subsonic Ultra Green Aircraft Research (SUGAR) concept, various advanced technologies and configurations were analyzed. Five configurations were

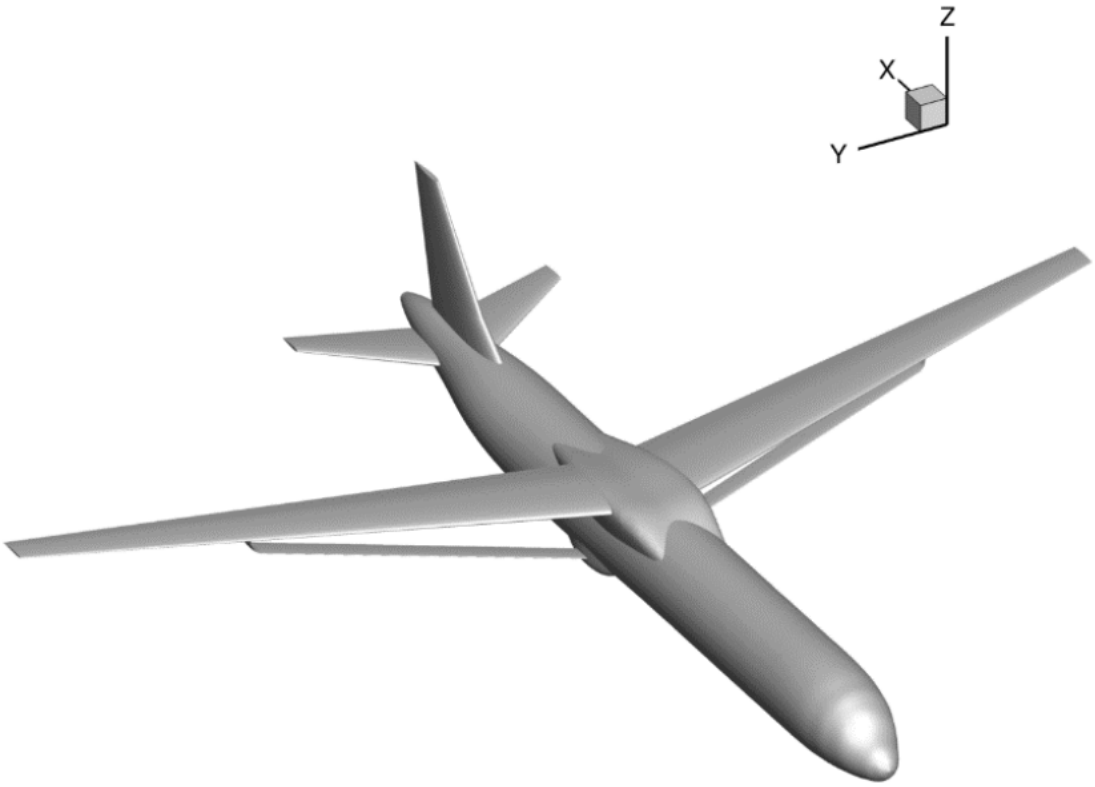

Figure 2.1. Reconstruction of the ONERA ALBATROS (Strut-Braced Wing concept) configuration using ESP/EGADS tools [16].

detailed for analysis: the SUGAR Free as a current technology baseline, Refined SUGAR with a basic conventional configuration including General Electric's "gFan" engine, SUGAR Volt with a battery gas turbine hybrid "hFan" engine, SUGAR Ray, a Hybrid Wing Body design focused on noise reduction while maintaining high performance, and SUGAR High with a high-span strut-braced wing [16, 34, 38, 17] and General Electric's "gFan+" engine. The initial release of the 765-095 SUGAR High configuration was generated during the first phase of the SUGAR program, with Phase II set to further develop this configuration.

In Phase II, an extension of the SUGAR High configuration, the TBW (Truss-Braced Wing) configuration, was studied for future Boeing 737-sized transports. The TBW design represents a compromise between reduced weight due to structural efficiency and the added drag caused by the truss [3]. Figure 2.2 and Figure 2.3 shows an image of a Truss-Braced Wing (TBW)

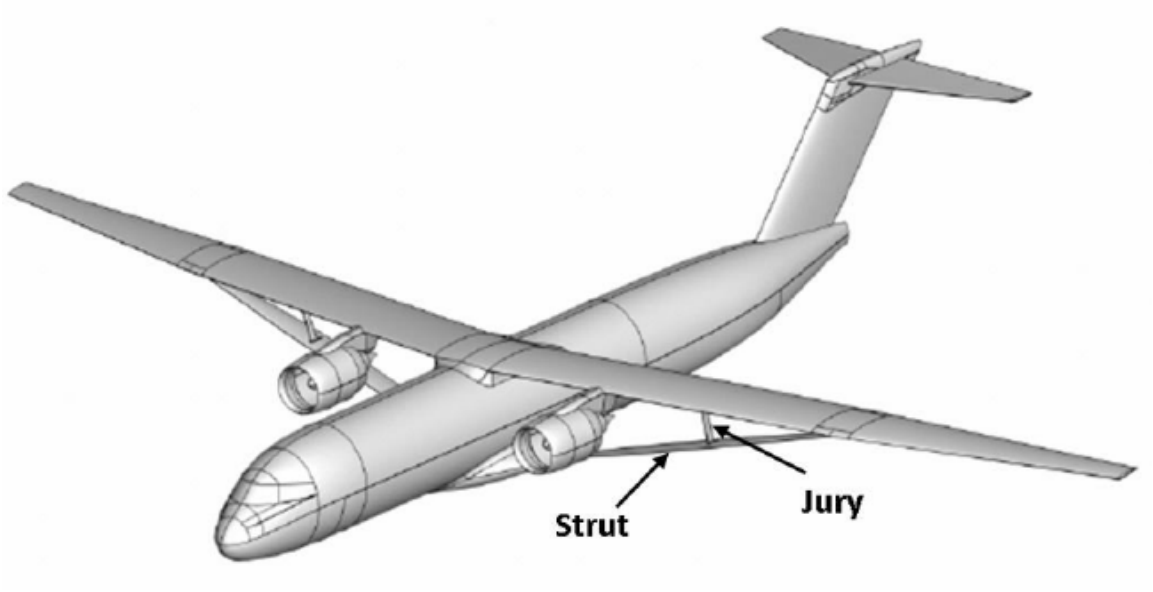

Figure 2.2. Subsonic Ultra Green Aircraft Research (SUGAR) initiated by National Aeronautics and Space Administration (NASA) has resulted in the Truss-Braced Wing (TBW) concept [131].

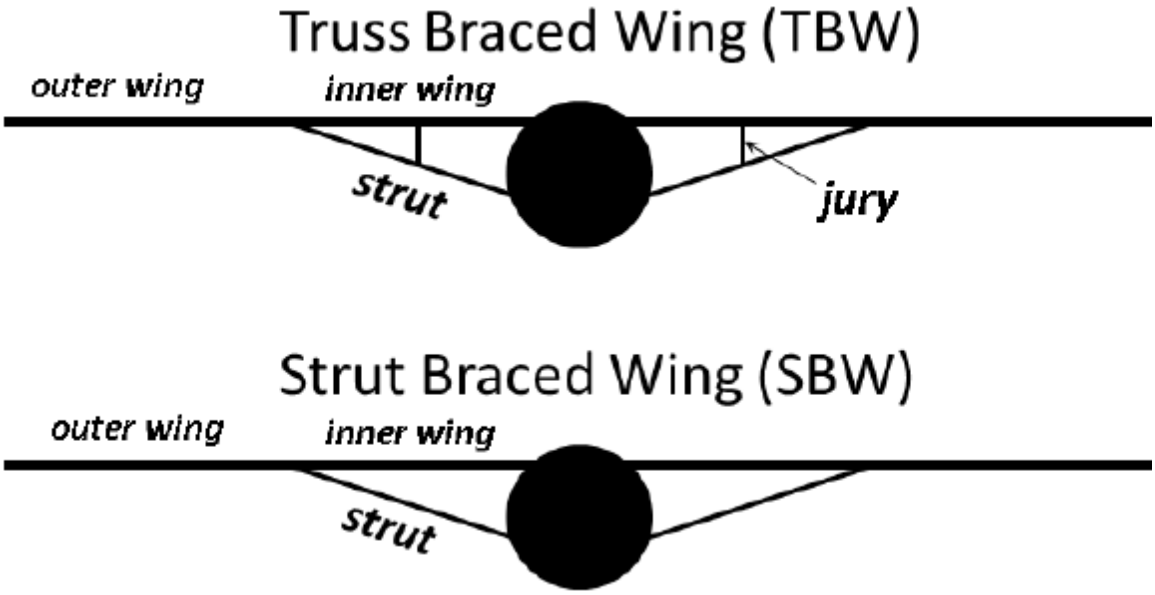

Figure 2.3. Truss-Braced Wing (TBW) (top) includes a vertical truss member, jury, not found on the simple Strut-Braced Wing Aircraft (bottom) [131].

concept from NASA and a comparison of the TBW and Strut-Braced Wing (Figure 2.1 shows a Strut-Braced Wing configuration [16]) respectively [131]. It has been proven that the TBW configuration is able to achieve larger reductions in fuel consumption than other unconventional

configurations [130].

Engineered for enhanced aerodynamic efficiency, this aircraft employs a substantially higher aspect ratio compared to traditional cantilever wings, achieved by utilizing truss structures to alleviate the wing root bending moment. This design allows for a noteworthy increase in the wing aspect ratio. Without structural bracing, the increase in the wing root bending moment would require a significant structural reinforcement which would lead to an increase in the structural weight that would offset the aerodynamic benefit of the high aspect ratio wing [76]. Hence, the primary wings are strategically braced near mid-span by two main struts, supplemented by two jury struts, each positioned on one wing, providing additional reinforcement. This design allows the main wing spar and skin to become thinner and lighter with reduced chord and thus reduced Reynolds number. The reduced wing thickness results in decreased wave drag. This also allows the wing to unsweep, thereby reducing span-wise cross flow disturbances. The combined effect of decreased cross flow and the reduced chord Reynolds number result in increased laminar flow. The expansive inboard wing areas with laminar flow experience reduced skin friction drag [101, 83]. However, it is acknowledged that the introduction of these braced structures induces certain aerodynamic impacts on the wing.

Thus, the design of a Truss-Braced Wing (TBW) is a Multidisciplinary Design Optimization (MDO) [70] process, aiming to strike a delicate balance between aerodynamic and structural efficiencies. At each stage of development, MDO studies have been conducted to enhance wing aerodynamics, structural efficiency, and flight performance, incorporating advanced N+4 turbofan engines. Initial investigations have successfully demonstrated the structural feasibility and potential advantages associated with the Truss-Braced Wing (TBW) in enhancing both aerodynamic performance and structural efficiency. A study conducted by Manav Bhatia et al. [8] laid the foundation for subsequent examinations into the nuanced challenges and opportunities inherent in this aircraft configuration. Sonia Lebofsky et al. [62] made significant contributions by addressing specific facets of aerodynamic performance and structural considerations within a specified Mach range. However, the lack of robust aerodynamic and structural modeling

for Mach numbers surpassing 0.70, limited their study to Mach numbers below 0.70. It is imperative to address these limitations for a more comprehensive understanding of the behavior and performance of the TBW under diverse operational conditions.

In a conventional MDO process, a diverse array of tools with varying fidelity is employed for tasks such as aerodynamic prediction and static aero-structural analysis. Despite ongoing efforts to develop high-fidelity Reynolds-Averaged Navier-Stokes (RANS) Computational Fluid Dynamics (CFD) models for Truss-Braced Wing (TBW) aerodynamic design and performance analysis, these models are often decoupled from the TBW structure. It is crucial to perform aeroelastic analysis for the TBW configuration, focusing on aero-structural coupling. This coupling has substantial implications for aerodynamics, as well as the stability and control of the vehicle. Consequently, aero-structural coupling emerges as a pivotal consideration in the development of TBW configurations. To facilitate this analytical capability, one viable approach involves the utilization of a lower-order aerodynamic tool capable of adequately capturing transonic and viscous flow effects for coupling with a finite-element model of the TBW structure. This strategy offers a swift analysis capability, streamlining vehicle optimization while incorporating aeroelastic constraints.

In a series of published works by Nguyen [77, 125, 128, 127, 78], meticulous consideration was given to a coupled aero-structural optimization. The studies utilized a low-fidelity vortex-lattice model and a mid-fidelity panel model to capture steady-state aerodynamics. Furthermore, a structural dynamic finite-element model was employed, encompassing the geometric nonlinear effect induced by tension in the struts, resulting in a deflection-dependent nonlinear stiffness. Despite the progress made in existing literature, this current study seeks to address specific research gaps. Notably, no prior research has explored the TBW design while considering both OML and structural variables. Furthermore, there is a lack of work incorporating coupled aeroelastic analysis through gradient-based optimization.

Recent advancements in Multidisciplinary Design Optimization (MDO) [111] underscore the efficacy of gradient-based optimization techniques in refining the initial design space

for distinctive aircraft concepts, even in the presence of numerous variables, numbering in the hundreds. Exemplifying the current state-of-the-art, Hwang and Ning employ the widely adopted OpenMDAO [39] framework to maximize the range of NASA's X-57 Maxwell electric aircraft [50]. The optimized design reveals a notable 12% increase in range, with the optimization problem being successfully resolved in less than ten hours. Both instances of aircraft design optimization benefit from the implementation of an automatically computed adjoint method for derivative calculations [49]. The adjoint method demonstrates scalability with an increasing number of design variables, establishing itself as a pivotal enabler for large-scale aircraft design optimization algorithms.

Table 2.1. Literature Review of Aero-Structural Solvers

	Mach number	**Aerodynamic Modeling**	**Wing-Strut Interference Effect**	**Wing, Strut and Jury Lifting Surfaces**	**Structural Modeling**	**Buckling Constraint**	**Aeroelastic Analysis**
Gur [43]	0.85	Various Solvers for Drag and FLOPS	No	None	Beam Model	No	Yes
Bhatia [8]	≥0.7	N/A	No	None	Beam Idealization considering only beam stiffness and static analysis	Yes	No
		Steady and Unsteady Double Lattice Method	No	Wing and Strut	Finite Element Based sizing considering aero-elastic Optimization	No	Yes
Nguyen [76]	0.745	Vortex Lattice Method using VSP Aero	Yes	Wing and Sturt	Beam Model	No	Yes
Nguyen [78]							
Xiong [125]							
Xiong [129]	0.8						
Xiong [127]							
Xiong [128]							
Solano [106]	0.7	N/A	No	All	Beam and Shell Model	Yes	No
Our Approach	0.7	Vortex Lattice Method with various drag solvers for interference, wave, and viscous forces.	Yes	All	Beam Model	Yes	Yes

These MDO studies have iteratively refined the wing geometry and configuration layout, incorporating trade studies focused on minimizing induced drag, profile drag, and wave drag resulting from the incorporation of the main strut and jury struts. While previous studies have determined the optimal number of jury and struts for the TBW, there has been limited investigation into the specific impact of wing-strut location. Sarojini et al.[99] and Solano et al.[106] explored the influence of wing-strut positioning on the structural weight of the

TBW. However, they did not perform an aeroelastic optimization to account for various drag components, particularly wave drag, which is critical in transonic conditions. This gap becomes more significant when transitioning to a Transonic Truss-Braced Wing (TBW) operating at Mach 0.80, where the wing-strut interference effects are amplified.

Furthermore, to perform a conceptual design of the Truss-Braced Wing (TBW), a mission and constraint analysis is crucial. Gur et al. [41] developed a framework for conceptual design of the Truss-Braced Wing (TBW) using FLight OPtimization System (FLOPS) for weight estimation, and semi-empirical methods for aerodynamic analysis. Chakraborty et al. [21] compared the strut-braced Wing configuration against the one-jury TBW configuration and the MDO study by including a mission analysis study for a climb, cruise, and descent mission profile. The study indicated that the one-jury TBW outperformed the strut-braced wing configuration for all span limits in terms of fuel burn. Adding one more jury only offered only marginal improvements for spans longer than 170 ft(approximately (approx.) 51.816 metres), which suggested that there was no need to investigate more complex truss systems such as three-jury or four-jury TBW. Meadows et. al [74] performed a comparison between a conventional cantilever wing design, a Strut-Braced Wing design, and a one-jury Truss-Braced Wing (TBW) design resulting in a similar conclusion as Chakraborty et. al. While these designs have led to advancements in the design of the Truss-Braced Wing (TBW) there have been very few studies that have done a combined mission and constraint analysis that could further lead to regulations on the stall speed, climb gradient and more.

This thesis seeks to address certain limitations from these papers. Firstly, by applying Outer Mold Line (OML) geometric parameterization (similar to the work detailed in Ruh et al.[92]) through Free-Form Deformation (FFD) to interconnected components like the wing, strut, and jury to the Truss-Braced Wing (TBW) configuration. This geometric parameterization study provides more precise control over aerodynamic shapes and structural integrity, which are vital for overall aircraft performance. Additionally, the research seeks to introduce a comprehensive optimization framework for the Truss-Braced Wing (TBW) configuration that includes OML,

Table 2.2. Literature Review Highlighting the Research Gap

	OML Defined	**Geometry Parameterized**	**Gradient Based Optimization**	**Nominal and off-nominal Mission Segments**	**Wing-Strut Location Analysis**	**Total Number of Variables and Constraints**
Gur [43]	No	No	Yes	Yes	No	< 50
Bhatia [8]	No	No	No	Yes -	No	< 50
	Yes	No	Yes	Yes	No	< 100
Nguyen [76]	No	No	No	No	No	< 100
Xiong [129]						
Nguyen [78]						
Xiong [125]						
Xiong [127]						
Xiong [128]				Yes		
Solano [106]	Yes	Yes	Yes	Yes	Yes	< 200
Our Approach	Yes	Yes	Yes	Yes	Yes	600+

structural, and trim design variables. This framework facilitates a more thorough exploration of the design space, enabling the identification of optimal configurations that meet performance, weight, and stability criteria. Table 2.1 outlines the aero-structural literature review detailed above and Table 2.2 outlines the research gap this thesis highlights.

This section, in full, is currently being prepared for submission for publication of the material. Darshan Sarojini, and John T.Hwang. The thesis author was the primary investigator and author of this material.

2.2 Multidisciplinary Design Optimization (MDO)

Multidisciplinary Design Optimization (MDO) is an approach that aims to optimize complex engineering systems by considering multiple disciplines simultaneously [26]. By integrating and coordinating the design of various subsystems or disciplines, such as structures, aerodynamics, controls, and more, MDO seeks to achieve an optimal overall system design.

Gradient-free methods, also known as derivative-free methods, are optimization techniques that do not rely on gradient information of the objective and constraint functions. These methods can be useful when the objective and constraint functions are non-differentiable or when the gradient information is costly or unavailable. Gradient-based methods, on the other hand, utilize gradient information (first-order derivatives) of the objective and constraint functions to

guide the search for optimal solutions. When available, gradient information provides gradient-based methods with several advantages over gradient-free methods. Gradient-based methods can converge to an optimal solution faster than gradient-free methods, especially when the design space is large or when the number of design variables is high. Gradient-based methods can handle large-scale optimization problems with a large number of design variables and constraints more effectively.

The challenges of MDO include the need to automate efficient and accurate sensitivity analysis for the complex problems typically encountered in this field. Additionally, there is a requirement to eliminate obstacles in the implementation of software that simulates system behavior based on a given model description. Understanding the properties of the physical system's behavior, as well as the program's run-time performance, from the model's structure is another significant challenge. Furthermore, reformulating model descriptions to address numerical difficulties specific to MDO problems is crucial for improving the robustness and effectiveness of optimization processes.

2.2.1 Computational System Design Language (CSDL)

Computational System Design Language (CSDL) [33] is an embedded domain-specific language designed to address Multidisciplinary Design Optimization (MDO) challenges. It allows engineers to work at a high level of abstraction, eliminating the need to manually implement low-level algorithms, such as those for derivative computation. CSDL automates the computation of derivatives both at the level of individual operations and across interconnected disciplines, making it ideal for solving optimization problems using gradient-based approaches.

CSDL simulations are written, compiled, and executed within a Python script. The CSDL compiler translates Python code that represents model behavior into low-level implementation code used to simulate the model, with users accessing the executable object through a Python object. The CSDL compiler operates as a three-stage compiler, consisting of a front end, which generates an intermediate representation of the code; a middle end, which performs

implementation-independent optimizations on this intermediate representation; and a back end, which generates executable code. The intermediate representation of the model captures dependency relationships between variables and operations, enabling different formulations, such as forward or reverse mode differentiation, depending on the structure of the intermediate representation. The executable code can be generated in any language. The front end and middle end of the CSDL compiler are implemented in one Python package, while the back end (code generator) is implemented in a separate package. This separation allows users to choose a code generator based on performance and memory requirements for simulating the model without needing to modify the model code [32].

2.3 Comprehensive Analysis and high-Dimensional DEsign Environment (CADDEE)

2.3.1 Aircraft Design Tools

The initial stages of aircraft design are intricate and involve navigating a vast design space to identify a suitable candidate that meets the top-level aircraft requirements (TLARs). These requirements are shaped by factors such as market demands, performance goals, and environmental concerns. Figure 2.4 illustrates a conceptual overview of the role that early-stage sizing tools play in aircraft design. The complexity of this process stems from the multidisciplinary and system-of-systems nature of aircraft design. The aircraft itself can be viewed as a system, which is composed of the interactions between its various components. A physical breakdown of the aircraft reveals parts such as the wing, empennage, fuselage, and engines. On a more detailed level, components like control surfaces and load-bearing members must also be considered. Analyzing the aircraft as an integrated system, or focusing on the interactions between its components, involves considerations from various disciplines, including aerodynamics, propulsion, structures, power systems, loads, flight mechanics, controls, noise, emissions, and cost.

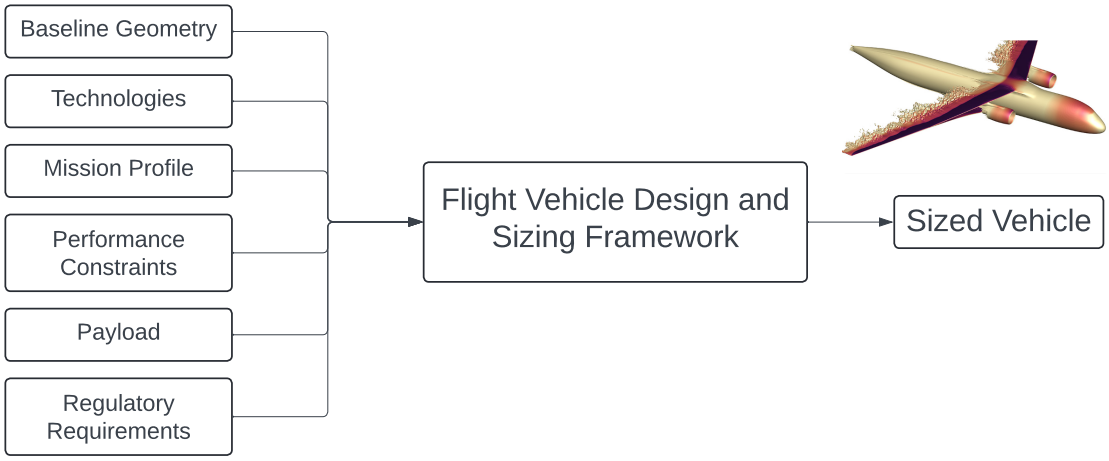

Figure 2.4. Sizing of a flight vehicle modified from Sarojini et al. [98]

Therefore, aircraft design is inherently a multidisciplinary system-of-systems challenge. Traditionally, early-stage aircraft design has relied on regression analyses or a limited set of parameters related to aerodynamics, propulsion, and flight conditions [87, 115]. NASA developed the tool FLight OPtimization System (FLOPS) [72] to address this need. FLOPS uses regressions to predict key aircraft parameters, such as the lift-to-drag ratio, engine thrust, and overall aircraft weight. These regressions are highly reliable due to decades of accumulated data, and they perform well for conventional aircraft designs. The mission segments are broken down into smaller time increments to provide greater detail throughout the mission. However, the regressions employed by early-stage design tools like FLOPS were specifically developed for traditional tube-and-wing aircraft and are not applicable to novel aircraft concepts and unconventional propulsion systems.

Recognizing these constraints, various physics-based sizing and analysis tools have been introduced in the literature. Welstead et al. [122] presented an energy-based approach for a new sizing tool called the Layered and Extensible Aircraft Performance System (LEAPS), which is under development at NASA to enhance the capabilities of the existing FLOPS. SUAVE [65] is a conceptual-level aircraft design environment that employs physics-based methods to size

innovative configurations and unconventional propulsion systems. An et al. [4] outlined a comprehensive sizing process that includes constraint analysis, electric propulsion system sizing, mission analysis, and structural weight estimation, with regressions developed for disciplinary analysis based on simulations and experimental data. Chakraborty et al. [20] introduced an energy-based sizing framework named PEACE, which represents disciplines in a functional form, allowing for disciplinary analysis using tables, surrogates, physics-based solvers, or a combination of these methods. The energy-based approach broadens the applicability of sizing to novel concepts and unconventional propulsion architectures. Additionally, Johnson and Silva [53] provide a survey of aircraft concepts and computational tools for advanced air mobility (AAM) developed by NASA.

The methods discussed in the literature aim to enhance various aspects of the sizing process. Sarojini et. al [98] and Ruh et. al [92] presented a new aircraft sizing framework named Comprehensive Analysis and high-Dimensional DEsign Environment (CADDEE). The features of this framework are(rephrased from [98]):

- Geometry-centric approach to MDO. Starting from a baseline OML geometry defined by B-splines, parametric changes can be made to the geometry that can be propagated to each physics-based analysis.

- Modular functional-form-based-framework. The framework is designed to be invariant to the vehicle concept, the propulsion system architecture, or the physics-based analysis methods used. Thus conventional aircraft or novel concepts, fuel-based or new propulsion system architectures can be sized.

- CADDEE relies upon physics-based models for weight estimation, aerodynamics, propulsion, stability and more. These models are all written in the Computational System Design Language (CSDL)(Section 2.2.1) which uses algorithms that act on computational graphs in order to automate adjoint-based sensitivity analysis for nearly any combination of

mathematical operations. This significantly speeds up the process of model development and integration within an MDO framework.

- As safety is a key consideration during aircraft design, the framework is designed to handle scenarios such as state-of-charge at the end of the mission, engine inoperative conditions, and flutter.

Now, we summarize CADDEE's features such as its geometry-centric approach, its strategy for data transfer, and general framework architecture. The following sections will examine the framework of CADDEE, which is primarily based on the work detailed in [98] and [92], with almost all of the succeeding sections serving as a rephrasing and adaptation of their original methodologies.

2.3.2 Geometry

The Truss-Braced Wing (TBW) model is first generated in OpenVSP [73] and CADDEE's geometry tool generates and maintains a high-fidelity, analytical model of the system, utilizing Basis Spline (B-Spline) due to their smoothness, analytical derivatives, and efficiency in representing complex geometries with minimal control points [14].

CSDL automatically calculates the analytical derivatives, allowing for gradient-based optimization without requiring extra implementation work. To enhance usability, the tool is designed with a user-friendly Python interface and utilizes object-oriented programming, which also supports the tool's modularity, making it simple to extend and upgrade. Figure 2.5 illustrates the flowchart of the geometry tool.

2.3.3 Modular Data Transfer

The Solver-Independent Field Representation (SIFR) methodology developed by Warner et al. [121] aims to enhance modularity among different solvers in an MDO problem by linking each solver to a common, framework-level representation of all field quantities, rather than

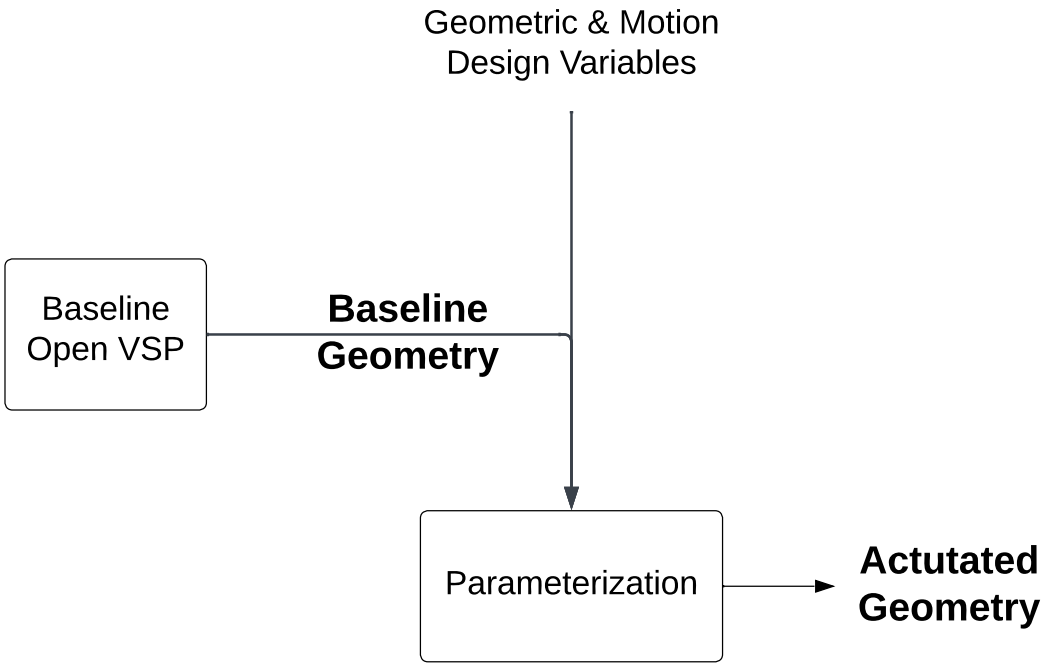

Figure 2.5. Flowchart of the geometry tool modified from Sarojini et al. [98].

directly interfacing solvers with one another. This approach standardizes the representation of spatially-distributed quantities, including states, design variables, and other key metrics. In the SIFR methodology, field quantities are handled similarly to geometry. Just as each geometric sub-surface maps from its parametric space to physical space, each field quantity is mapped from parametric space to the appropriate state space. This results in a unified, framework-level representation of field quantities, which provides data to solvers through evaluations at a mesh of spatial points.

2.3.3.1 Solver-Independent Field Representation (SIFR)

Within a geometry-centric framework, the geometry is consistently defined by a mapping from a parametric space to a physical space, with each sub-surface being treated as a geometry function chosen from an arbitrary function space. The SIFR methodology applies this same

approach to represent a given field at the framework level. This Solver-Independent Field Representation (SIFR) is composed of field functions, which are mappings from parametric space to the relevant field space. Importantly, the parametric space used for the geometry is the same as that used for the field representation, thereby integrating the field representation within the geometry. Although they share a parametric space, there are no additional constraints on the geometry function and the state function.

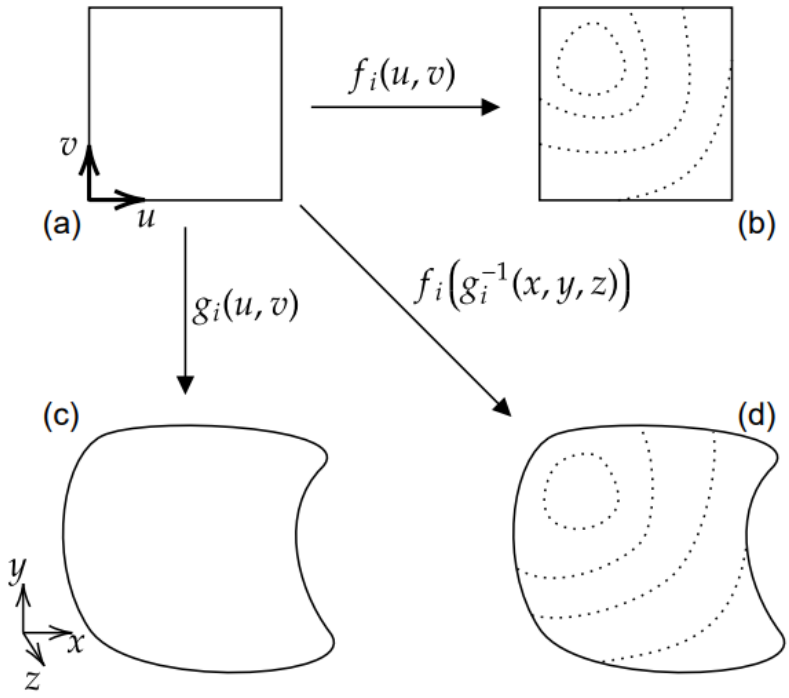

Figure 2.6. Diagram of the solver independent field representation: (a) parametric space, (b) contour plot of field quantity corresponding to patch i, (c) geometry patch i in physical space, (d) contour plot of field quantity in physical space. Originally from Warner et al. [121].

Warner et al. [121] aims to give a map between physical space and field space by defining a *geometry function* and a *field function*. This is shown in Figure 2.6.

A *geometry function* will be made of a union of B-Spline surfaces, and hence they define a function that represents the entire geometry.

$$G(i,u,v) = g_i(u,v) \tag{2.1}$$

where (u,v) is the input parametric coordinate, $I \times u \times v$ is an indexed parametric space where I = (1,2,3,....l) where l is the number of B-Splines in the geometry and $g_i(u,v)$ is the geometry function of the form that represents a set of B-Spline surfaces [30] corresponding to index $i \in I$.

A *field* may be defined over an arbitrary subset of the geometry, dubbed the field domain. The parametric field domain is an indexed parametric space of the form $\bar{I} \times u \times v$, where $\bar{I} \subseteq I$. A function to represent the field over the full field domain is:

$$F(i,u,v) = f_i(u,v) \tag{2.2}$$

where $f_i(u,v)$ is the field function of the form that represents a set of B-Spline surfaces [30] corresponding to index $i \in \bar{I}$.

2.3.3.2 Three-Column Data Transfer

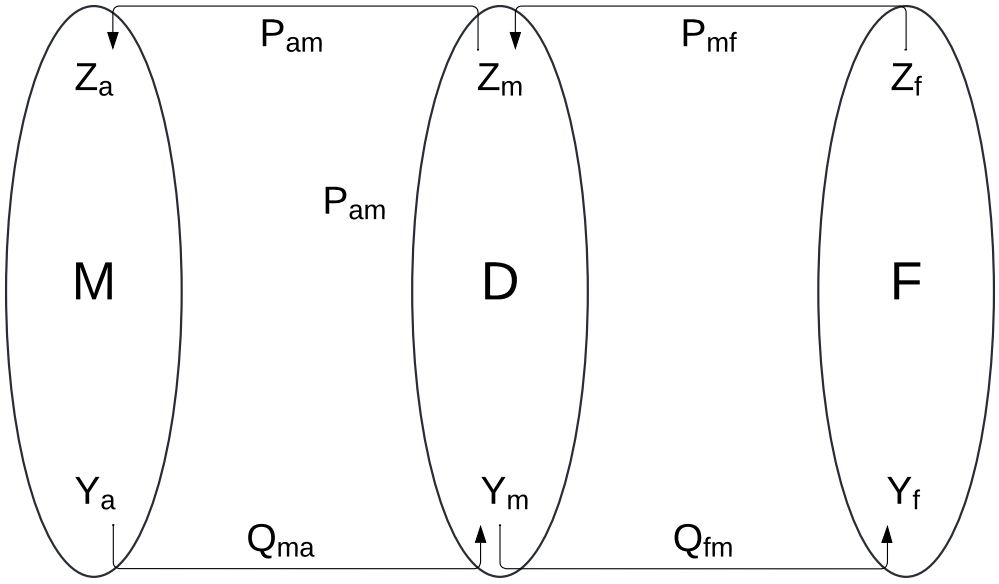

Figure 2.7. Illustration of the SIFR process between framework (F) and model (M) with input Z and output Y: P_{mf} framework evaluation, P_{am} model input, Q_{ma} model output, Q_{fm} framework fitting. Originally from Warner et al. [121].

After establishing the Solver-Independent Field Representation (SIFR), it must be evaluated to transfer data to solvers and fit it to solver outputs. Warner et al. ensure that this data transfer process is divided into three distinct stages, with the data representation changing at each stage. Figure 2.7 illustrates this process. Moving from right to left, the three stages are the framework representation (F), the discrete nodal representation (D), and the internal representation within the solver model (M).

Let Z represent a specific input field to the solver model, and Y represent a specific output field. Then, Z_f and Y_f are the solver-independent field representations of these quantities, and Z_a and Y_a are their representations within a particular solver. These representations are typically continuous, as is the case in this thesis. The discrete nodal representation serves as the bridge between these two functional representations, comprising a set of points over the field domain where one functional representation is evaluated and the other is fitted. For the input and output fields, Z_m and Y_m are the discrete representations.

To compute Z_m, the Solver-Independent Field Representation (SIFR) is evaluated at the chosen discrete locations, with P_{mf} being the resulting matrix that maps the framework representation to the discrete representation. The solver then computes the matrix P_{am}, which maps the discrete representation to the solver's internal representation. This process is unique to each solver and may involve specific assumptions and interpolation techniques relevant to that solver. This process is reversed for the output, with Q_{ma}, computed by the solver, mapping the solver's internal representation to the discrete representation. Finally, the nodal representation is fitted to the framework representation using the matrix Q_{fm}.

2.3.4 Mass Properties Estimation

Estimating the aircraft mass properties is a challenging multidisciplinary problem. The total aircraft mass properties can be computed as a build-up from 'component' mass properties. Broadly, we can categorize the 'components' as structural components, subsystem components, and energy components. This section is a combination of previous work published in CADDEE

and a more detailed overview can be seen at [98].

2.3.4.1 Structural Components

The typical procedure for sizing structural components involves several steps: First, static and dynamic maneuvers are simulated by integrating aerodynamics, structural dynamics, flight mechanics, and controls [103, 94, 86]. Next, the dynamic and static loads are converted into a set of critical static load cases [59, 55]. Finally, the structure is represented either as a shell model [57, 58, 85] or a beam model [112, 23, 105, 96] and sized based on these critical load cases. The structural weight estimation model calculates the aircraft-level mass properties, which are specified by 10 scalars: mass, three components of the center of gravity relative to an axis system, and six components of the symmetric mass moment of inertia tensor relative to the same axis system. For large transport category aircraft, the conditions to be considered are defined by 14-CFR. The coupled multidisciplinary analysis, which includes aerodynamics, structural dynamics, and propulsion, is combined with a controller and the equations of motion (EoM) to simulate maneuvers and determine the loads [95]. The structure is then sized by enforcing material failure and buckling constraints under the specified load conditions.

2.3.4.2 Subsystem Components

Subsystem components pertain to the aircraft's equipment systems that utilize secondary (non-propulsive) power to carry out functions crucial for vehicle performance, safety, controllability, and passenger comfort. In MDO studies, the structural weight of the aircraft is usually scaled to include these subsystem components. A common scaling factor of 1.25 is applied for large transport category aircraft [15]. In this work, the scope is limited by not incorporating physics-based subsystem sizing, instead relying on a scaling factor to account for the subsystems.

2.3.4.3 Energy Components

In this study, we define energy components broadly as elements that contribute to the propulsion of the flight vehicle. For a traditional fuel-powered aircraft, the engine serves as the

main propulsive mechanism, and fuel is stored on board to complete the mission. Therefore, the mass properties of both the engine and fuel are categorized under energy components.

2.3.5 Mission Segment Aeromechanics

The aeromechanics analysis must be conducted for each mission segment, and at a high level, a multidisciplinary analysis involving coupled aerodynamic, propulsive, and structural dynamics is performed to determine the aerodynamic and propulsive loads on the aircraft. These loads, along with the inertial loads, are then input into the equations of motion (EoM). The EoM is used either to trim the aircraft for the specific mission segment [95] or to assess the aircraft's dynamic response. This section is a combination of previous work published in CADDEE and a more detailed overview can be seen at [98].

2.3.5.1 Vehicle State

Twelve rigid-body states are defined:

- Body-fixed axis, velocity in x-direction u
- Body-fixed axis, velocity in y-direction v
- Body-fixed axis, velocity in z-direction w
- Inertial axis, position in x-direction X
- Inertial axis, position in y-direction Y
- Inertial axis, position in z-direction Z
- Body-fixed axis, roll-rate about x-direction p
- Body-fixed axis, pitch-rate about y-direction q
- Body-fixed axis, roll-rate about z-direction r

- Inertial axis, roll angle, attitude about x-direction ϕ
- Inertial axis, pitch angle, attitude about y-direction θ
- Inertial axis, yaw angle, attitude about z-direction ψ

Properties expressed within the wind-fixed axis frame are treated as dependent states. These states can be computed as dependent properties using transformation relationships. The velocity, angle of attack, and sideslip angle, respectively in the wind-fixed axis frame are computed as

$$V = \sqrt{u^2 + v^2 + w^2} \tag{2.3}$$

$$\alpha = \tan^{-1}(w/u) \tag{2.4}$$

$$\beta = \sin^{-1}(v/V) \tag{2.5}$$

The state vector is denoted $\vec{x}$ = {u,v,w,p,q,r,ϕ, θ, ψ, X, Y, Z}. This vector can be split into two parts, a dynamic portion $\vec{x_d}$, and a kinematic portion $\vec{x_k}$ as:

$$\vec{x} = \{\vec{x_d}, \vec{x_k}\} = \{\{u, v, w, p, q, r\}, \{\phi, \theta, \psi, X, Y, Z\}\} \tag{2.6}$$

2.3.5.2 Vehicle Controls

The controls on a flight vehicle pertains to the features which allow for the vehicle to be maneuvered in flight. CADDEE considers two types of control surfaces:

1. Basic control surface: most conventional control surfaces such as elevators, ailerons, flaps, etc fall under this category. A deflection value can be specified between an upper and lower bound.

2. Scheduled control surface: the deflection value of this control surface depends on a basic control surface deflection value. The user must provide the mapping relation between the two. A combination of the two types of control surfaces allows for most vehicles to be defined.

2.3.5.3 Inertial Loads

The gravitational force vector in body-fixed axis is

$$\vec{F}_g = \begin{bmatrix} Mg\sin\theta \\ Mg\cos\theta\sin\phi \\ Mg\cos\theta\cos\phi \end{bmatrix} \tag{2.7}$$

where M is the mass of the aircraft, and g the acceleration due to gravity, θ the pitch angle, and ϕ the bank angle. The corresponding moment is computed about the reference point using the offset vector from reference point to center of gravity, $\vec{r_g}$. Thus,

$$\vec{M}_g = \vec{r_g} \times \vec{F}_g \tag{2.8}$$

2.3.5.4 Aerodynamics

The purpose of the aerodynamics solver is to obtain the distributed loads and net loads on the vehicle at every time step as a function of the current state and control vectors:

$$\vec{f}_a, \vec{F}_a = f(\vec{x}, \vec{u_a}) \tag{2.9}$$

$$\vec{m}_a, \vec{M}_a = f(\vec{x}, \vec{u_a}) \tag{2.10}$$

where $\vec{F}_a$ and $\vec{M}_a$ are the net forces and moments on the aircraft respectively,$\vec{f}_a$ and $\vec{m}_a$ the distributed forces and moments respectively, and $\vec{u_a}$ the vector of deflections of all control surfaces on the aircraft. The deflection of each control surface is denoted as $\delta^{\text{(Mission segment)}}_{\text{(Control surface)}}$.

The net loads, $\vec{F}_a$ and $\vec{M}_a$ feed into the equations of motion block, whereas the distributed loads, $\vec{f}_a$ and $\vec{m}_a$,are inputs to the structural solvers.

2.3.5.5 Propulsion

The purpose of the propulsion solver is similar to that of the aerodynamics, i.e., it provides the loads on the vehicle at every time step as a function of the current state and control vectors. The vehicle is, in general, composed on a number of propulsive devices $n_p = 1, \ldots N_P$. The loads from each propulsion device is summed up to give the net loads on the aircraft:

$$\vec{F}_p = \sum_{n_p=1}^{N_P} f(\vec{x}, n_p u_p) \tag{2.11}$$

$$\vec{M}_p = \sum_{n_p=1}^{N_P} f(\vec{x}, n_p u_p) \tag{2.12}$$

In addition, the loads from each propulsive device are provided as point loads to the structural solvers.

2.3.5.6 Equations of Motion

CADDEE allows the user to specify any equation system describing the motion of the vehicle. The equation system may be specified as:

$$\dot{\vec{x}} = f(\vec{x}, \vec{u}) \tag{2.13}$$

if the state vector derivative can be explicitly written as a function of the state and control vectors. If such a formulation is not possible, a residual system of the following form can be specified:

$$\mathtt{R} = f(\dot{\vec{x}}, \vec{x}, \vec{u}) \tag{2.14}$$

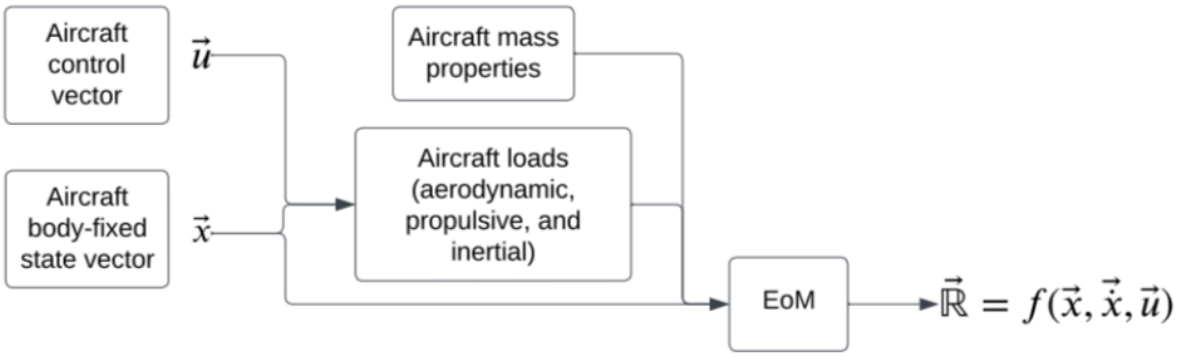

Figure 2.8. Computation of EoM residuals, inspired from Sarojini et al. [98].

The residual form is more general and allows the framework to be coupled to other analysis such as aerodynamics and structures to allow for flexible aircraft flight dynamics. For chosen values of $\vec{x}$, $\vec{u}$ by the optimizer, the total loads on the aircraft is computed. The loads, along with the aircraft mass properties, and $\vec{x}$ are given to the equations of motion block which computes $\mathtt{R} = \dot{\vec{x}} = \{\vec{x_d}, \vec{x_k}\}$. Figure 2.8 shows this computation as a flowchart.

$$\dot{\vec{x}} = f(\vec{x}, \vec{u}) \tag{2.15}$$

It is essential to ensure the aircraft can be trimmed at each mission segment in the mission profile. Each mission segment is treated as a case of dynamic equilibrium which involves finding the state and control vector such that

$$\vec{x_d} = f(\vec{x}, \vec{u}) = \vec{0} \tag{2.16}$$

where $\vec{x}$ is an aircraft body-fixed state vector and $\vec{u}$ is an aircraft control vector.

For each mission segment, a scalar constraint of the residuals is imposed on the optimizer, thus ensuring the aircraft is trimmed at each mission segment:

$$\mathtt{R} = (\vec{x_d})^T \cdot [W] \cdot \vec{x_d} \tag{2.17}$$

where [W] is a symmetric positive-definite, $\mathtt{R}$ is the trim residual, square matrix of

weights yielding a non-negative constraint [27].

2.3.6 Comprehensive Analysis

CADDEE is equipped to simulate various aircraft design disciplines across multiple mission segments, allowing for different levels of model fidelity. By using vectorization techniques, models of the same type can be efficiently applied across different mission segments. These mission segments fall into three categories. The first type, trim-state segments, represent steady operational conditions like cruise or hover, and are relatively simple to analyze. We will look at this type in detail, looking at the various analysis models (Section 3.2) used to compute these mission segments and also look at the results (Chapter 4) we have obtained from using these analysis models and this framework.

To guarantee a steady flight condition, we enforce a condition that all loads (aerodynamic, propulsive, and inertial) are balanced. We accomplish this by using the following equations of motion to compute a trim residual which is driven to zero. The stability analysis is limited to trimming the aircraft in each mission segment, such that the net forces and moments are zero. The equations of motion assume that the surface of the Earth is flat, rotational effect are negligible, and the atmosphere is at rest. In addition, the moments of inertia are treated as constant.

$$F_x - mg\sin\theta = m(\dot{u} + qw - rv) \tag{2.18}$$

$$F_y + mg\cos\theta\sin\phi = m(\dot{v} + ru - pw) \tag{2.19}$$

$$F_z + mg\cos\theta\cos\phi = m(\dot{w} + pv - qu) \tag{2.20}$$

$$L = I_x\dot{p} - I_{yz}(q^2 - r^2) - I_{zx}(\dot{r} + pq) - I_{xy}(\dot{q} - rp) - (I_y - I_z)qr \tag{2.21}$$

$$M = I_y\dot{q} - I_{zx}(r^2 - p^2) - I_{xy}(\dot{p} + qr) - I_{yz}(\dot{r} - pq) - (I_z - I_x)rp \tag{2.22}$$

$$N = I_z\dot{r} - I_{xy}(p^2 - q^2) - I_{yz}(\dot{q} + rp) - I_{zx}(\dot{p} - qr) - (I_x - I_y)pq \tag{2.23}$$

Equations 2.18 to 2.23 represents the total forces about the x, y, and z axes are F_x, F_y, and F_z respectively. The moments are L, M, and N. The linear velocity terms are u, v, and w, and the rotational velocities are p, q, and r. The Euler angles that rotate the body-fixed frame are ϕ, θ, and ψ. This work requires a 3 DoF system rather than a 6 DoF system.

The second type, transient segments, involve time integration schemes to capture dynamic transitions or gust responses, making them more computationally intensive. The third type focuses on off-design conditions, such as flutter or aeroelastic divergence.

2.3.7 Framework architecture

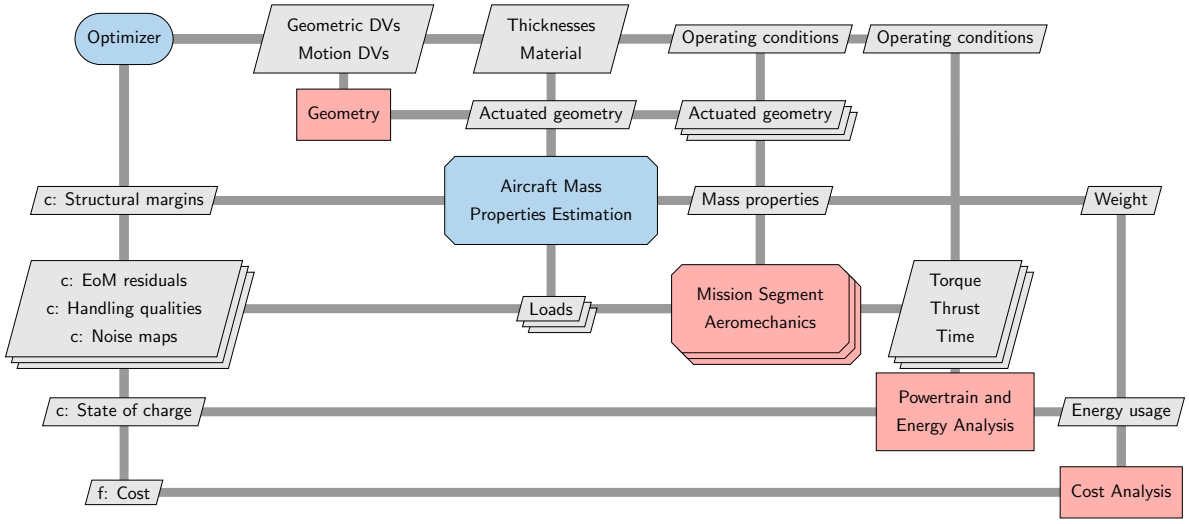

Figure 2.9. Architecture of the CADDEE design framework [98]

In Figure 2.9 we show the general architecture of the CADDEE framework in the form of a XDSM for a general example of an aircraft design problem for which CADDEE could be used. The diagram shows how disciplines are connected, what constraints are enforced (indicated by c) and what variables are optimized (i.e., design variables). The elements described above are incorporated into the overall CADDEE framework as shown in the XDSM in Figure 2.9. We set up an optimization problem for the top-level model in CADDEE containing all the

discipline-level submodels. In this example, the cost analysis outputs the objective function (indicated by f). In general, this can be any other quantity of interest such as gross weight, range, noise etc.

We apply constraints on the structural margins, EoM residuals, handling qualities and more in this example. The design variables for optimization originate from various submodels within the top-level model. The CADDEE model computes the objective, constraints, and their first derivatives and issues them to an optimizer from an interfaced optimizer library that contains multiple general-purpose optimization algorithms. The optimizer evaluates the CADDEE model repeatedly until the optimality and feasiblility criteria are met and thereupon outputs the optimal design variables. An additional cost analysis can also be included in the framework. The cost model provides an estimate of the capital expenses and operating expenses of the flight vehicle. The optimization problem can then be formulated as a minimization of cost. A similar such approach is taken in this thesis with the optimization problem being that of minimizing the fuel burn of the Truss-Braced Wing (TBW) aircraft during cruise, climb and descent.

Chapter 3

Methodology

This chapter presents a methodology to perform a fuel-burn analysis of the Truss-Braced Wing (TBW). An aircraft sizing framework named Comprehensive Analysis and high-Dimensional DEsign Environment (CADDEE) enables the creation of multidisciplinary models of aircrafts (and similar systems) to support analysis and design, using large-scale MDO. Section 2.1 details why a new aircraft sizing framework is required to analyze the TBW. In this chapter, Section 3.1 details the geometry parameterization performed on the Truss-Braced Wing (TBW) configuration, Section 3.4 details the optimization methodologies and Section 3.2 looks at the analysis models that are used in this thesis.

3.1 Design Parameterization

The design is parameterized using a high-fidelity representation of the Outer Mold Line (OML). To achieve this, Basis Spline (B-Spline) surfaces are used due to their analytical form and their ability to effectively represent complex geometries with a small number of control points. These B-Spline surfaces are then used to establish connections between any given set of external points and the central geometry using mapped arrays. A mapped array is a set of points resulting from the evaluation of a parametric map, which is determined by projecting points onto the OML.

Mapped arrays serve various purposes, such as extracting meshes, determining geometric

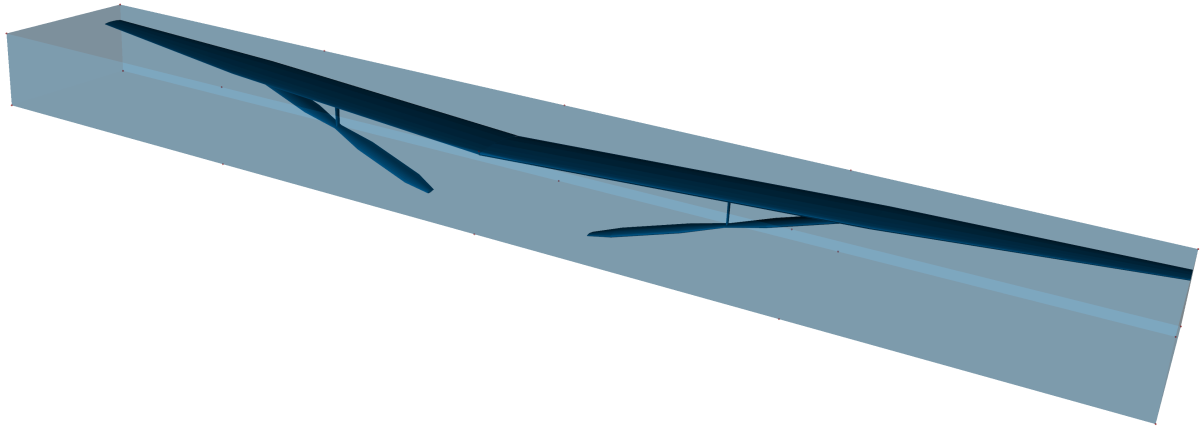

Figure 3.1. The Truss-Braced Wing (TBW), sturt and jury are enclosed within Free-Form Deformation (FFD) blocks, which scale the components during optimization.

variables (e.g., wing area, rotation axes), and defining parameters for bulk actuation (e.g., tilting wing). By defining these mapped arrays based on the B-Spline surfaces, any modifications made to the design geometry can be efficiently propagated through a simple matrix multiplication. At a level higher, the user can specify Free-Form Deformation (FFD) blocks, and set the FFD control points as design variables. At the second-to-highest level, the parameterization is further abstracted to the manipulation of FFD section properties in order to further reduce the dimensionality of the design space.

Figure 3.1 is a visualization of the Free-Form Deformation (FFD) blocks. For the Truss-Braced Wing (TBW) configuration it is essential to ensure that the Wing-Strut connection, Jury-strut connection and Wing-Jury connection is maintained throughout. This was done by the use of Free-Form Deformation (FFD) blocks. During the optimization every component has it's own FFD block, making the choice of contracting or expanding of each component independent to each other.

The capability of FFD in CADDEE proves particularly valuable during optimization processes for the TBW, where accurate representation of geometric variable changes, such as wing span or wing sweep, and is crucial for disciplines like aerodynamics and propulsion in order to capture the geometry changes.

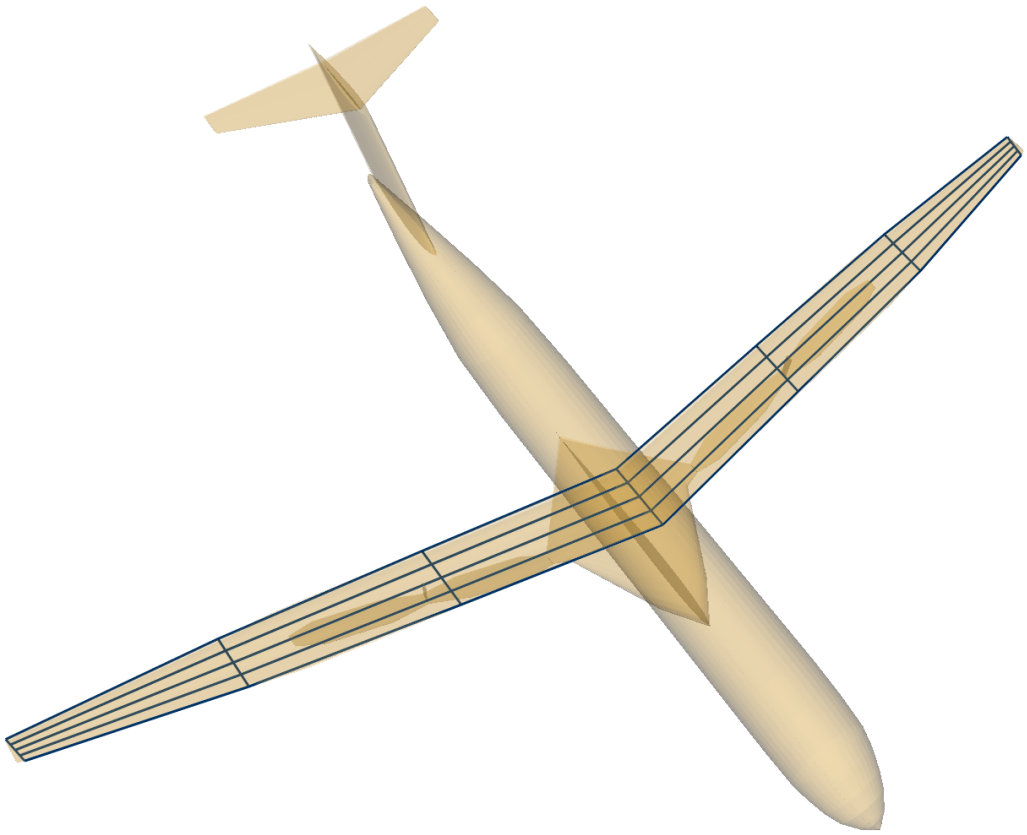

Figure 3.2. Wing Camber mesh.

Figure 3.2 illustrates the application of mapped arrays, showing the generation of a camber surface mesh for the wing superimposed with the B-spline geometry. In Figure 3.3, high-level sizing parameters like wing span and wing chord are derived from relative distances using mapped arrays, visually depicted by the blue points.

3.2 Analysis Models

We know look at the analysis model used in CADDEE to perform aeroelastic analysis on the Truss-Braced Wing (TBW) aircraft. This section modifies the framework mentioned in Section **??** to the Truss-Braced Wing (TBW) and describes CADDEE in a functional form.

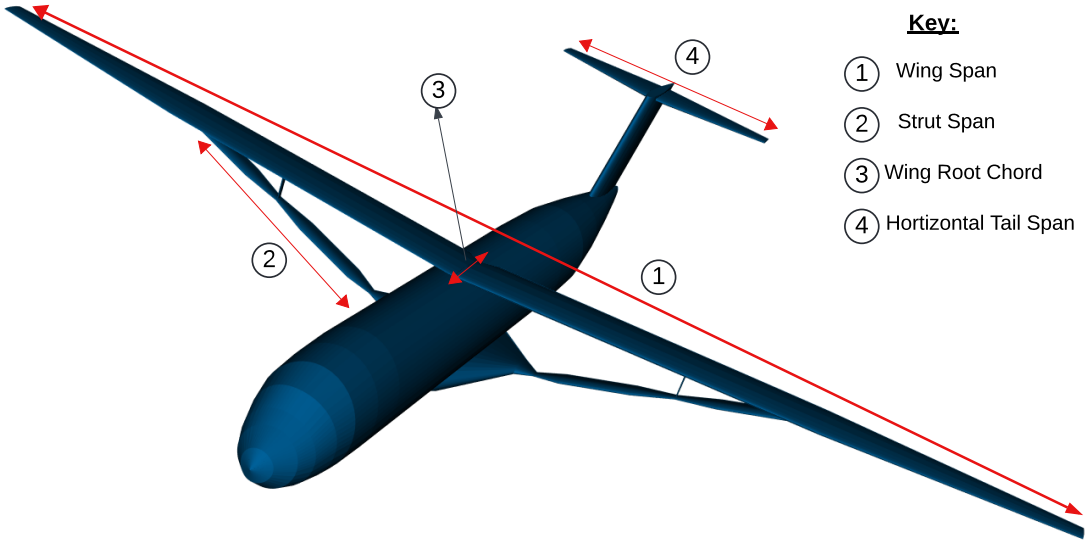

Figure 3.3. High Level Geometric Quantities.

3.2.1 Aerodynamic Analysis

This section takes a look at the various aerodynamic models used for analysis. Vortex Lattice Method (VLM) is discussed in Section 3.2.1.1, and the Section 3.2.1.2 discusses the various drag models that are accounted for in this study.

3.2.1.1 Vortex Lattice Method (VLM)

The aerodynamic solver is used to compute the total aerodynamic forces and moments on the aircraft. A fluid solver called Vortex-based Aerodynamic Solver Toolkit (VAST) was used for the aerodynamic analysis. It has multiple solver options: lifting-line method (LLT), Vortex Lattice Method (VLM) [124, 97, 113], and vortex panel method. VAST has options for both static and dynamic simulations. Vortex-based methods are a set of commonly used methods to analyze the aerodynamic performance, such as force or pressure distribution of lifting surfaces [6].

VLM assumes the flow to be potential, characterized by an irrotational velocity field,

which is given by

$$\nabla^2 \Phi = 0 \,, \tag{3.1}$$

where Φ is the fluid potential.

Other assumptions of the VLM include that 1) the fluid is incompressible and inviscid; and 2) the lifting surfaces are thin with a small angle of attack and sideslip. Figure. 3.4 demonstrates

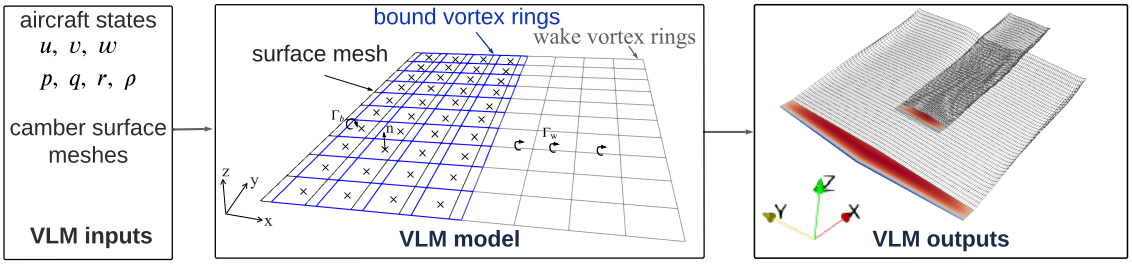

Figure 3.4. Aerodynamic analysis solution process using Figures as shown by Ruh et al. [92]

the inputs, model, and outputs of our VLM model. The inputs of the VLM model are the meshes and the states of the lifting surfaces. The VLM uses structured quadrilateral panels. It uses vortex rings located at the quarter-chord of each panel for computation. The system of equations to be solved corresponds to the flow-tangency condition meaning zero normal velocity on the lifting surface panels.

$$A\Gamma_\mathrm{b} + B\Gamma_\mathrm{w} + v \cdot n = 0 \tag{3.2}$$

where v is the kinematic velocity; n is the normal vector of the lifting surface panels; where Γ_b, Γ_w are the bound and the wake vortex circulation strengths, respectively; A and B are the aerodynamic influence coefficient matrices. The output of the VLM model is the traction forces on each panel given by panel forces divided by the area. The panel forces are calculated using the Kutta–Joukowski theorem [56]

$$F = \rho \Gamma_\mathrm{b} v_\mathrm{ind} \times s \tag{3.3}$$

where ρ is the density of the air; v_{ind} is the induced velocity evaluated on the bound vortex collocation points; and s is the bound vector.

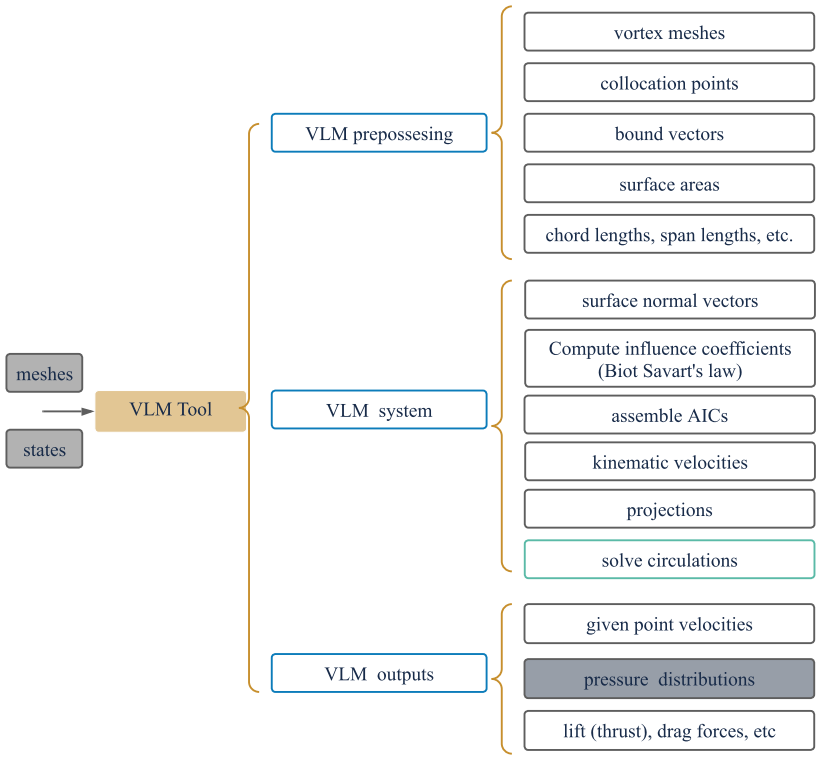

Figure 3.5. Aerodynamic analysis solution process in Tabular Form as shown by Ruh et al. [92]

We implement the VLM in CSDL(Section 2.2.1 with automated derivative computation (visualized in Fig. 3.5). It is implemented in an inertia frame with a constant freestream velocity and assumes steady-state conditions during each mission segment.

The summation of panel forces is executed in the chord-wise direction, and the computation of moments is conducted with respect to the quarter-chord point. The resultant one-dimensional load vectors are subsequently linked to the one-dimensional beam model, operating under the presumption that all forces are conservative. Although this assumption is constraining, it allows for the retrieval of first-order effects governing alterations in structural stress as lifting surfaces undergo scaling during optimization. The employment of VLM facilitates the accurate representation of lift forces including wing, horizontal tail and strut forces, as well as

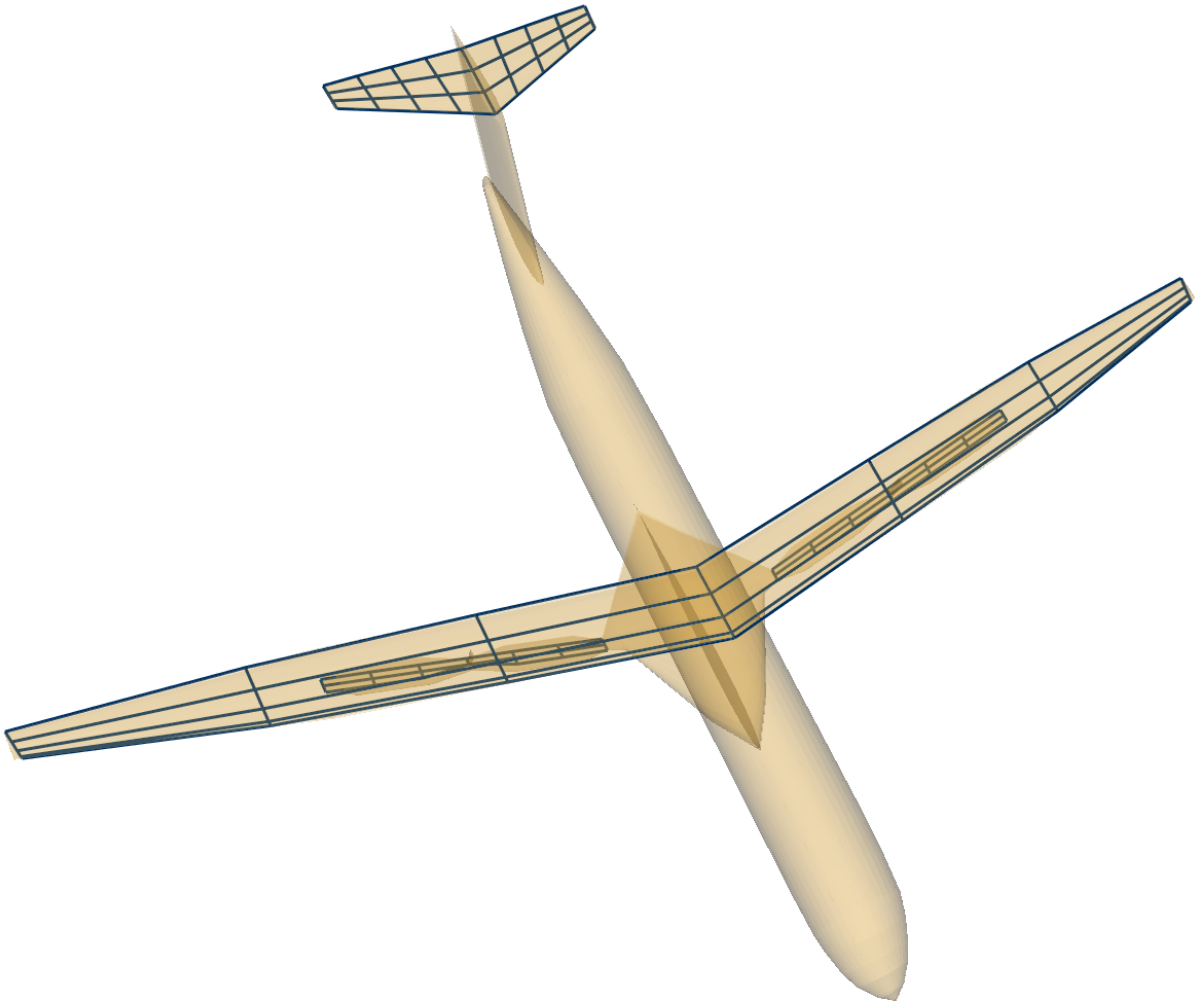

Figure 3.6. VLM Panels (dark blue) on the Truss-Braced Wing (TBW), strut and horizontal tail in CADDEE.

lift-induced drag and drag attributable to Mach number correction. Therefore, VLM outputs pressure distributions on the lifting surfaces, which are then coupled with the structural solver. A picture of VLM panels on the TBW, horizontal tail and the strut are shown in Figure 3.6.

3.2.1.1.1 Oswald Factor

In order to calculate the induced drag the Oswald efficiency factor is plays a crucial role. Various approaches to calculate this factor are detailed in [117, 80], but the TBW configuration is a non-planar configuration, and even though Kroo et. al [61] researched most of the non-planar configurations, Nitá et al. [80] displayed that the most promising results come from the box wing

configuration [100], where the two wings are connected via winglets. The proposed factor for calculating the Oswald factor is given as:

$$\frac{e_{box}}{e_{ref}} = \frac{k_3 + k_4 \times (h/b)}{k_1 + k_2 \times (h/b)} \tag{3.4}$$

where h and b are the wing span and root chord respectively, the factors k_1, k_2, k_3, k_4 are from different literature sources [84, 90] and the equation was created with the help of a tool called iDrag [37].

3.2.1.2 Drag Models

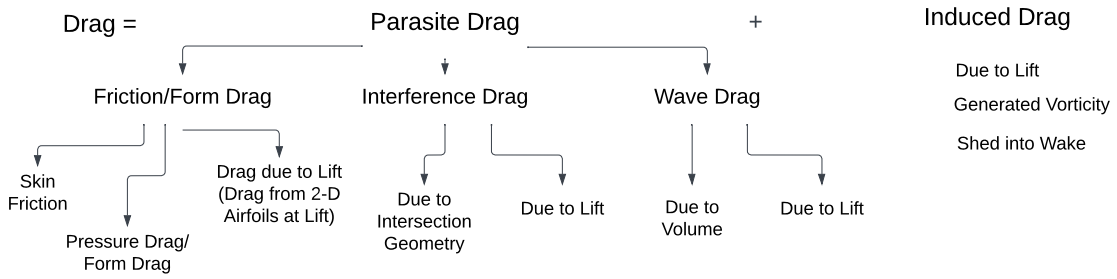

Figure 3.7. Drag Breakdown used in this thesis.

The aerodynamic performance of a Truss-Braced Wing (TBW) configuration is heavily influenced by various drag components, each contributing differently depending on the flight regime. Parasitic drag comprises both skin friction/viscous drag, interference drag and pressure drag, which arise from the interaction of the aircraft surface with the air. Due to the extended structure and multiple exposed components in a TBW, the parasitic drag can be significant. Induced drag results from the generation of lift, particularly prominent at lower speeds and higher angles of attack, where the wing's efficiency is reduced by the downwash created by vortices. The TBW's unique configuration, with its struts and bracing, offers potential reductions in induced drag by allowing for a higher aspect ratio wing. However, these benefits must be balanced against the structural penalties of the bracing system. At higher speeds, particularly

near transonic regimes, wave drag becomes a critical factor. Wave drag arises due to shock waves formed as the flow around the wing reaches and exceeds the speed of sound, leading to a significant increase in drag [127, 128, 62]. The TBW's aerodynamic design must carefully consider these shock wave effects to optimize performance at cruising speeds. Understanding these drag components and their interplay is essential for assessing the overall efficiency and viability of the truss-braced wing configuration in modern aircraft designs [5, 89]. Figure 3.7 gives a breakdown of the drag used in this thesis.

The VLM solver in Section 3.2.1.1 accounts for induced drag. Solvers for pressure drag, interference drag, wave drag and viscous drag are detailed below.

3.2.1.2.1 Pressure Drag

A form factor is used to represent the drag correction due to both thickness and pressure drag, which is sometimes referred to as profile drag. Many form-factor models exist [46, 116, 52, 104, 79], and this thesis uses the Grumman lifting-surface form factor FF_{wing} for the wing, truss members and tail:

$$FF_{wing} = 1 + 1.8\frac{t}{c} + 50(\frac{t}{c})^4 \tag{3.5}$$

where t/c is the maximum cross-sectional thickness ratio [43].

3.2.1.2.2 Viscous Drag

The viscous drag calculation is based on the wetted area and uses predictions of skin-friction models and form-factor estimations. The skin-friction prediction uses laminar and turbulent boundary-layer models. For laminar flow, the Eckert reference-temperature method [123] is used, and for turbulent flow, the Van Driest II method [48, 47] (based on the von Kármán–Schoenherr model) is used. The total skin-friction coefficient is based on a composition of the laminar/turbulent flow. Several composition formulas are available [63, 25, 19] but for this thesis the following relationships form the basis for approximating viscous skin friction drag

as described by Abbott and Von Doenhoff [1]:

$$c_{D_{f,wing}} = kc_f \times \frac{S_{w_{wing}}}{S_{ref}} \tag{3.6}$$

The key parameters in these expressions are the calculation of skin friction coefficient, c_f, and the corresponding form factors for airfoil, k, shapes. The airfoil form factor k is given by reference [108, 107] as a function of the thickness-to-chord ratio t/c, Mach number M, and wing sweep angle Λ.

$$FF_{wing} = 1 + \frac{0.6}{\bar{cos^2}\Lambda} + 100(\frac{t/c}{M})^4) \tag{3.7}$$

The calculation of skin friction coefficient associated with the wing and fuselage is performed using flat plate approximation. The resulting expression for c_f that captures the effect of laminar-to-turbulent flow transition is as follows:

$$c_f = \frac{x_c}{\bar{c}}(1.328 \times Re_{x_c}^{-0.5}) + (0.072 \times (Re_{\bar{c}})^{-0.2}) - \frac{x_c}{\bar{c}}(0.072 \times (Re_{x_{\bar{c}}})^{-0.2}) \tag{3.8}$$

where $Re_{\bar{c}}$ is the Reynolds number based on the mean aerodynamic chord.

To estimate the transition length x_c which is the distance from the leading edge of the wing or nose of the fuselage where the flow transitions from laminar to turbulent flow, the following expression is used:

$$x_c = \frac{(Re_{x_c} \times \mu)}{(\rho \times V)} \tag{3.9}$$

where the value ofRe_{x_c} is the transition Reynolds number, μ is the kinetic viscosity, ρ is the density, and V is the airspeed.

3.2.1.2.3 Wave Drag

The wave drag is a result of the shock waves created over the vehicle; thus, it becomes important at high subsonic speeds. The wave drag model used here is based on the Korn equation extended to swept wings [71, 7] with a Korn factor of 0.95, implying the use of supercritical airfoils. Along with Lock's fourth power law [51, 67, 45] the drag rise, critical Mach number, and drag-divergence Mach number can be estimated. For the aggressive-technology case, a highly supercritical airfoil is used: namely, a Korn factor of 0.95. The formula's are listed below:

$$M_{DD} + 0.1C_L + (\frac{t}{c}) = k_A \tag{3.10}$$

$$M_{Cr} = M_{DD} - (0.00125)^{(1/3)} \tag{3.11}$$

$$C_{D_{wave}} = 20(M - M_{Cr})^4 \tag{3.12}$$

where M_{DD} is the Drag Divergence Mach number, C_L is the coefficient of lift, t is the thickness of the airfoil, c is the chord-length of the airfoil and k_A is the korn factor of the airfoil.

3.2.1.2.4 Interference Drag

The interference drag estimation is based of Hoerner's Fluid-Dynamic Drag [46]. Five fundamental interference drag effects were identified from the Hoerner data. These five effects are combined in different ways to calculate the interference drag for a wing-fuselage intersection, and a wing-strut intersection. The first effect is the interference drag due to a wing intersecting a flat wall at a perpendicular angle. The drag coefficient due to this effect is given by:

$$C_{D_{wall}} = (0.8(\frac{t}{c})^3 - 0.0003)\frac{c^2}{S_{ref}} \tag{3.13}$$

The second effect is the interference drag due to a streamlined section intersecting another

streamlined section at a perpendicular angle. This is equivalent to a perpendicular wing-strut intersection. The drag coefficient due to this effect is given by:

$$C_{D_{strut}} = (17\frac{t}{c}^4 - 0.005\frac{t}{c}^2)\frac{c^2}{S_{ref}} \tag{3.14}$$

The t/c and c in this equation are the average values of the wing and strut.

The third effect is the interference drag due to the lift coefficient. The drag coefficient due to this effect is given by:

$$C_{D_{cl}} = (0.1C_L^2)\frac{c^2}{S_{ref}} \tag{3.15}$$

This equation comes from the Hoerner's statement, "At any rate, the interference drag approximately increases as the square of the lift coefficient." The value of 0.1 is a scaling factor. The fourth effect is the interference drag reduction due the sweep of the intersection. The drag coefficient due to this effect is given by:

$$C_{D_{sweep}} = (-0.000018\alpha^2 + 0.00009\alpha)\frac{c^2}{S_{ref}} \tag{3.16}$$

The sweepback angle α is defined as 0° for a perpendicular intersection in the side view.

The fifth effect is the interference drag due the inclination angle of the intersection. The drag coefficient due to this effect is given by:

$$C_{D_{inclin}} = (-0.000006\beta^2 + 0.0015\beta)\frac{c^2}{S_{ref}} \tag{3.17}$$

The inclination angle β is defined as 0° for a perpendicular intersection in the front view.

The five effects shown above are combined in the following ways to form the total interference drag for the wing-fuselage and wing-strut intersections.

Wing-fuselage :

$$C_{D_{interference}} = C_{D_{wall}} + C_{D_{cl}} + C_{D_{sweep}} + C_{D_{inclin}} \tag{3.18}$$

Wing-strut :

$$C_{D_{interference}} = C_{D_{strut}} + C_{D_{cl}} + C_{D_{sweep}} + C_{D_{inclin}} \tag{3.19}$$

All of the interference drag equations above assume that no fillets are being used at the intersections of the surfaces. Hoerner states: "the interference drag of a strut junction can thus be reduced to 10% of the unfaired configuration or less by means of a fairing extending one strut chord beyond the trailing edges." Therefore the interference drag calculated above is reduced by a factor of 10 [36]. In previous cases these equations weren't meant to provide an accurate measure of interference drag, but simply an indication of the trend. However by utilizing the wing-strut interference effects solver we can account for accurate representations of the interference drag.

Wing-Strut Interference Effects A method to enhance potential flow methodologies by addressing transonic and viscous aerodynamic effects encountered in many transport aircraft involves the utilization of a directly coupled transonic small disturbance (TSD) and integral boundary layer (IBL) framework. This approach aims to comprehensively account for the intricate physics associated with transonic and viscous flow phenomena.[22]. The corrections for transonic and viscous flows utilizing the TSD/IBL method are typically applicable to a single-element airfoil. However, the TBW configuration presents a complex geometry, encompassing a strut juncture region where interference aerodynamics can exert an influence on the overall aerodynamic performance of the aircraft. As the strut approaches the wing from below, the validity of transonic and viscous flow corrections using the TSD/IBL method diminishes due to interactions between the wing airfoil and strut airfoil [31].

To address these interference aerodynamics, Computational Fluid Dynamics (CFD)

models are established for both the wing-strut configuration and the wing-alone configuration of the TBW jig shape geometry using FUN3D. To isolate the interference aerodynamic effects for the wing and strut, the nacelle, pylon, and horizontal tail are excluded from the models. Surface pressure coefficients are then computed for both configurations at various wing stations. A comparison of the wing-strut data with the wing-alone data reveals the induction of a suction peak along the lower surface of the wing near the wing-strut juncture due to the presence of the strut [126].

A wing-strut interference correction method was developed by Fugate et al. [31] to correct the VLM model. The correction method is applied to the VLM model to update the section lift, drag, and pitching moment coefficient of each wing section. The interference correction, Δc_{IC}, that is applied to the model is calculated using the following equation:

$$\Delta c_{IC} = \Delta c_{FUN3D} - \Delta c_{VLM} \tag{3.20}$$

where c represents a key aerodynamic parameter such as C_L, or C_D, and Δ represents the change in the given parameter between the wing-strut configuration and wing-alone configuration. A model using the results of the thesis is implemented in CADDEE to account for the wing-strut interference effects.

3.2.2 Propulsion Analysis

We now look at the propulsion model used to determine the thrust by the engines. The model used here is a simple 1-D linear model that is dependent on the throttle of the TBW aircraft. The maximum thrust is obtained from the NASA TBW report [12] and simple equations are used determine the Force on each engine. Figure 3.8 shows this linear model. The engine used here is a gFan+ as mentioned in the above mentioned report.

$$F_{left_{engine}} = Throttle \times \frac{T_{max}}{2} \tag{3.21}$$

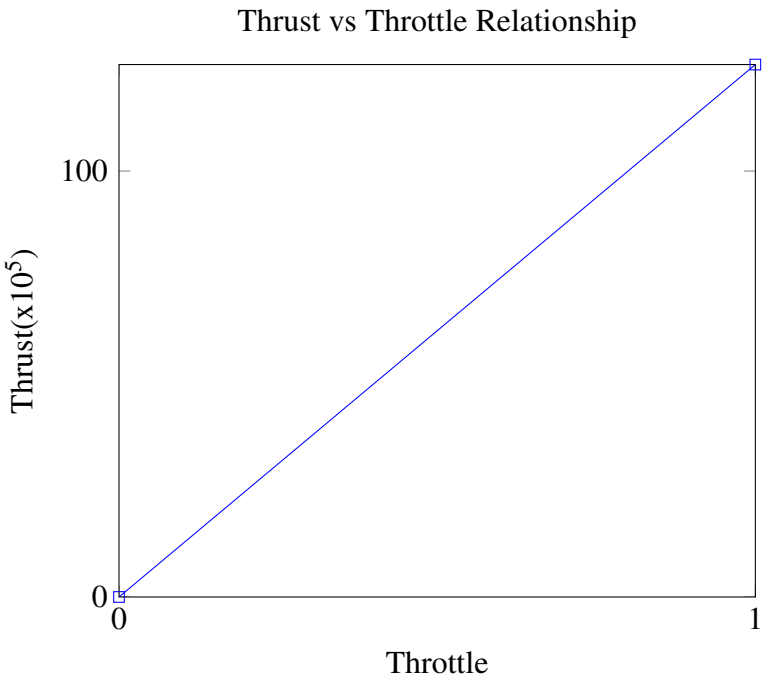

Figure 3.8. Relationship between throttle and thrust.

where $F_{left_{engine}}$ is the force on the left engine, T_{max} is the maximum thrust in Newtons. The total propulsion force on the engine is obtained from the below equation.

$$F_{total_{engine}} = F_{left_{engine}} + F_{right_{engine}} \tag{3.22}$$

3.2.3 Structural Weight Estimation

Numerous weight estimation methodologies utilized in preliminary aircraft design commonly rely on statistical methods or uncomplicated energy-based formulas. These approaches empower designers to approximate the weight of conventional concepts effectively. In the structural weight estimation model developed by Orndorff et. al [82], one-dimensional meshes (Figure 3.10) are derived from the overarching aircraft geometry, representing various slender components like the wing and fuselage. Assigning cross-sectional properties to each element within these meshes, the system is then solved to derive elemental stresses. By iteratively adjusting the structure to align with maximum allowable stress constraints, a reliable estimate of

the structural weight for any given component can be attained.

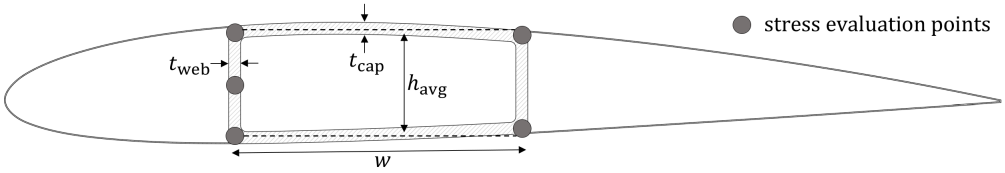

Figure 3.9. The wing box structure is shown here with the stress evaluation points marked with circles - as shown by Ordnorff et al. [82]

To streamline the structural analysis, Orndorff et. al employed a simplification wherein they characterized the wing-box structure as a hollow rectangular box-beam. This approach aligns with analyses conducted by Chauhan and Martins [23] and by Sarojini [93]. The thicknesses of the box-beam web and cap (t_{web} and t_{cap}) were treated as design variables in the optimization problem, while the width and height of the beams are determined from the wing meshes as ratios of the chord and the wing thickness. Utilizing these box-beam elements, Orndorff et. al constructed a global stiffness matrix $[K]$ using 12×12 frame stiffness elements [64]. By amalgamating aerodynamic, inertial, and propulsive loads, we form the stiffness matrix F, and subsequently solve the linear system $F = [K]U$ to ascertain the displacements U.

Following the solution of the linear system, Orndorff et al. conducted a stress recovery process, employing local displacements to calculate the loads acting on each element within the global beam mesh. Utilizing these loads, Ordnorff et al. computed the stress at five specific points along the box beam, corresponding to the anticipated locations of maximum bending and shear stresses. To account for various loading conditions, including -1g, +2.5g, and sizing scenarios, the aerodynamic and inertial loads in F were multiplied by a load factor. As no buckling models were incorporated, Orndorff et al. applied a conservative two-times safety factor during the assessment of the resulting Von-Mises stress at each of the five stress-evaluation points (Figure 3.9). This thesis replicates this exact methodology and Figure 3.10 depicts this.

As mentioned in Section 2.3.3 and 3.2.1 there is a transfer of data between the aerodynamic and structural solvers. This full data transfer scheme can be seen by the following the

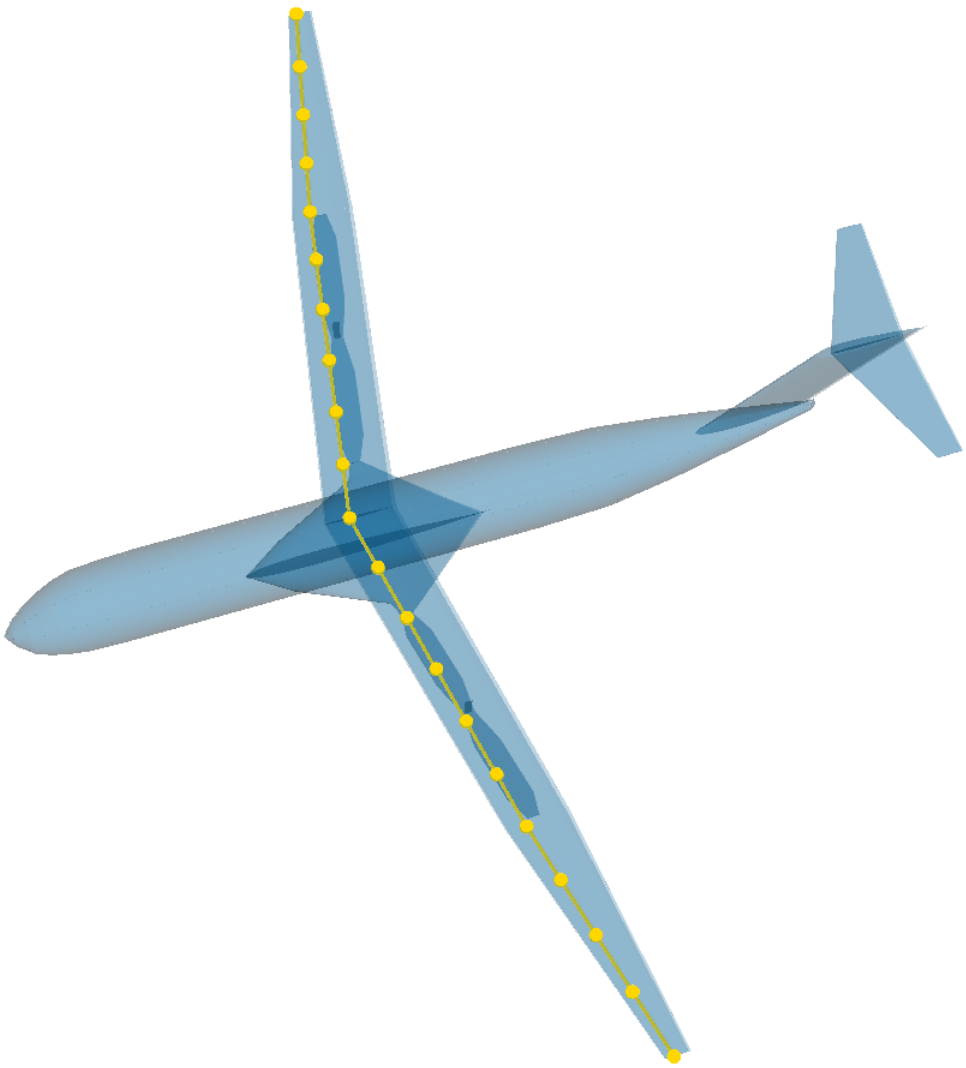

Figure 3.10. The one-dimensional stick model representation of the aircraft structure (in gold).

data transfer diagram shown in Figure 3.11. Starting with the aerodynamics solver (A), the map $T_{aa'}$ is computed by the machine learning airfoil model to transfer the forces from the VLM camber mesh to a nodal distribution on the wing surface. Next $T_{f'a}$ is computed using the above mentioned beam model, to transfer these nodal forces into the framework representation. The framework representation is then evaluated at the nodes of the structural meshes, resulting in the map $P_{sf'}$. These nodal forces are then ingested by the structural solver via the map $P_{ss'}$, resulting in the solver's finite element representation of the forces. The structural solver then computes the resulting displacements, which are transferred to a nodal representation by evaluating the

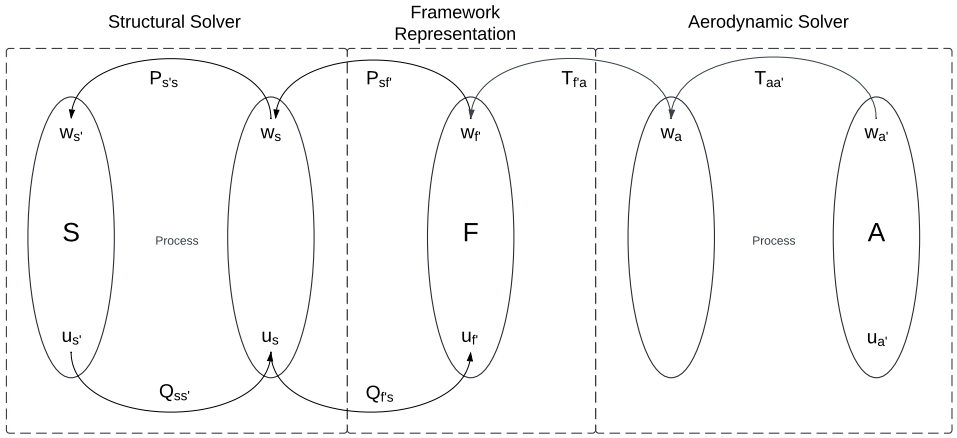

Figure 3.11. Data transfer between structural and aerodynamic solver using the SIFR methodology with respect to the various solvers used in this thesis.

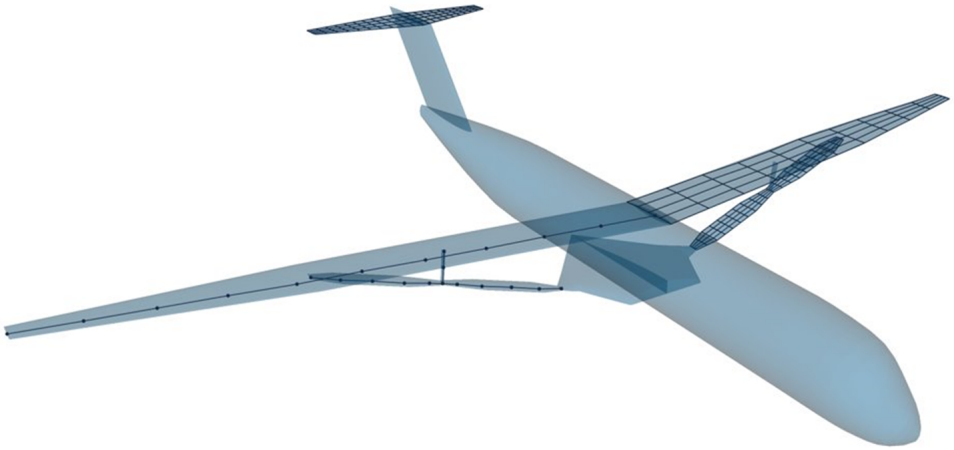

Figure 3.12. Vortex Lattice Method (Section 3.2.1.1) and 1-D beam mesh on the Truss-Braced Wing (TBW).

finite element representation of the displacements at a dense grid of points, resulting in the map $Q_{ss'}$. The B-Spline framework representation is then fit to the displacements at a dense grid of points, resulting in the map $Q_{f's}$. Figures 3.12 and 3.13 show one half of the wing depicting a VLM mesh and the other depicting a beam mesh on the wing, horiztontal tail and sturt for the VLM mesh and on the wing, strut and jury for the beam mesh.

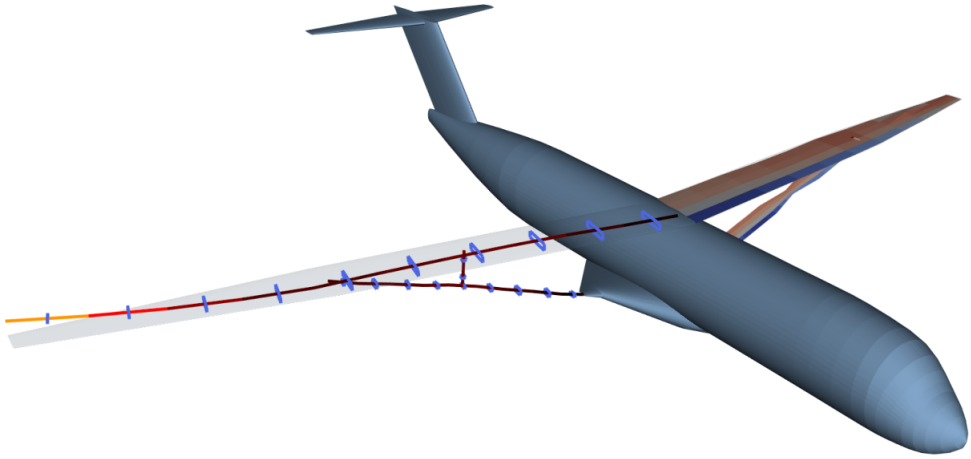

Figure 3.13. The one-dimensional stick model representation of the aircraft structure (with exaggerated deflections) - on the left side and a surface mesh look of the VLM on the right.

3.2.4 Mission Analysis

In Figure 3.14 we show the mission profile that we consider in this study, which is adopted from a study by Bradley et. al [12]. The red color indicates the various mission segments that we model, namely: cruise, climb and descent.

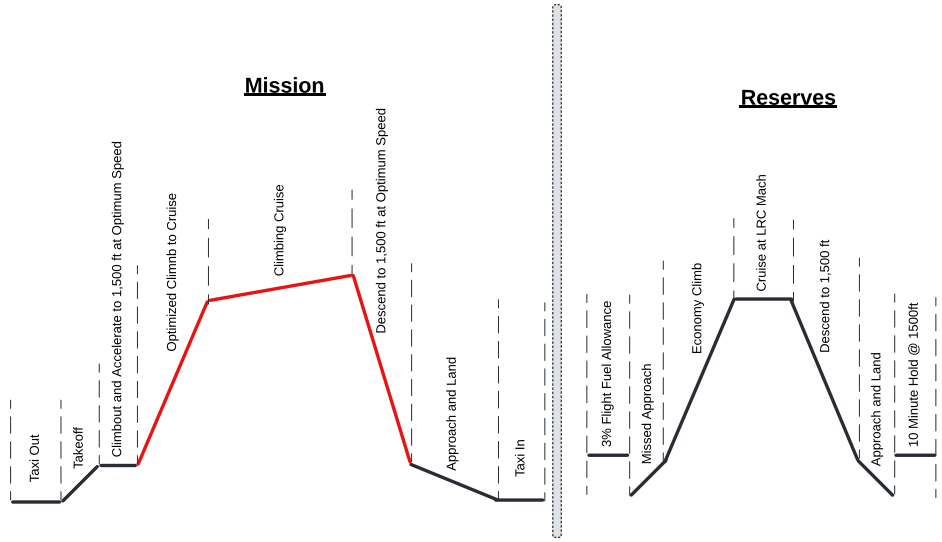

Figure 3.14. Mission Profile for the Truss-Braced Wing (TBW).

The complete aircraft design problem involves the simultaneous optimization of the

aerodynamic shape of a configuration, the structure to support the loads, and the propulsion system to provide the sufficient thrust required for flight at the desired airspeeds. Therefore, the objective function to be optimized requires a combination of aerodynamic, propulsion performance and structural weight.

This thesis focuses on studying fuel burn across various mission profiles, namely, cruise, climb, and descent—each with a distinct fuel-burn equation. The unique solvers addressing these variations are detailed below.

3.2.4.1 Fuel Burn during Climb

The equations that are used to calculate the fuel burn during climb are detailed below:

$$h_{gain} = h_{f_{climb}} - h_{i_{climb}} \tag{3.23}$$

$$t_{climb} = \frac{h_{gain} \times 3600}{V sin(\gamma_{climb})} \tag{3.24}$$

where $h_{i_{climb}}$ and $h_{f_{climb}}$ are the initial and final altitudes of climb and h_gain is the altitude gain in Equation 3.23 and V is the free stream velocity at the given mach number (0.70), γ_{climb} is the flight path angle during climb and t_{climb} is the time to climb in Equation 3.24.

Furthermore, the fuel burned during climb ($\dot{m}_{f\,climb}$) is calculated by the following equation:

$$\dot{m}_{f\,climb} = T_{climb} \times SFC_{climb} \times t_{climb} \tag{3.25}$$

where the Specific Fuel consumption is denoted by SFC_{climb}, and Thrust produced by the engines during climb is denoted by T_{climb} in Equation 3.25, where all are in SI units.

3.2.4.2 Fuel Burn during Cruise

The Bréguet range equation [18]:

$$Range = \frac{V}{c}\frac{L}{D}\ln\frac{W_i}{W_f} \tag{3.26}$$

is a fundamental formula used to estimate the range of an aircraft as it combines aerodynamic $(\frac{VL}{D})$, propulsion (c) and structural (W_i/W_f) figures of the aircraft. In the above equation V stands for the flight speed, L/D is the Lift-to-Drag ratio, c is the specific fuel consumption, W_i is the initial weight of the aircraft before take off or the Maximum Gross Weight of the aeroplane, W_f is the final weight of the aircraft after the mission - mainly taking into account fuel burn, as shown in the equation below.

$$W_f = W_i - \dot{m}_{f_{cruise}} \tag{3.27}$$

Equations 3.26 and 3.27 can be rewritten in terms of fuel burn($\dot{m}_{f_{cruise}}$) as follows:

$$\dot{m}_{f_{cruise}} = W_i(1 - \frac{1}{e^{ratio}}) \tag{3.28}$$

where ratio is:

$$ratio = \frac{R \times c}{V \times L/D} \tag{3.29}$$

This equation is suitable for use during cruise due to the following assumptions:

1. The equation assumes the aircraft to be flying at a constant altitude and speed, with no changes in flight path angle.

2. The aerodynamic performance of the aircraft is assumed to be constant throughout the flight. This implies that both the lift and drag remain proportional and that the aircraft is flying at an optimal angle of attack.

3. The only significant weight reduction over time is due to fuel consumption. Changes in

other parameters like payload are ignored.

4. The analysis assumes no external wind forces, so the aircraft's ground speed is equal to its airspeed.

3.2.4.3 Fuel Burn during Descent

The equations that are used to calculate the fuel burn during descent are detailed below:

$$h_{loss} = (h_{f_{descent}} - h_{i_{descent}}) \tag{3.30}$$

$$t_{descent} = \frac{h_{loss} \times 3600}{V sin(\gamma_{descent})} \tag{3.31}$$

where $h_{i_{descent}}$ and $h_{f_{descent}}$ are the initial and final altitudes of descent and h_{loss} is the altitude loss in Equation 3.30 and V is the free stream velocity at the given mach number (0.70), $\gamma_{descent}$ is the flight path angle during and $t_{descent}$ is the time to descent in Equation 3.31. It is clear that h_loss will be negative and the $\gamma_{descent}$ would also be negative hence cancelling each other out.

Furthermore, the fuel burned during descent ($\dot{m}_{f_{descent}}$) is calculated by the following equation:

$$\dot{m}_{f_{descent}} = T_{descent} \times SFC_{descent} \times t_{descent} \tag{3.32}$$

where the Specific Fuel consumption is denoted by $SFC_{descent}$, and Thrust produced by the engines during is denoted by $T_{descent}$ in Equation 3.32, where all are in SI units.

3.2.4.4 Total Fuel Burn

The total fuel burnt during climb, cruise and descent is give by equation 3.33

$$\dot{m}_{f_{total}} = \dot{m}_{f_{climb}} + \dot{m}_{f_{cruise}} + \dot{m}_{f_{descent}} \tag{3.33}$$

3.2.5 Constraint Analysis

In addition to the mission and aero-structural analysis mentioned in previous sections a constraint analysis is also added to the optimization study.

Constraint analysis is a fundamental method in aircraft design used to determine the optimal wing size and engine specifications that meet various performance requirements. This approach evaluates the interplay between key design variables and performance constraints to ensure a balanced and efficient aircraft configuration.

The design Variables in Constraint Analysis:

- Wing Loading (W/S): The aircraft's weight (W) divided by the wing's surface area (S). This parameter influences takeoff and landing performance, as well as overall aerodynamic efficiency.
- Thrust-to-Weight Ratio (T/W): The engine's thrust (T) divided by the aircraft's weight (W). This ratio affects the aircraft's acceleration, climb rate, and top speed.

Some of the Performance Constraints in Constraint Analysis:

- Takeoff and Landing Distances: The aircraft must be capable of taking off and landing within specified runway lengths.
- Climb Rate: A minimum rate of ascent is required to meet regulatory and operational standards.
- Stall Speed: The minimum speed at which the aircraft can maintain level flight without stalling.
- Cruise Speed: The aircraft should maintain a specified speed during level flight for efficiency and scheduling.

In addition to the above mentioned performance constraints, Maneuver constraints are also utilized in this preliminary analysis. We will dive in depth about the Stall-Speed, Climb and Constraint Maneuvers because of it's importance in forming the optimization problem for the full-scale optimization.

Stall-speed is the minimum speed at which an aircraft can maintain level flight. Below this speed, the aircraft's wings cannot generate enough lift to counteract its weight, leading to a loss of control known as a stall. In preliminary performance analysis, stall-speed helps determine the safe operating range of the aircraft. It's crucial for evaluating takeoff and landing distances, and for ensuring safe maneuvering at low speeds [68].

Climb performance refers to how well an aircraft can gain altitude. It is typically measured in terms of rate of climb (feet per minute or meters per second) and climb gradient (the angle or percentage of climb relative to horizontal). Analyzing climb performance is essential for understanding how an aircraft performs under various conditions, such as after takeoff or in emergency situations. It affects route planning, especially in mountainous terrain or when operating out of short or high-altitude runways. Maneuver constraints are limitations related to the aircraft's ability to safely perform various maneuvers. These include considerations for maximum bank angles, turn rates, and load factors (G-forces) that the aircraft can withstand without exceeding its design limits or causing undue stress [69]. Evaluating maneuver constraints ensures that the aircraft can safely perform required maneuvers under different flight conditions. This is vital for mission planning, avoiding structural damage, and maintaining safety margins [91, 88, 102]. Equations 3.34, 3.35, 3.36 give the stall speed, climb and maneuver constraints used in the optimization problem.

$$\frac{W}{S} \leq 0.9 C_{l_{max}} cos(\Lambda) \frac{1}{2} \rho (V_{stall})^2 \tag{3.34}$$

$$\frac{T}{W} \geq G + \frac{W/S}{\pi \times e \times AR \times q} + \frac{C_{D_0} q}{W/S} \tag{3.35}$$

$$\frac{T}{W} \geq \frac{C_{D_0} q}{W/S} + \frac{n^2}{\pi \times e \times AR \times q} W/S \tag{3.36}$$

where W/S is the Weight-by-area of the wing, $C_{l_{max}}$ is the 2-D maximum lift coefficient, Λ is the wing sweep of quarter-chord line, ρ is the density of the air, V_{stall} is the stall velocity, G is the climb gradient, e is the Oswald Factor(Using the same formula in Section 3.2.1.1.1), AR is the aspect ratio, q is the dynamic pressure, T/W is the Thrust-to-Weight ratio, C_{D_0} is the coefficient of drag with 0^o angle of attack, and n is the load factor where n is specified in Equation 3.37.

The values of n, G, and V_{stall} are taken with respect to the Boeing 737 flight as a reference.

$$n = \frac{Lift}{Weight} \tag{3.37}$$

The conditions introduce two additional constraints in the optimization problem. Specifically, Equation 3.38 and Equation 3.39 define the climb gradient and stall speed requirements, respectively. Although these equations are straightforward, they are still incorporated into the optimization problem to ensure compliance.

$$G = \frac{T - D}{W} \tag{3.38}$$

$$V_{Mach=0.7} \geq V_{stall} \tag{3.39}$$

In addition to the above constraints, takeoff (Equation 3.40) and landing (Equation 3.41) distances as well as cruise speed (Equation 3.42) are also taken as constraints.

$$\frac{W}{S} \leq \mathrm{TOP}\, \sigma C_{L_{\mathrm{takeoff}}} \frac{T}{W} \tag{3.40}$$

$$\frac{W}{S} \leq \left(S_{\mathrm{landing}} - Sa\right) \sigma C_{L_{\max}} \frac{1}{80\,\mathrm{ft}} \tag{3.41}$$

$$\frac{T}{W} \geq \frac{k}{q}\frac{W}{S} + \frac{qC_{D_0}}{W/S} \tag{3.42}$$

3.3 Optimization Problem Formulation

The optimization problem will be broken down into two sets. In Section 3.3.1, we focus on sub-scale MDO where we show the optimization problem of a structural sizing optimization and a trim analysis. In Section 3.3.2 we present the optimization problem of our full-scale optimization study, in which the optimizer can change all (including geometric) variables of the design.

3.3.1 Sub-scale MDO

Due to the complexity of this high-dimensional optimization problem, we begin the system-level optimization with sub-scale optimizations to establish a good starting point for the large-scale optimization. In these preliminary optimizations, we keep the aircraft geometry unchanged and focus solely on finding an effective initial solution.

Initially, we size the wing, strut and jury structures using two specific conditions outlined in Table 3.1, where the aircraft is subjected to loads of +2.5g and -1g. These conditions will determine the thickness of the wing's, strut's and jury's top and bottom skins, as well as the spar thickness. The objective is to minimize the wing weight while adhering to constraints related to buckling, stress, and displacements. This sizing is performed for various wing-strut locations' (η) in order to give us a good starting point to perform our optimization. by studying the resulting mass properties we aim to establish a good starting point for the wing-strut location as well. We perform this for a range of η locations from 0.40 to 0.80, where if η is = 1 then the wing tip chord and the strut coincide.

Figure 3.15 and Figure 3.16 show the strut location for $\eta = 0.40$ and $\eta = 0.80$ respectively.

Subsequently, we conduct an aircraft trim optimization (Table 3.2) for all the various

Table 3.1. Sizing Design Variables and Constraints

	Variable/Function	Quantity
minimize	Minimize Wing + Strut + Jury Structural Mass	1

w.r.t	Wing beam Top Skin thickness	21
	Wing beam Bottom Skin thickness	21
	Wing beam Spar thickness	21
	Strut beam Top Skin thickness	18
	Strut beam Bottom Skin thickness	18
	Strut beam Spar thickness	18
	Jury beam Top Skin thickness	6
	Jury beam Bottom Skin thickness	6
	Jury beam Spar thickness	6
	Incidence Angle	2
	Pitch Angle	2
	Throttle	2
	# of Design Variables	***141***

subject to	Wing Top Buckling	20
	Wing Maximum Stress (21x5)x2	210
	Wing Displacement (21x3)x2	126
	Trim Residual/ Aircraft Acceleration	2
	Wing Bottom Buckling	20
	Width of Wing Beam (20x2)	40
	Height of Wing Beam (20x2)	40
	Width of Strut Beam (16x2)	32
	Height of Strut Beam (16x2)	32
	Width of Jury Beam (4x2)	8
	Height of Jury Beam (4x2)	8
	Wing Beam Top Skin Thickness Symmetry	10
	Wing Beam Bottom Skin Thickness Symmetry	10
	Wing Beam Spar Thickness Symmetry	10
	# of Constraints	***568***

wing-strut locations, to ensure that the forces and moments during each steady design condition are nearly zero. In this phase, the optimizer is limited to adjusting trim variables such as the aircraft pitch angle and elevator deflection.

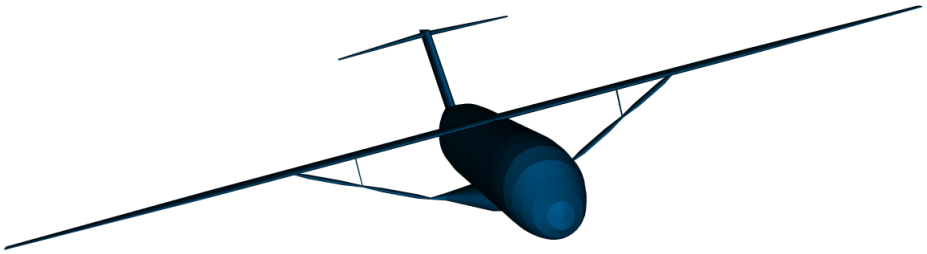

Figure 3.15. Wing Strut Location(η) = 0.40.

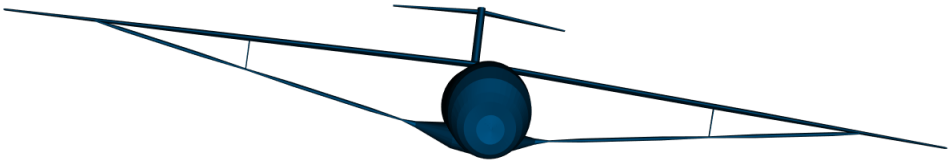

Figure 3.16. Wing Strut Location(η) = 0.80.

Table 3.2. Trim Design Variables and Constraints

		Variable/Function	**Quantity**
Cruise	minimize	Trim Residual	1
	w.r.t	Incidence Angle	1
		Pitch Angle	1
		Throttle	1
		# of Design Variables	***3***
Climb	minimize	Trim Residual	1
	w.r.t	Incidence Angle	1
		Pitch Angle	1
		Throttle	1
		Flight Path Angle	1
		# of Design Variables	***4***
Descent	minimize	Trim Residual	1
	w.r.t	Incidence Angle	1
		Pitch Angle	1
		Throttle	1
		Flight Path Angle	1
		# of Design Variables	***4***

3.3.2 Full-scale MDO

In this section, we detail the full-scale MDO problem we solve, minimize the full burn during a specified mission. Fuel burn is considered a viable full-scale MDO problem because for conceptual design the minimizing of fuel burn entails minimizing weight while maximizing aerodynamic efficiency especially during cruise, as detailed in Equation 3.29 and Equation 3.28. Therefore we include geometric parameters and perform constraint analysis for stall, maneuver and climb.

Using the physics-based models presented previously, we formulate an optimization problem that allows us to optimize the Truss-Braced Wing (TBW). As mentioned previously, the objective of our optimization is to minimize fuel burn for a mission of climb, cruise and descent. We choose to minimize fuel burn because we can assess the aerodynamic efficiency, and fuel economy of the TBW aircraft, by analyzing the Lift-to-Drag (L/D) ratio and can also assess the performance and cost by sizing the TBW and reducing the mass of the wing, strut and jury while ensuring various stability conditions are met.

At a high level, the design variables can be categorized into geometric (e.g., wing span and sweep), operational (e.g., aircraft pitch), and sizing variables (e.g., skin thickness). The geometric design variables comprise the span, sweep, twist, chord, and horizontal-tail incidence, representing the minimum necessary elements for the optimizer to determine a viable solution. Notably, the horizontal-tail incidence holds significance in the computation of the trim residual (R), as it counterbalances the aerodynamic moment from the wing. Unlike the wing incidence angle, the pitch angle for the entire airplane serves as a design variable, thereby effectively altering the wing's incidence.

Another important constraint is the maximum allowable wing stress and the maximum wing displacement due to the stresses. Because an important constraint of the optimization problem is the total mass, the structural solution will inherently be driven to the maximum stress constraint. To limit the total number of constraints, we use maximum and minimum

Table 3.3. Design Variables to Minimize Fuel Burn

	Variable/Function	Quantity
	Wing Span	1
	Wing Root Chord	1
	Wing Mid Chord	1
	Wing Tip Chord	1
	Wing Sweep	3
	Wing Twist	3
	Wing beam Top Skin thickness	21
	Wing beam Bottom Skin thickness	21
	Wing beam Spar thickness	21
	Strut beam Top Skin thickness	18
	Strut beam Bottom Skin thickness	18
	Strut beam Spar thickness	18
	Jury beam Top Skin thickness	6
	Jury beam Bottom Skin thickness	6
	Jury beam Spar thickness	6
	Incidence Angle	2
	Pitch Angle	2
	Throttle	2
Cruise	Incidence Angle	1
	Pitch Angle	1
	Throttle	1
Climb	Incidence Angle	1
	Pitch Angle	1
	Throttle	1
	Flight Path Angle	1
Descent	Incidence Angle	1
	Pitch Angle	1
	Throttle	1
	Flight Path Angle	1
	# of Design Variables	***162***

operators on all the vectorized constraints (e.g., maximum stress). Since the maximum and minimum operations are non-differentiable we approximate these constraints using Kreisselmeier-Steinhauser functions.

Table 3.3 gives a breakdown of the design variables and Table 3.4 gives a breakdown of

Table 3.4. Constraints to Minimize Fuel Burn

	Variable/Function	Quantity
	Wing Top Buckling	20
	Wing Maximum Stress (21x5)x2	210
	Wing Displacement (21x3)x2	126
	Trim Residual/ Aircraft Acceleration	2
	Wing Bottom Buckling	20
	Width of Wing Beam (20x2)	40
	Height of Wing Beam (20x2)	40
	Width of Strut Beam (16x2)	32
	Height of Strut Beam (16x2)	32
	Width of Jury Beam (4x2)	8
	Height of Jury Beam (4x2)	8
	Wing Beam Top Skin Thickness Symmetry	10
	Wing Beam Bottom Skin Thickness Symmetry	10
	Wing Beam Spar Thickness Symmetry	10
	Sweep Constraint	1
	Twist Constraint	1
	Minimize Total Mass	1
Cruise	Trim Residual/ Aircraft Acceleration	1
	Maximize L/D	1
	Constraint Analysis(Stall Speed)	2
	Constraint Analysis(Maneuver)	1
Climb	Trim Residual/ Aircraft Acceleration	1
	Time to Climb	1
	Distance to Climb	1
	Constraint Analysis(Climb)	2
Descent	Trim Residual/ Aircraft Acceleration	1
	Time to Descent	1
	Distance to Descent	1
	# of Constraints	***584***

Table 3.5. Summary of the Optimization Problem

Objective	Minimize Fuel
Number of Design Variables	162
Number of Constraints	584

the constraints in the optimization problem. The optimization problem consists of three different conditions where the constraints will be trimmed at, namely +1g, and at -1g, and 2.5g according to the 14-CFR Part 25-Code of federal regulations, and this is summarized in Table 3.5.

The designated cruising altitude is set at 13,106.4 meters (43,000 feet), and the payload weight is specified as 13,970.645 kilograms (30,800 pounds), inclusive of 12 first-class and 142 economy-class seats. These parameters are considered constant in governing the cruise condition. Conversely, variables such as throttle and pitch angle are treated as design parameters. The atmospheric properties, encompassing density, pressure, and temperature at this altitude, are obtained from a standard-atmosphere surrogate model established through a sixth-order polynomial regression. Table 3.5 summarizes the optimization problem detailed above.

We first solve the optimization problem for the configuration yielding the lowest mass, as determined from the analysis of various wing-strut configurations in Section 3.3.1. The goal is to identify an appropriate wing-strut location for conducting the aforementioned optimization process.

3.4 Computational Approach

The computational approach used in this thesis is detailed below. We discuss the optimization techniques used to solve the optimization problem.

Our target optimization problem is large-scale, involving hundreds of design variables and multiple constraints. Sequential quadratic programming (SQP) and interior point (IP) methods have demonstrated high efficiency in solving such large-scale problems, typically requiring only a few hundred model evaluations or less. For our problem, we plan to use the SNOPT [35] (sparse nonlinear optimizer)optimization algorithm, which is based on the SQP method. SNOPT

solves a series of quadratic programming (QP) subproblems to reach a feasible local minima for a nonlinear programmming problem. Each QP subproblem minimizes a quadratic approximation of a modified Lagrangian subject to linearized constraints to obtain a search direction towards the next design iterate. Additionally, we used the Sequential Least Squares Programming (SLSQP) method ([60]) from modOpt: A modular development environment and library for optimization algorithms [54] to determine a few initial trim results.

Given that our system model incorporates multiple subdiscipline models, the design variables may vary significantly in magnitude, leading to poor scaling and a lack of reliable initial guesses for some variables. These factors could potentially cause convergence issues during optimization. To address this, we will conduct optimizations at the subsystem level first and use those solutions to appropriately scale and initialize the broader system-level optimization problem.

This chapter, in full, is currently being prepared for submission for publication of the material. Darshan Sarojini, and John T.Hwang. The thesis author was the primary investigator and author of this material.

Chapter 4

Results

In this chapter we present two sets of results. In Section 4.1 we show the results of a structural sizing optimization. In Section 4.2 we present the results of our full-scale optimization study, in which the optimizer can change all (including geometric) variables of the design. All studies within this chapter were executed on a desktop with an 8-core Ryzen 7 @ 3.6 GHz processor and 32 GB of RAM. We do not implement multi-threading or parallelization with GPUs in any of our numerical experiments.

4.1 Sub-Scale MDO

This section presents the findings from the sub-scale Multidisciplinary Design Optimization (MDO) of the Truss-Braced Wing (TBW) aircraft configuration. As mentioned in Section 3.3.1 we aim to minimize the (Wing + Strut + Jury) Structural Mass and perform a trim analysis for different mission segments.

As mentioned previously, the wing loads are calculated and applied to a structural analysis module. Figures 4.1, 4.2, 4.3, 4.4, 4.5, 4.6, 4.7, and 4.8 show the physical thicknesses of the top and the bottom skin of the box beam after applying the plus 2.5g and minus 1g load cases for different wing-strut locations(from η=0.40 to η=0.80). As expected, the load cases size the top and bottom skin thicknesses differently with the plus 2.5g load case sizing the top skin and the minus 1g sizing the bottom skin, which is thinner at the top.

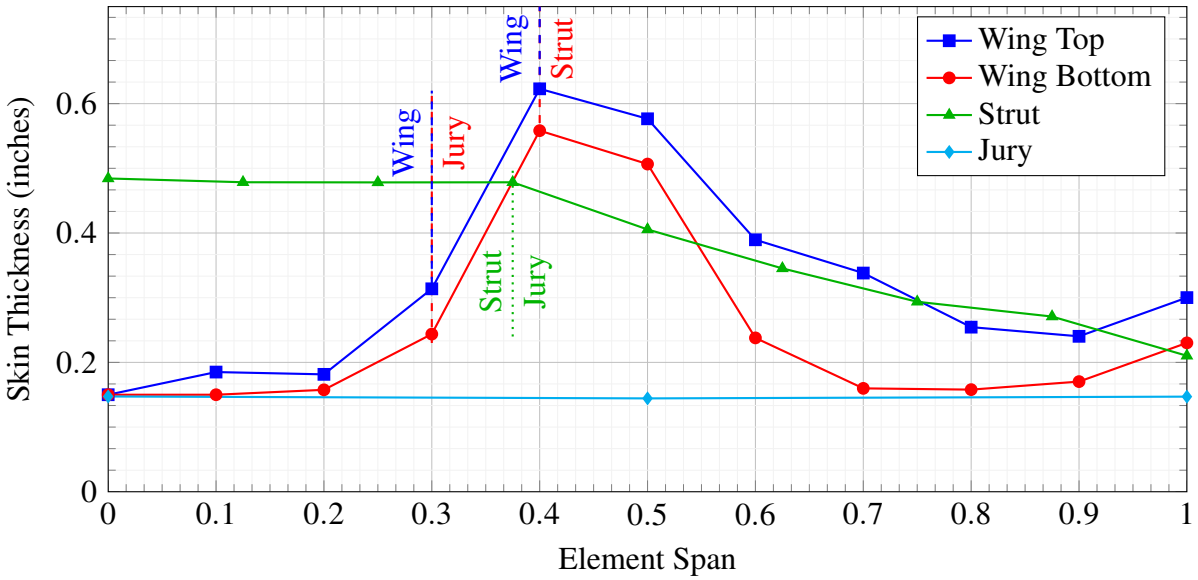

Figure 4.1. Sized Skin Thickness ($\eta = 0.40$).

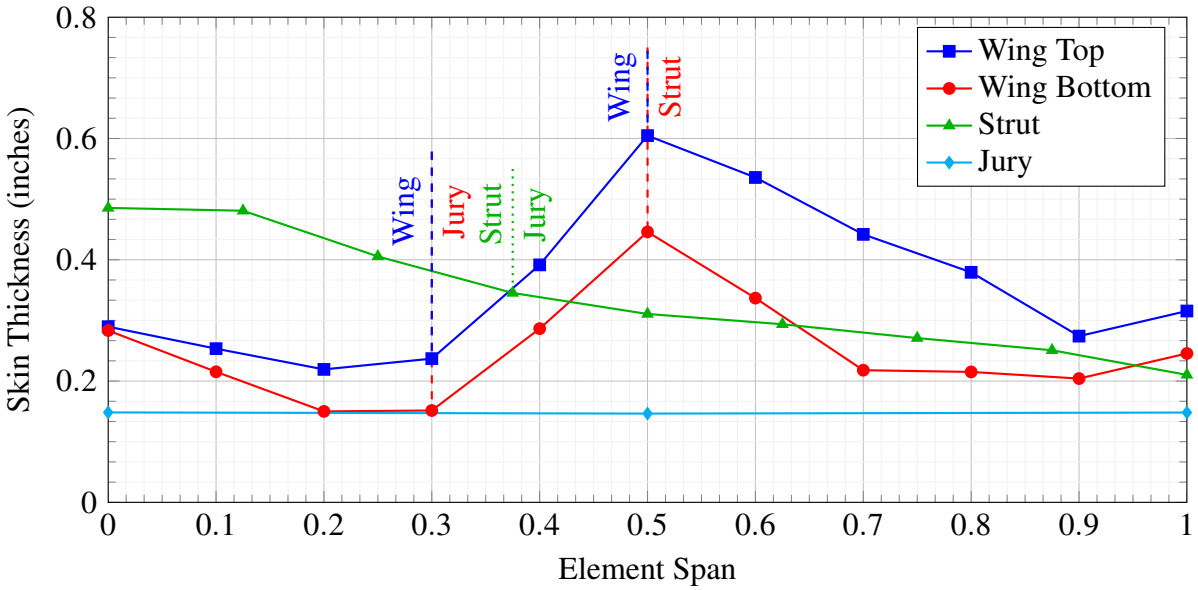

Figure 4.2. Sized Skin Thickness ($\eta = 0.45$).

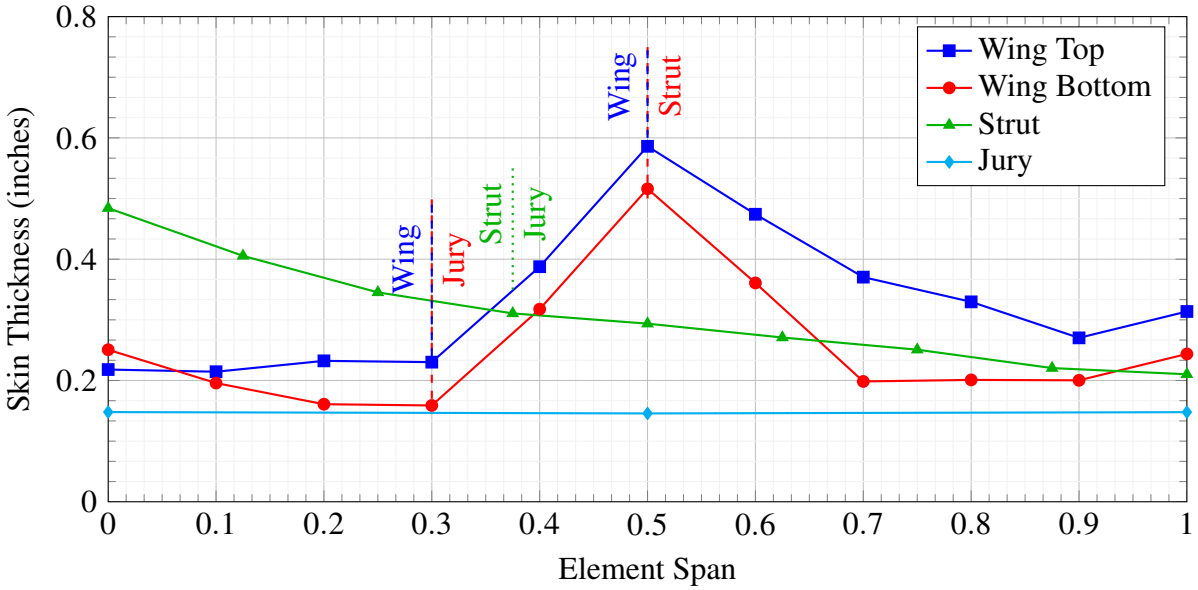

Figure 4.3. Sized Skin Thickness ($\eta = 0.51$).

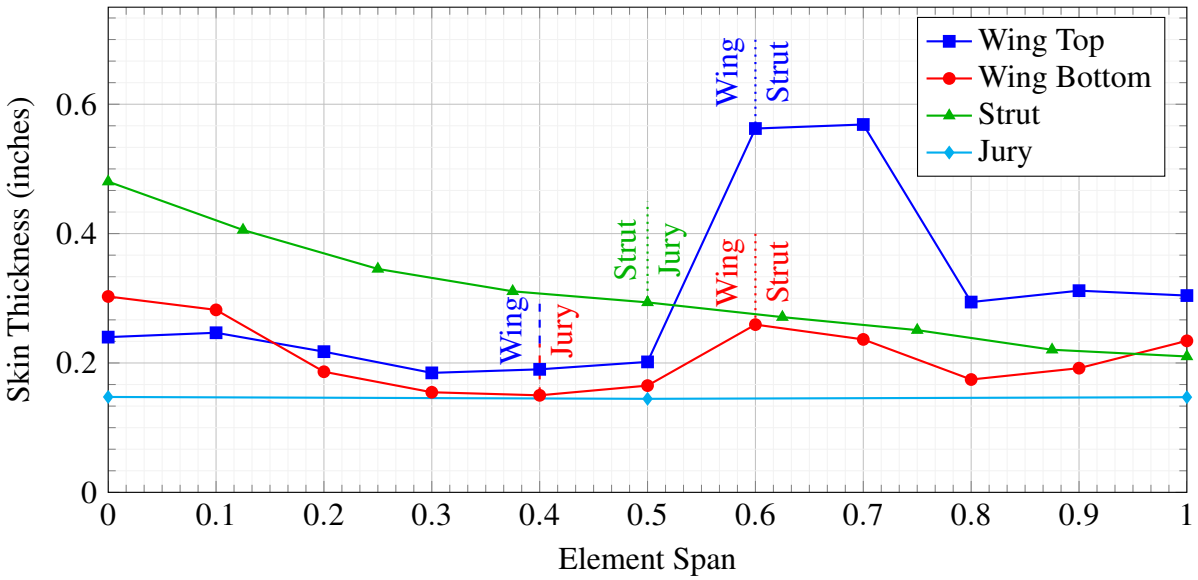

Figure 4.4. Sized Skin Thickness ($\eta = 0.57$).

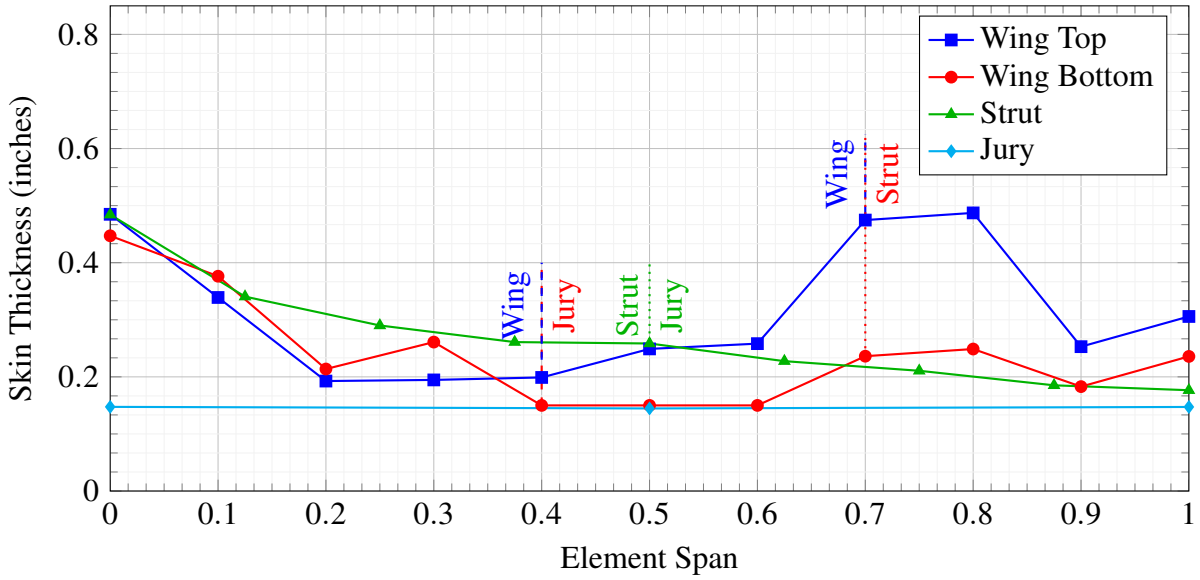

Figure 4.5. Sized Skin Thickness ($\eta = 0.63$).

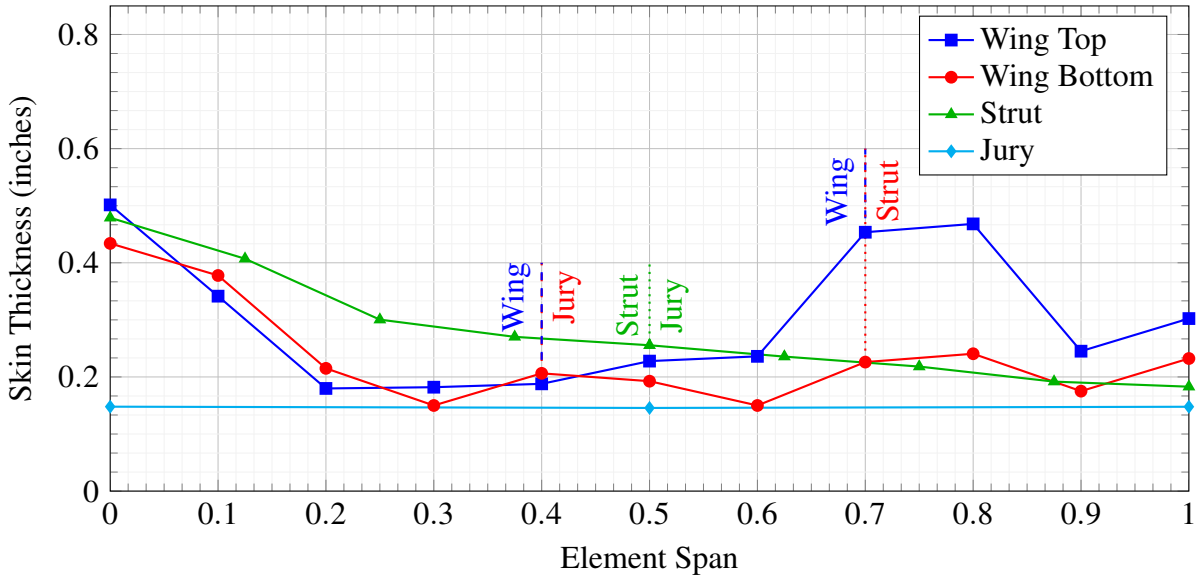

Figure 4.6. Sized Skin Thickness ($\eta = 0.69$).

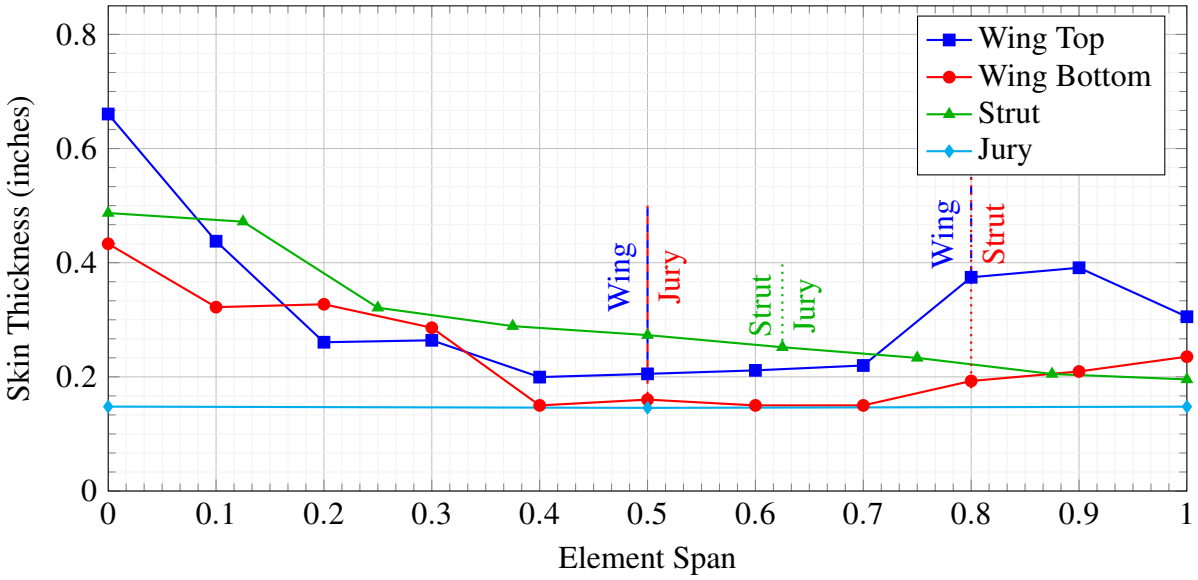

Figure 4.7. Sized Skin Thickness ($\eta = 0.76$).

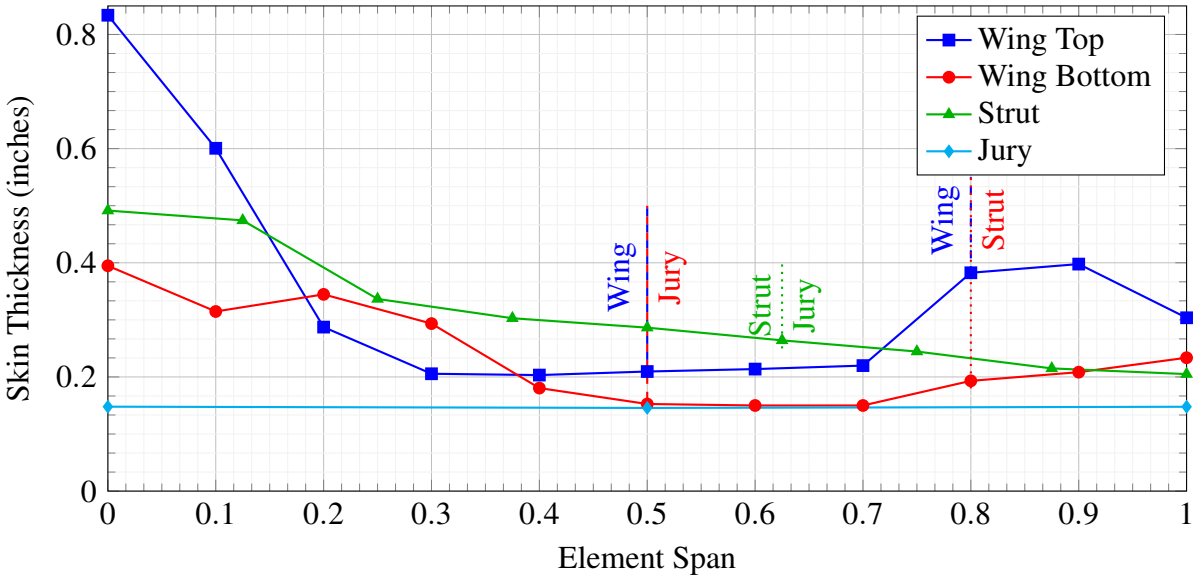

Figure 4.8. Sized Skin Thickness ($\eta = 0.80$).

We find that stress and buckling constraints are the sizing criterion and the displacement constraints are inactive. A trend is seen as detailed below:

The stress in the wing structure generally decreases as the strut is moved farther outboard (closer to the wing tip).

At Lower Values of η, when the strut is placed closer to the wing root (e.g., at 0.40 of the span), the wing experiences higher bending moments because the strut supports the wing at a point closer to the root, leaving a larger portion of the wing unsupported. This configuration increases the internal stresses, especially near the root and along the main wing structure, as the larger unsupported span from the strut to the tip results in higher bending loads on the wing itself.

As the strut moves farther outboard, the effective span of the wing that the strut supports increases. This reduces the bending moment at the root and along the wing, leading to a reduction in stress. The wing load is better distributed, as the support point from the strut reduces the distance over which the wing must carry loads, thereby reducing the bending stresses.

When the strut is placed near 0.70 - 0.80 of the span, the majority of the wing is supported by the strut. The bending moments decrease significantly, especially near the wing root, leading to a substantial reduction in stress. The outboard location of the strut effectively reduces the wing's deflection, further lowering internal stresses.

Similarly for buckling we see that the buckling behavior in a truss-braced wing is heavily influenced by the location of the wing strut, particularly due to changes in how the wing is supported and how loads are distributed along its span.

When the strut is positioned closer to the wing root (e.g., at 0.40), a larger portion of the wing is left unsupported toward the tip. This increases the likelihood of buckling, particularly in compression-dominated regions of the wing. The bending moments are higher toward the wing tip, which induces higher compression forces on the upper surface of the wing, making it more prone to local buckling in those areas. Additionally, the increased bending moments result in higher stresses near the root, which can also cause the web and cap to buckle.

Table 4.1. Sized (Wing + Strut + Jury) Mass after Sub-Scale MDO.

Wing-Strut Location	Sized Mass
0.4	8534.55
0.45	8335.92
0.51	8216.06
0.57	8024.3
0.63	8130.45
0.69	8268.79
0.76	8381.27
0.8	8463.47

As the strut moves farther outboard, the effective length of the unsupported wing section shortens. This reduces the risk of buckling in both local (panel or skin buckling) and global (overall wing flexure) modes. With the strut placed more outboard, the load is distributed more evenly, reducing the concentrated compressive forces that would otherwise promote buckling near the unsupported wing regions.

When the strut is located at higher values of η, the majority of the wing is supported, drastically reducing the compressive loads on the unsupported sections. The reduced length of the unsupported span decreases the likelihood of global buckling. The wing experiences less bending near the root, where structural buckling can be most critical. With the strut close to the tip, the upper wing surface experiences lower compressive forces, reducing the risk of buckling even further. The stress, displacement, nodal forces and spar thicknesses for different η can be found in Section A.1 to Chapter A.8

The general trend can be seen as follows:

- η = 0.40: Highest stress, larger bending moments on the wing. Highest buckling risk, large unsupported span leads to higher compressive forces.
- η = 0.50: Stress begins to decrease, improved load distribution. Buckling risk starts to reduce, supported span decreases. Further reduction in buckling risk as load distribution improves.

- η = 0.60: Noticeable reduction in stress as the strut location optimizes load support. Further reduction in buckling risk as load distribution improves.
- η = 0.70: Low stress, bending moments reduced significantly. Low buckling risk, much of the wing is supported by the strut.
- η = 0.80: Lowest stress, strut optimally supports the wing, minimizing bending. Lowest buckling risk, minimal compressive forces, most of the wing is supported.

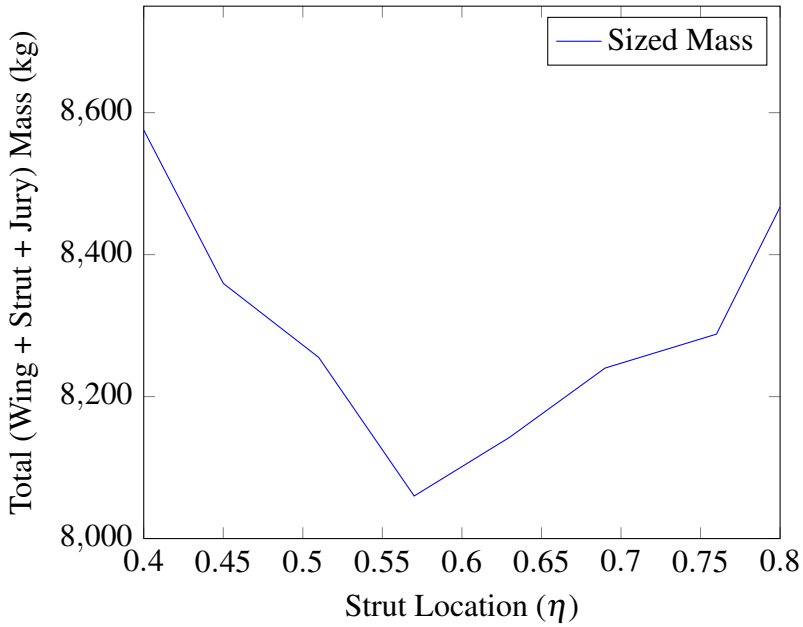

Figure 4.9. Change of structural weight for total sizing when the strut location (η) is varied on the baseline configuration.

When comparing the (Wing + Strut + Jury) box mass for the initial wing geometry for all configurations (i,e before the full-scale optimization) the combined box mass for various wing-strut configurations is shown in Table 4.1 and Figure 4.9 displays these results in a graphical format.

From the results, we see that the sweet-spot for the wing-strut location is η=0.57 which has the lowest mass after sizing. Coincidentally this is the wing-strut location utilized by Boeing and NASA in their various reports. We then perform a trim analysis for various mission segments.

Table 4.2. Trim during Cruise, Climb and Descent for $\eta = 0.57$

Parameter	1g	2.5g	-1g	Climb	Descent
Pitch (deg)	1.08	4.2	-3.26	-0.69	-7.48
Tail deflection (deg)	-0.22	-2.57	3.45	-5.13	-5.9
Throttle setting (%)	63.42	94.78	68.34	83.66	10
L/D	27	-	-	19.25	21.54
Flight Path Angle	-	-	-	4.5	-2.2

Figure 4.10 shows which load conditions sized each node and illustrates which nodes are sized by buckling and strength. The graph shows skin thickness vs wing span and we see that at almost $\eta = 0.6$, the wing and strut coincide.

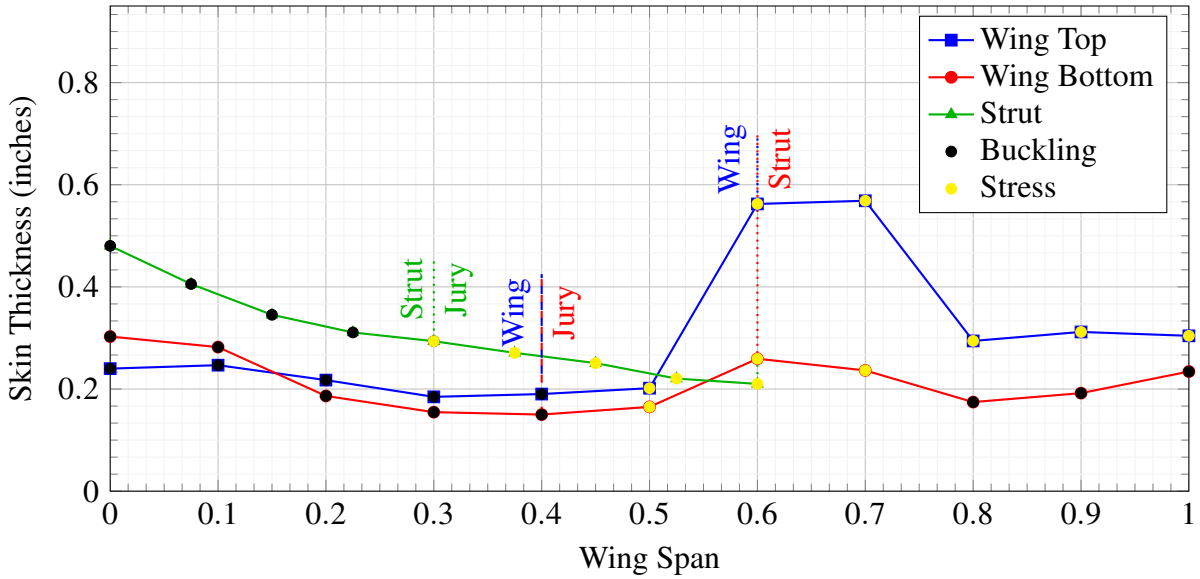

Figure 4.10. Sizing Skin Load Cases.

Table 4.2 details the various results from the trim analysis. The results we notice seem reasonable enough given that a higher aspect wing ration should have a L/D ratio around 27 and should have a higher throttle setting during climb and the least during descent.

In addition to this, the tail deflection during a 2.5g maneuver should be negative because the aircraft is experiencing an upward acceleration of 2.5 times the force of gravity, which means the aircraft is pulling up into a steep climb or turning maneuver. In that situation, the center of gravity (CG) of the aircraft is ahead of the center of lift, causing a nose-down pitching moment.

To counteract this, the horizontal tailplane needs to generate a downward force (negative lift) to balance the pitching moment and maintain controlled flight. This downward force stabilizes the aircraft by creating a moment that opposes the nose-down tendency. Negative tail force is typical in most conventional aircraft configurations during positive-g maneuvers. The larger the load factor (e.g., 2.5g), the more negative force the tail generates to balance the increased lift from the wings and maintain stability.

The pitch angle is negative for a -1g maneuver also seems resonable because the aircraft is experiencing a downward acceleration equivalent to the force of gravity but in the opposite direction (upside down or diving). To achieve this condition, the aircraft must pitch downward, which requires a negative pitch angle. A negative pitch angle implies that the nose of the aircraft is lower than the tail. This is necessary to balance the forces during the maneuver, as the aircraft needs to align its lift vector to provide the required downward acceleration to sustain a -1g load. A negative pitch angle ensures the aircraft can maintain controlled flight during negative-g maneuvers by adjusting the orientation of the wings relative to the airflow, keeping the aircraft in equilibrium.

4.2 Full-Scale MDO

Based on the results obtained in Section 4.1, we present the results of the full-scale optimization (minimum fuel burn across various mission segments) problem we solve. As mentioned in the previous sections the results we got above helped us get a reasonable starting point for the optimization for our full-scale optimization.

The mission fuel analysis for climb, cruise and takeoff is heavily dominated by the cruise fuel burn. As a result the goal of minimizing gross weight while maximizing aerodynamic efficiency to minimize fuel burn can be tackled using the Breguet Range Equation 3.28.

The results in Section 4.1 aid in getting a better understanding of a a detailed breakdown of the aircraft component weights before and after the optimization, and is shown in Figure 4.11.

The optimized gross weight is about 21550.41 kg which is a decrease of a about 8% and the majority of this reduction can be attributed to the wing and strut reduction which is about 1200 kg(5.5%).

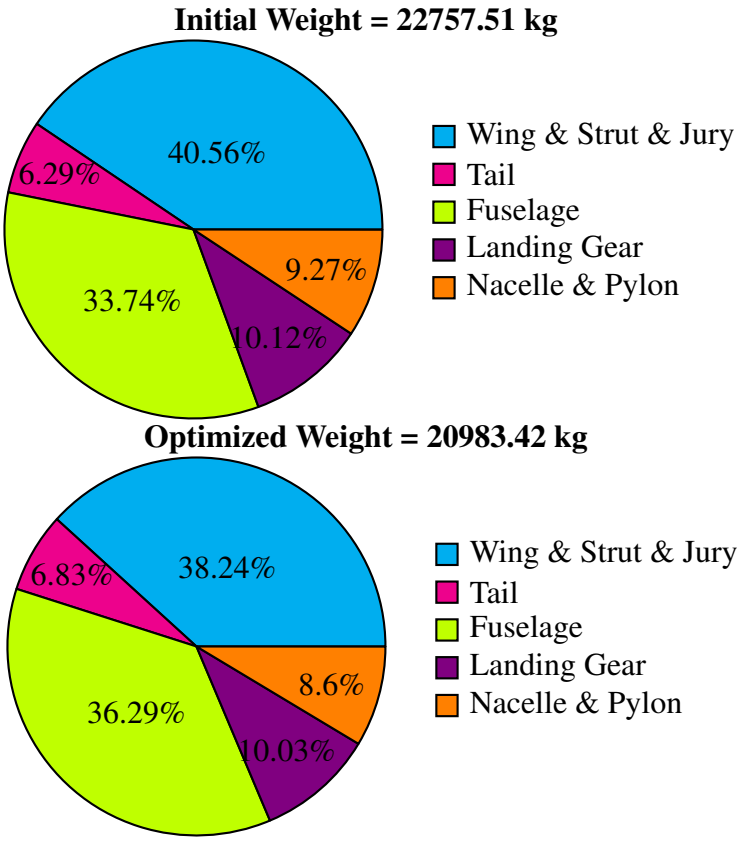

Figure 4.11. Weight Breakdown before & after Optimization (η = 0.57).

To demonstrate the optimized design's feasibility, we show multiple optimization constraints as a function of the optimization iteration in Figure 4.12. One of the key constraints is that the aircraft has to be trimmed for every steady design condition. To this end, we show the aircraft trim residual as a function of the optimization iteration for all steady design conditions. We observe a decrease of several orders of magnitude for all design conditions as the optimization progresses. Since the trim residual is a representation of the aircraft's linear and angular accelerations, we conclude that for steady design conditions, the optimized aircraft experiences net forces and moments on the order of a few Newton (meter), which demonstrates that the

Table 4.3. Summary of High-Level Design Variable Changes

Parameter	Initial	Optimized
Wing Span (ft)	170	177.05
Wing Root Chord (ft)	10.8	10.7
Wing Mid Chord (ft)	9.5	9.37
Wing Tip Chord (ft)	3.8	3.37
Wing Twist (deg)	0	-0.36
Wing Aspect Ratio	24	26.8
Wing Sweep (deg)	11.5	14.86

aircraft is trimmed.

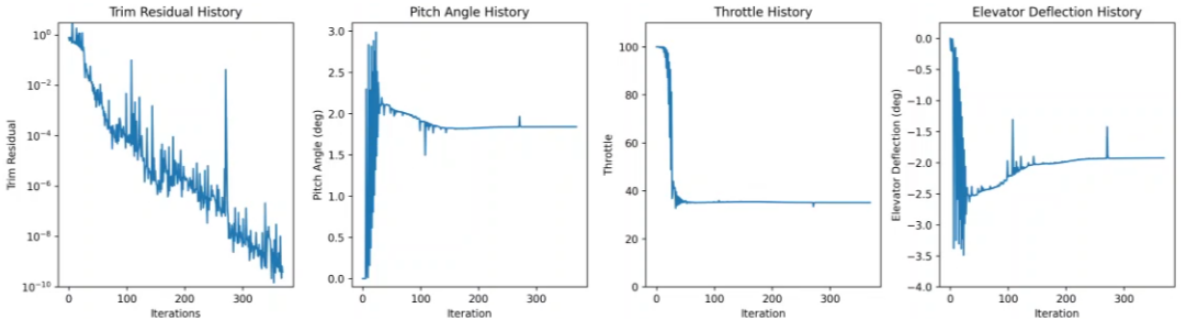

Figure 4.12. Trim vs Operation Iteration Limit.

We summarize the high-level design variables before and after optimization in Table 4.3. We note that for the wing tip chord, the optimizer reached the lower bounds set for those variables, suggesting that the vehicle gross weight could potentially be reduced further by relaxing those bounds due to a decrease in wing area, but those changes would have been very minute if so. Figure 4.13 shows Table 4.3's values.

Additionally, the wing span was increased from 170 ft to 177.05 ft, indicating that the optimization favored a longer span to improve aerodynamic efficiency by reducing induced drag. This longer span is typically associated with higher lift-to-drag ratios, which enhances fuel efficiency, especially in long-range applications. The wing root chord experienced a slight reduction from 10.8 ft to 10.7 ft, reflecting a minor refinement in the planform, likely aimed at improving aerodynamic performance without significantly altering the root's lift generation.

Additionally, both the wing mid chord and wing tip chord were reduced, with the mid

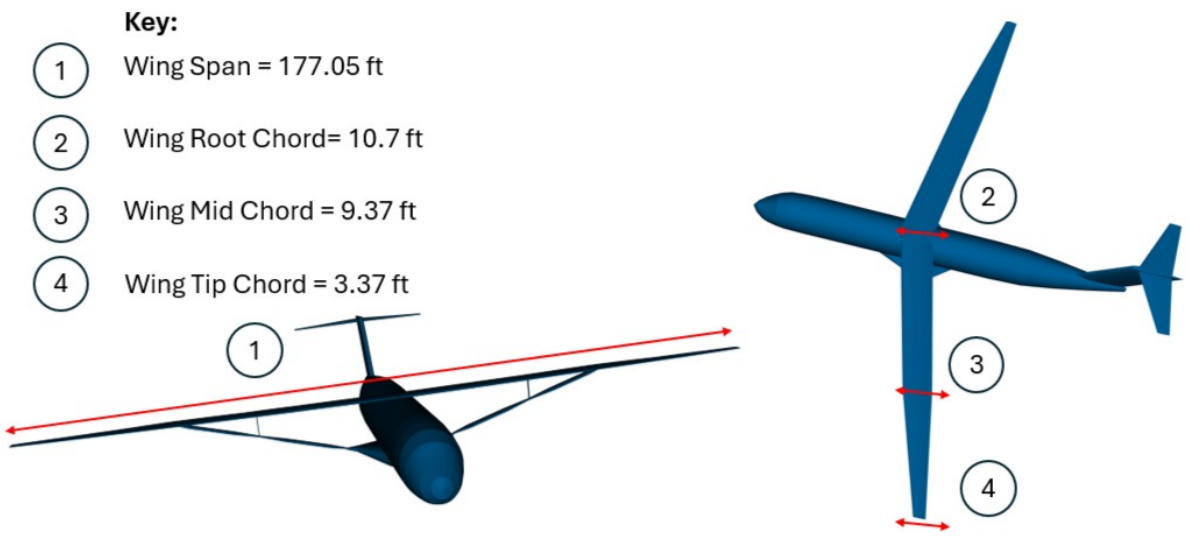

Figure 4.13. Geometric Design Variables.

chord shrinking from 9.5 ft to 9.37 ft and the tip chord decreasing from 3.8 ft to 3.37 ft. This reduction in the tip chord suggests a more tapered wing, which is effective in reducing tip drag and further enhancing aerodynamic performance. The optimized wing also introduces a negative twist of -0.36 degrees, compared to the initial 0 degrees, which helps prevent tip stall and distributes lift more efficiently along the span. This twist, contributes to better stability and performance.

The aspect ratio increased from 24 to 26.8, which seems reasonable given a higher aspect ratio generally improves aerodynamic efficiency However, this reduction likely represents a structural compromise to manage the increased stresses associated with the longer span. Finally, the wing sweep was increased from 11.5 degrees to 14.86 degrees, improving performance at higher speeds by delaying shockwave formation and reducing drag in the transonic flight regime. Overall, these design changes reflect a balance between aerodynamic efficiency, structural integrity, and performance at higher speeds.

With the sizing and geometrical changes, we now look at the effect these changes have on the fuel burn during cruise, climb and descent.

Table 4.4 summarizes the climb results which we get from the optimization. The throttle

Table 4.4. Summary of Climb Results for η = 0.57

Parameter	Value
Pitch (deg)	-0.69
Tail deflection (deg)	-5.13
Throttle setting (%)	83.66
Max Thrust(kg)	85594.56
Fuel (kg)	878.27
T/W	0.062
W/S(N/sq.m)	481.84
L/D	19.25
Climb Flight Path Angle (deg)	4.5
Time to Climb (minutes)	12.3
Distance to Climb (nm)	100.86

setting is set to maximum during the climb as it requires more propulsion during climb. The time and distance to climb is less than the 30 minutes and 200 nautical miles respectively, which formed our key constraints for this optimization problem.

The climb analysis results with an efficiency factor of 0.57 provide key insights into the aircraft's performance. The pitch angle during the climb is -0.69 degrees, indicating a slightly nose-down attitude, possibly due to the high lift generated by the wing design. The tail deflection is -5.13 degrees, which helps maintain stability during this phase. The throttle setting is at 83.66%, meaning the engine was not operating at full capacity, likely for efficiency or operational limits.

The maximum thrust generated during the climb is 85,594.56 kg, with 878.27 kg of fuel consumed. The aircraft's thrust-to-weight ratio (T/W) is 0.062, and the wing loading (W/S) is 481.84 N/m², both reflecting typical climb performance characteristics. The lift-to-drag ratio (L/D) is 19.25, indicating efficient aerodynamic performance. The climb flight path angle is 4.5 degrees, and the time to climb to the desired altitude is 12.3 minutes, covering a distance of 100.86 nautical miles.

The cruise analysis results for an efficiency factor of 0.57 show several important performance characteristics. The pitch angle during cruise is 1.08 degrees, indicating a slightly

Table 4.5. Summary of Cruise results for η = 0.57

Parameter	Cruise
Pitch (deg)	1.08
Tail deflection (deg)	-0.22
Throttle setting (%)	63.42
Taper Ratio	0.89/0.39
Aspect Ratio	21.25
Wing Sweep (deg)	14.86
Max Thrust(kg)	26761.66
Wing + Strut + Jury Weight (kg)	8024.3
Fuel (kg)	8672.2
T/W	0.043
W/S(N/sq.m)	367.79
L/D	27.45

nose-up attitude typical for steady-level flight. The tail deflection is minimal at -0.22 degrees, suggesting that only a small adjustment is needed for stability. The throttle setting is at 63.42%, reflecting moderate engine power usage during cruise.

The wing's taper ratio, varying from 0.89 to 0.39, and the aspect ratio of 21.25, highlight the wing's slender and efficient design, aiding in improved aerodynamic performance. The wing sweep is 14.86 degrees, which balances high-speed flight with stability. Maximum thrust during cruise is 26,761.66 kg, and the combined weight of the wing, strut, and jury is 8,024.3 kg.

Fuel consumption is measured at 8,672.2 kg, while the thrust-to-weight ratio (T/W) is 0.043, indicating moderate engine thrust relative to the aircraft's weight during cruise. The wing loading (W/S) is 367.79 N/m², and the lift-to-drag ratio (L/D) is 27.45, demonstrating the aircraft's high aerodynamic efficiency during this flight phase.

In the descent phase with an efficiency factor of 0.57, the lift-to-drag ratio (L/D) is 21.54, reflecting a good aerodynamic performance that helps maintain a smooth and controlled descent. A high L/D ratio during descent is crucial for reducing drag, which minimizes the need for excess power while still sustaining lift, allowing the aircraft to glide effectively.

The throttle setting during descent is very low at only 5%, meaning the engines are

Table 4.6. Summary of Descent Results for η = 0.57

Parameter	Descent
Pitch (deg)	-7.48
Tail deflection (deg)	-5.9
Throttle setting (%)	5
Max Thrust(kg)	5115.65
Fuel (kg)	322.48
L/D	21.54
Descent Flight Path Angle (deg)	-2.2
Time to Descent (minutes)	25.2

operating at a much lower power output compared to other phases of flight. This reduced throttle setting contributes to fuel efficiency, as demonstrated by the low fuel consumption of 322.48 kg during descent. The aircraft's pitch angle is -7.48 degrees, and the tail deflection is -5.9 degrees, providing stability in the descent path, which follows a flight path angle of -2.2 degrees.

As mentioned previously, Constraint analysis is essentially a way to look at aircraft weight, wing area, and engine thrust for various phases of flight and come to a decision about meaningful starting values of all three parameters for a given set of design objectives. Figure 4.14 does this by looking at two important ratios, the thrust-to-weight ratio (T/W), the wing loading or ratio of weight-to-planform area (W/S).

In Figure 4.14 the space above the climb and takeoff curves and to the left of the landing line is our acceptable design space. Any combination of W/S and T/W within that space will meet our design goals. What we want, however, is the "best" combination of these parameters for our design goals. The optimum will be found at the intersections of these curves. Figure 4.15 shows this intersection.

We see that there are two cases that can be used based on what the design goal is. By "optimum" we mean that we are looking for the minimum thrust-to-weight ratio that will enable the airplane to meet its performance goals and we would like to have the highest possible wing loading. The desire for minimum thrust is obvious, based on the need to minimize fuel

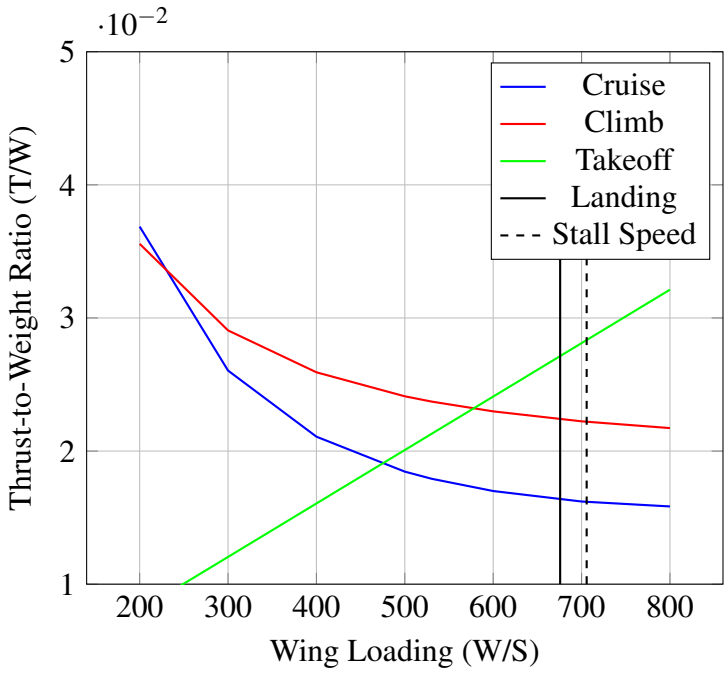

Figure 4.14. Constraint Analysis for $\eta = 0.57$.

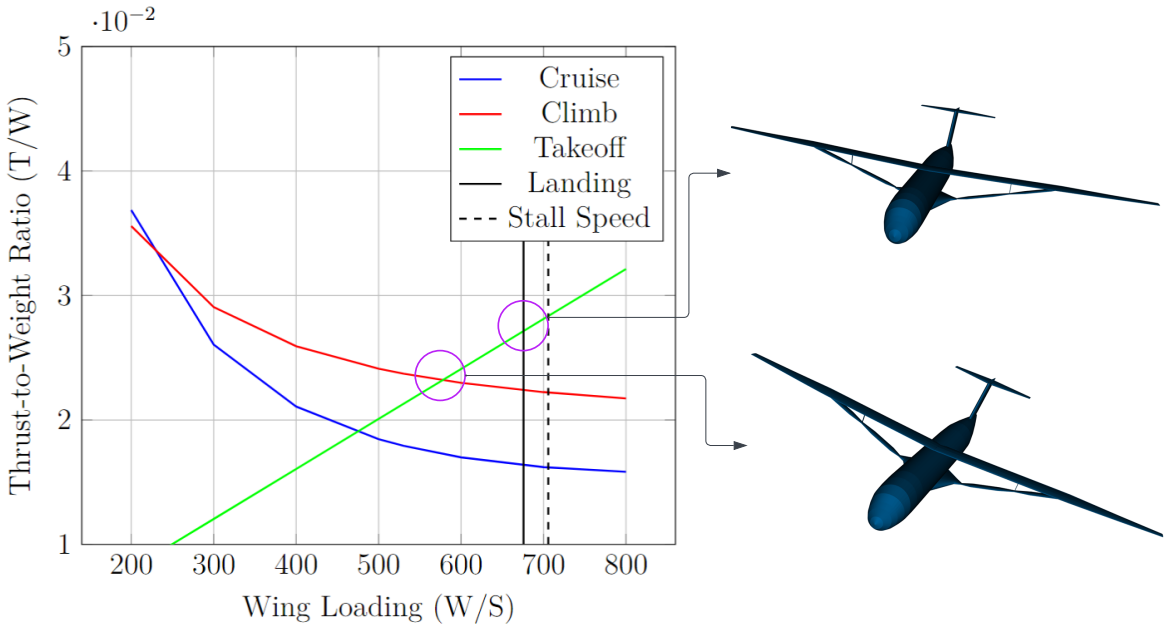

Figure 4.15. Constraint Analysis for $\eta = 0.57$ showing the optimum points.

consumption and engine cost. The goal of maximum wing loading may not be as obvious to the novice designer but this means the wing area is kept to a minimum which gives lower drag. It

also gives a better “ride” to the airplane passengers. As wing loading increases the effects of turbulence and gusts in flight are minimized, smoothing out the “bumps” in flight.

Figure 4.16 compares the fuel burnt across each mission segment, established from the data we get from each of the above tables. The sized group weights statement is shown in Table 4.7.

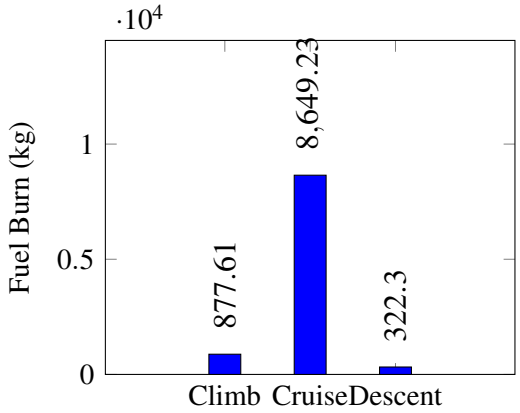

Figure 4.16. Fuel Burnt (kg) for Cruise, Climb, and Descent.

Table 4.7. Sized Group Weights

Group	**Initial**	**Optimized**
Wing + Strut + Jury	9262.35	8024.3
Tail	1433.35	1433.35
Fuselage	7679.31	7615.81
Landing Gear	2304.25	2104.67
Nacelle & Pylon	2109.20	1805.3
1. Engines	*5488.46*	*3093.5*
2. Fuel System	*752.96*	*698.53*
Propulsion (1. + 2.)	6241.43	3792.03
Flight Controls	1202.02	1034.19
I.Auxiliary Power Unit	*458.13*	*458.13*
II.Hydraulics	*344.73*	*290.3*
III.Electrical	*1043.26*	*1043.26*
Power Systems (I + II + III)	1846.12	1791.69
Instruments	349.27	349.27
Avionics & Autopilot	680.39	680.39
Furnishing & Equipment	4136.76	4136.76
Air Conditioning	653.17	653.17
Anti-Icing	54.43	45.36
Manufacturer's empty weight	**37952.04**	**33466.28**
1. Operational Items	3270.40	3270.4
Operational Empty Weight	**41222.44**	**36736.67**
1. Usable Fuel	12836.65	11702.67
2. Design Payload	13970.63	13970.63
Total Weight	**68038.8**	**62409.98**

This chapter, in full, is currently being prepared for submission for publication of the material. Darshan Sarojini, and John T.Hwang. The thesis author was the primary investigator and author of this material.

Chapter 5

Conclusion

In this thesis, we demonstrate the application of large-scale Multidisciplinary Design Optimization (MDO) to the the Truss-Braced Wing (TBW) configuration.

This thesis presents two key contributions to the conceptual design of the truss-braced wing (TBW) configuration. The first contribution investigates the impact of wing-strut location on the TBW, utilizing physics-based solvers to determine the optimal wing-strut placement. By systematically analyzing various configurations, this research identifies an optimal strut placement based on structural sizing, with a focus on minimizing wing, strut, and jury mass while maintaining aerodynamic efficiency. The second contribution applies novel optimization methodologies to minimize fuel consumption across different mission phases—climb, cruise, and descent—while addressing structural and constraint analyses. Through sub-scale optimization followed by full-scale optimization, this research identifies the optimal wing-strut location and performs a comprehensive trim analysis. To the author's knowledge, this methodology, which involves two sub-scale optimization problems and one full-scale optimization, represents a novel approach in the study of TBW configurations. The application of large-scale multidisciplinary design optimization (MDO) techniques, combined with gradient-based approaches, allows for rapid exploration of the design space, ensuring robust performance across both nominal and off-nominal mission segments. These contributions demonstrate the feasibility and effectiveness of applying large-scale MDO to conceptual aircraft design.

To solve the sub-scale MDO problems, a cruise condition was set up for the Truss-Braced Wing (TBW) configuration where the designated cruising altitude is set at 13,106.4 meters (43,000 feet), and the payload weight is specified as 13,970.645 kilograms (30,800 pounds), inclusive of 12 first-class and 142 economy-class seats. These parameters are considered constant in governing the cruise condition. The physics based models that were used to analyze the sub-scale MDO problems are detailed. A vortex-lattice model for steady-state aerodynamics, incorporating transonic and viscous flow corrections was developed. Addressing the intricate flow interactions near the strut attachment to the wing, a correction method based on the high-fidelity Computational Fluid Dynamics (CFD) solver FUN3D, as developed by Nguyen [31], was implemented in CADDEE and applied to the aerodynamic solver. A linear propulsion solver is used for this analysis and the structural solver is based on linear Euler-Bernoulli beam theory, with box cross-section assumptions. The 6 Degrees of Freedom (DoF) Euler flat-Earth equations of motion calculate geometric deformation under aerodynamic, inertial and propulsion forces. The constraints were trimmed at +1g, and at -1g, and 2.5g according to the 14CFR Part 25-Code of federal regulations. The first sub-scale MDO problem gave a wing-strut location of 57% of the wing's span to be the optimal solution and using the above mentioned physics based models a trim analysis for this configuration for different mission segments was performed.

Using the information from the sub-scale optimization, mission and constraint analysis namely for climb, cruise and descent is performed for the optimal TBW configuration. In addition to this, the geometric variables of the OML, and structural thickness variables are design variables for the optimization problem. Results show a gross weight reduction of about 8% over the initial design, and a reduction of fuel by about 9% with all major constraints (e.g., aircraft trim, constraint analysis) being satisfied.

To perform all the above mentioned analyses and optimization an integrative computational wrapper was used, seamlessly coupling low-fidelity aero-structural models, weight models, performance models, and propulsion models with the TBW structure to overcome existing decoupling challenges for the TBW configuration. Concurrently, the Outer Mold Line (OML)

was parameterized using Free-Form Deformation (FFD) blocks to allow for refinement, targeting interconnected components such as the wing, strut, and jury to enhance accuracy and versatility in aerodynamic design. Gradient-based optimization techniques were applied, focusing on both nominal and off-nominal mission segments. These results demonstrate the feasibility of applying large-scale MDO to the aircraft conceptual design problem to efficiently explore the design space, using physics-based models in combination with gradient-based optimization.

Chapter 6

Future Works

We identify multiple directions for future work for this topic. When exploring the wing-strut interference effect we would have to use higher fidelity modeling to fully understand this effect. In future iterations higher fidelity like Computational Fluid Dynamics (CFD) can be used to capture these effects. Furthermore, a linear Euler model is used for the Truss-Braced Wing (TBW) but there are many non-linear structures in the Truss-Braced Wing (TBW). Studying these wing-strut interference effects is crucial to understand the optimal wing-strut location of which preliminary analyses were conducted and some of the results are shown in Appendix B.

This thesis explores a one-way coupling scheme between the aerodynamic solver and the structural solver. The effects of adding two-way coupling to this problem, including both work-conservative and non-conservative force-displacement transfer is explored by van Schie et al [120]. A similar two-way coupling can be implemented for this problem and is being worked up on the next iteration of CADDEE.

There are also areas of improvement pertaining to raising the modeling fidelity of the aircraft sub-disciplines. For example, we plan to use the Reissner–Mindlin shell theory to more accurately model the wing structure. Lastly, we would like to further expand the scope of design conditions that we consider to also include fully dynamic cases such as a gust response or wing flutter which is key for the Truss-Braced Wing (TBW) configuration.

Appendix A

Sub-Scale MDO

A.1 η = 0.40

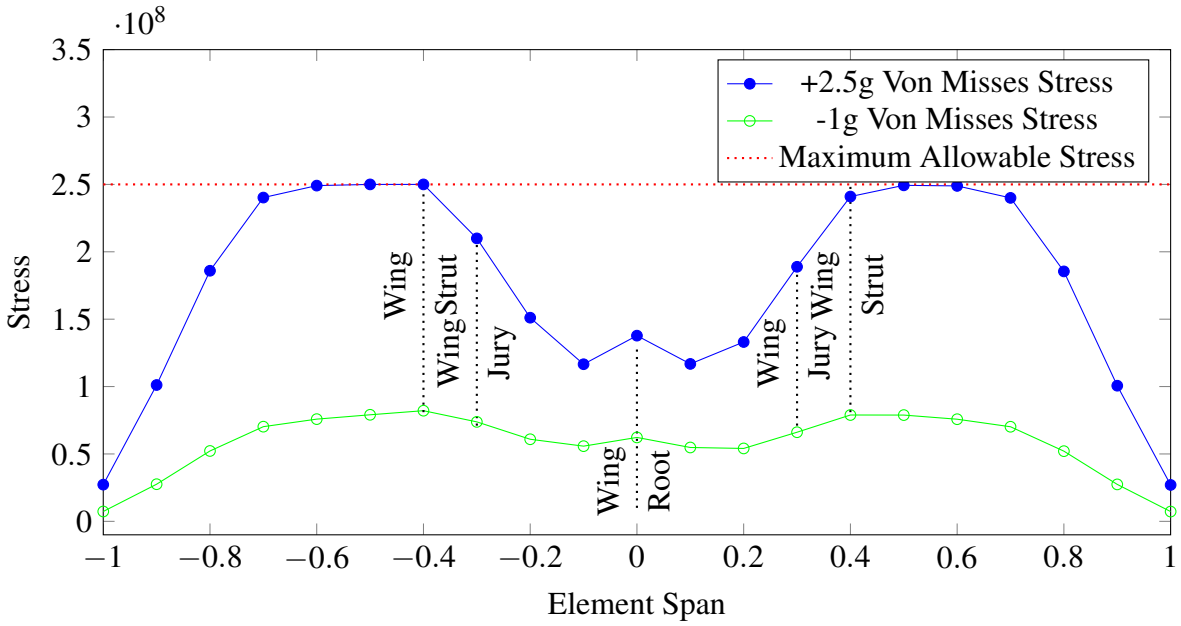

Figure A.1. Stress vs Element Span for η = 0.40.

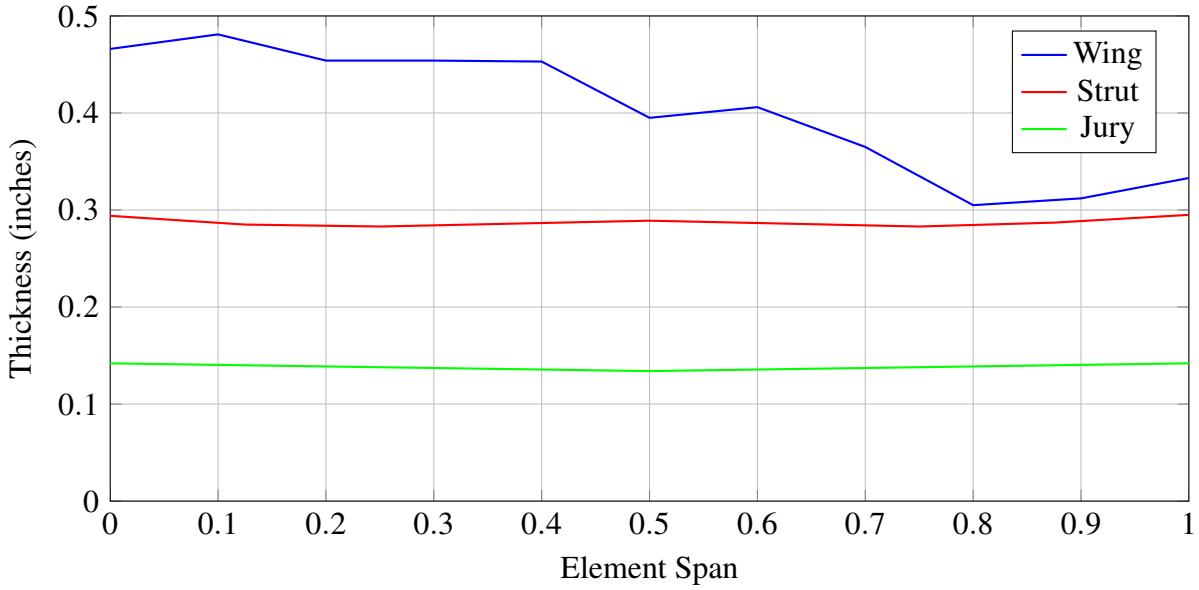

Figure A.2. Sized Spar Thickness ($\eta = 0.40$).

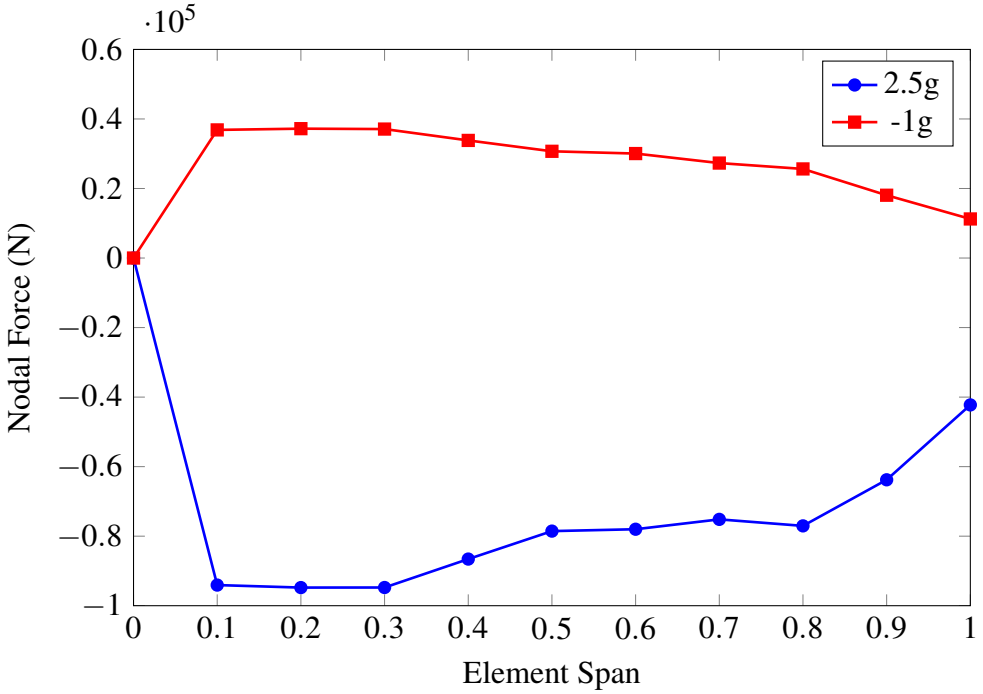

Figure A.3. Nodal Forces ($\eta = 0.40$).

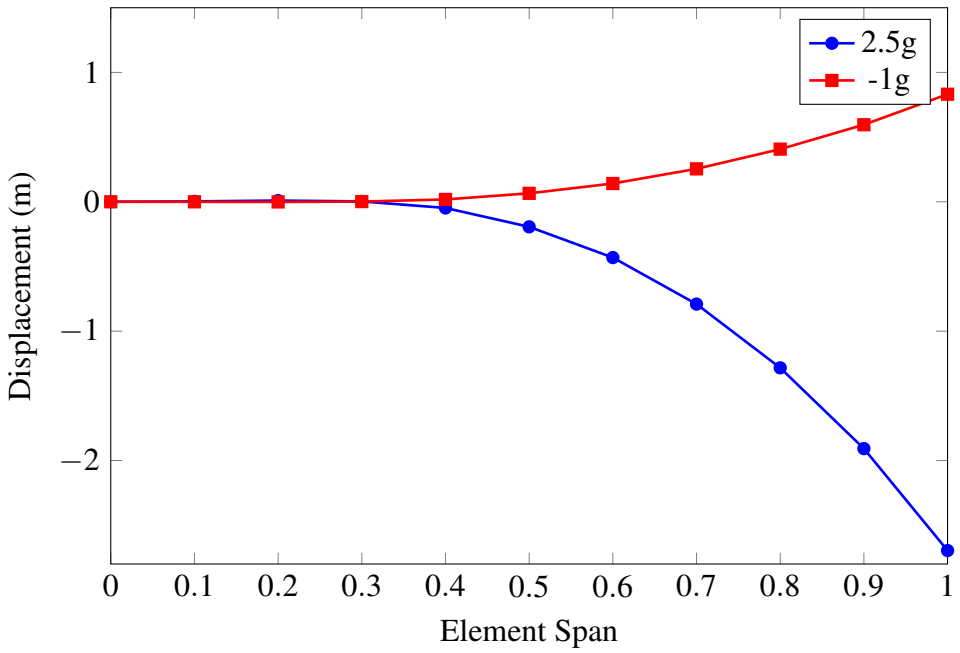

Figure A.4. Displacements ($\eta = 0.40$).

A.2 $\eta = 0.45$

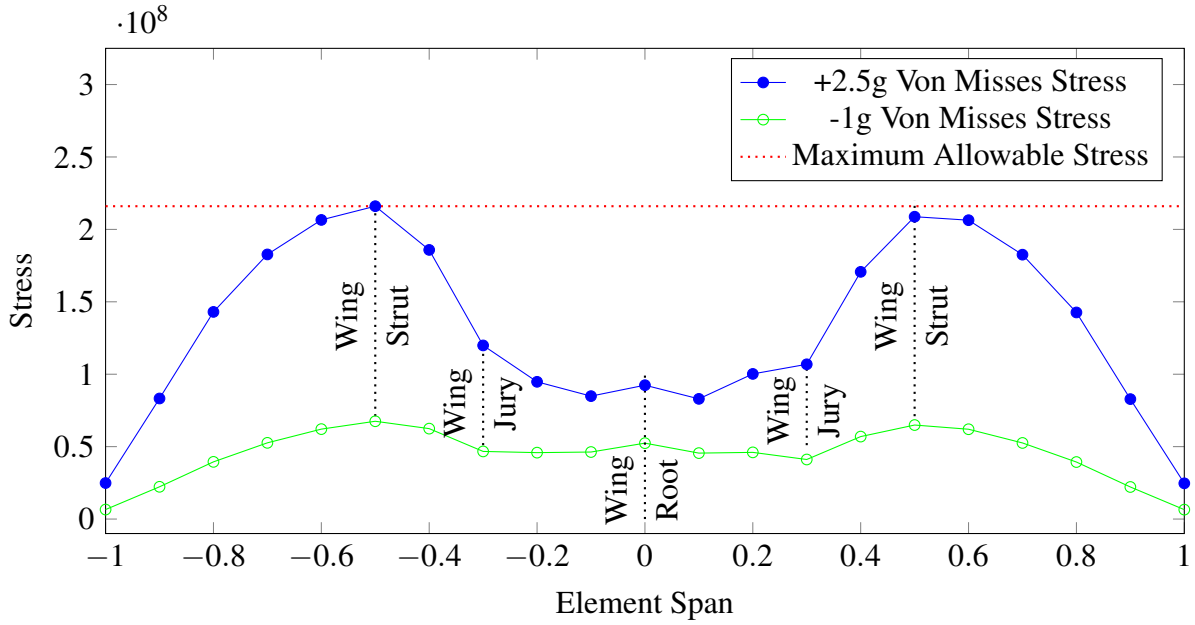

Figure A.5. Stress vs Element Span for $\eta = 0.45$.

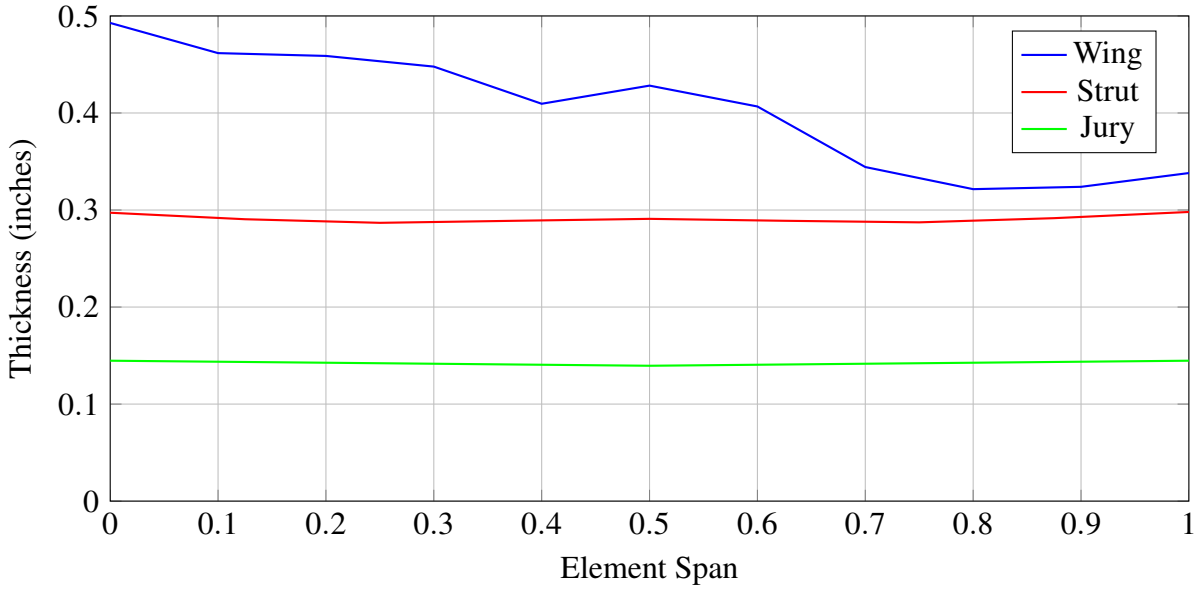

Figure A.6. Sized Spar Thickness ($\eta = 0.45$).

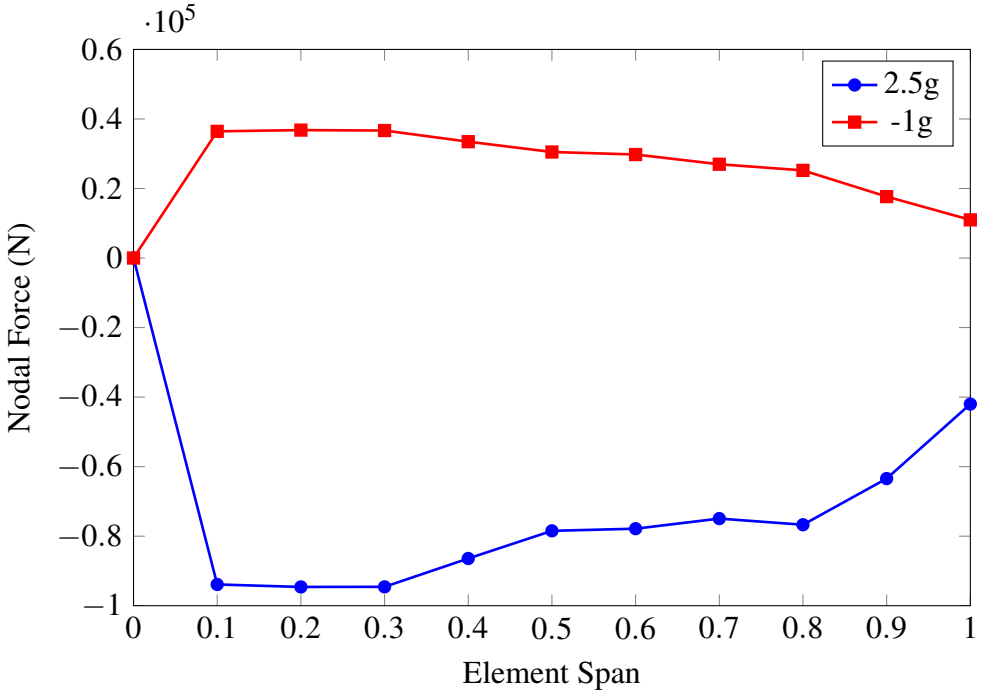

Figure A.7. Nodal Forces ($\eta = 0.45$).

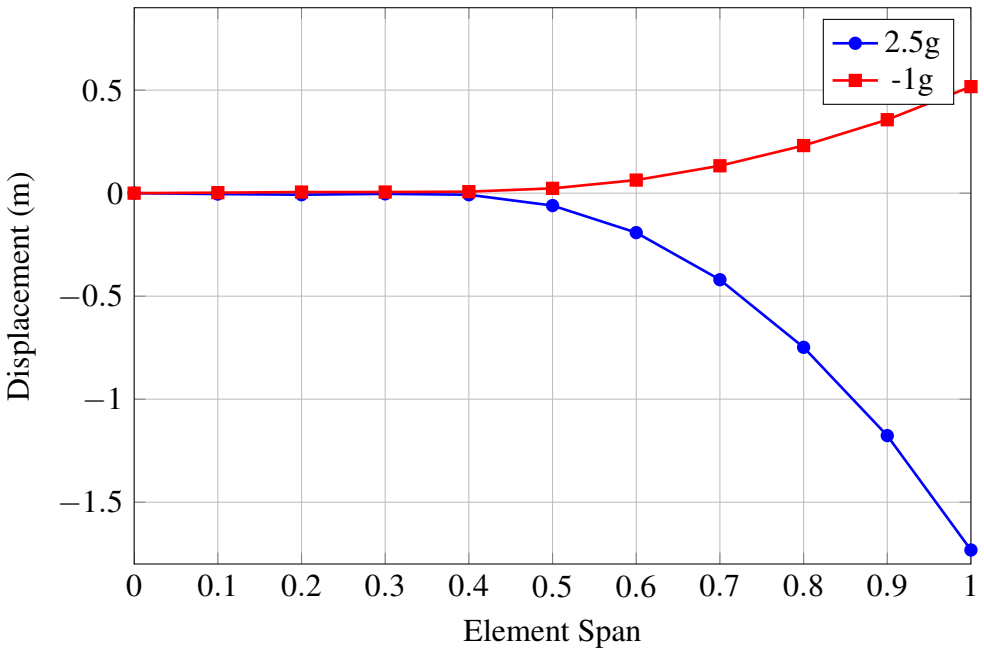

Figure A.8. Displacements ($\eta = 0.45$).

A.3 $\eta = 0.51$

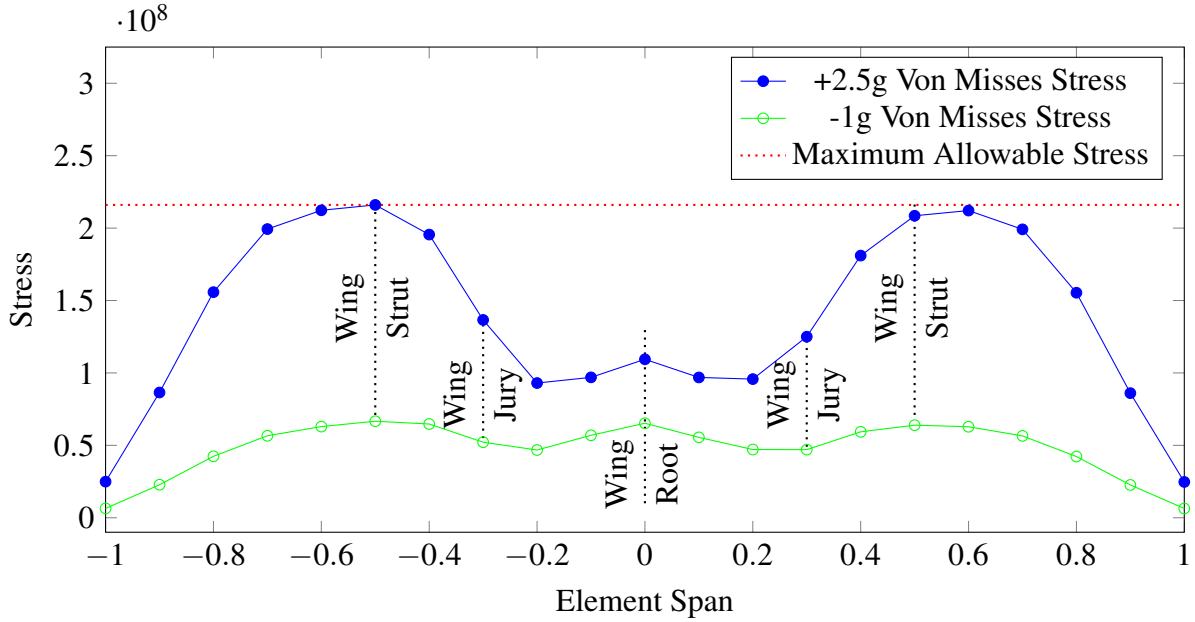

Figure A.9. Stress vs Element Span for $\eta = 0.51$

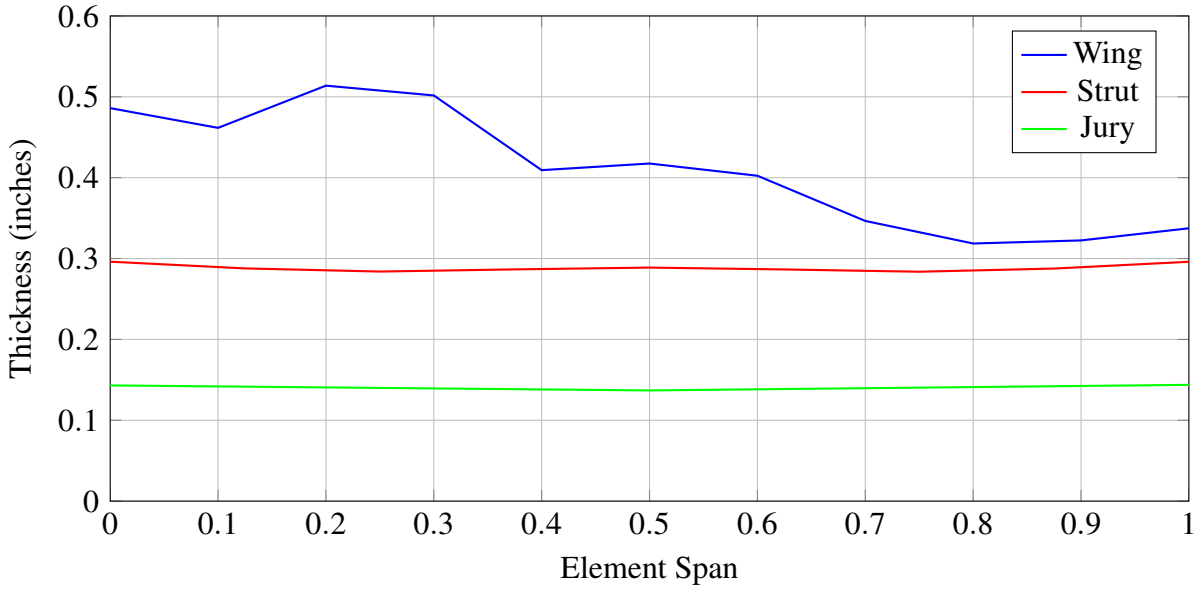

Figure A.10. Sized Spar Thickness ($\eta = 0.51$)

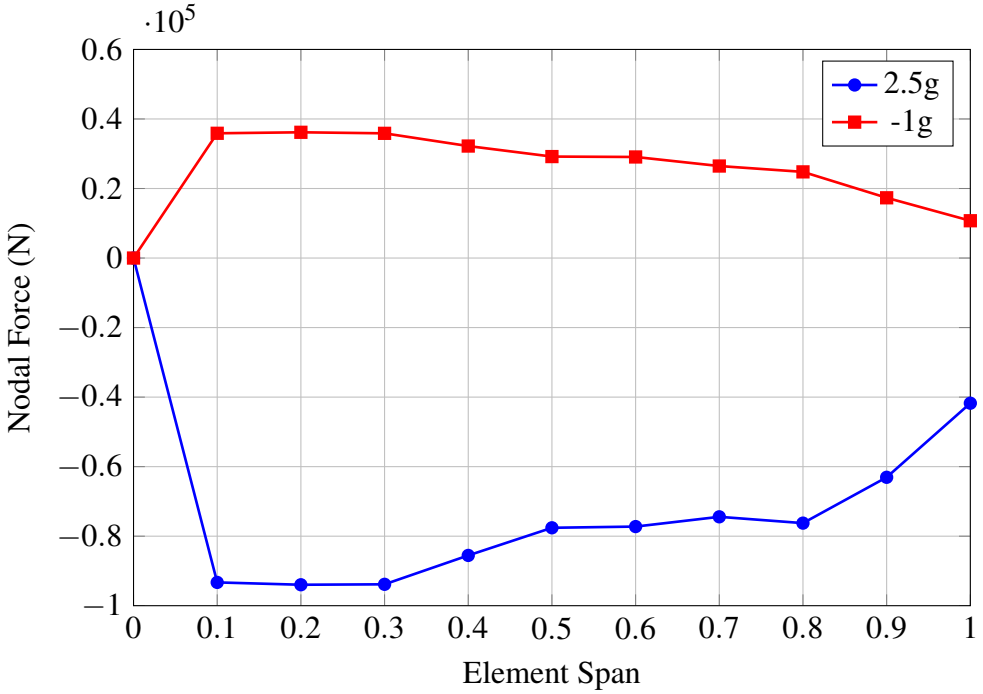

Figure A.11. Nodal Forces ($\eta = 0.51$)

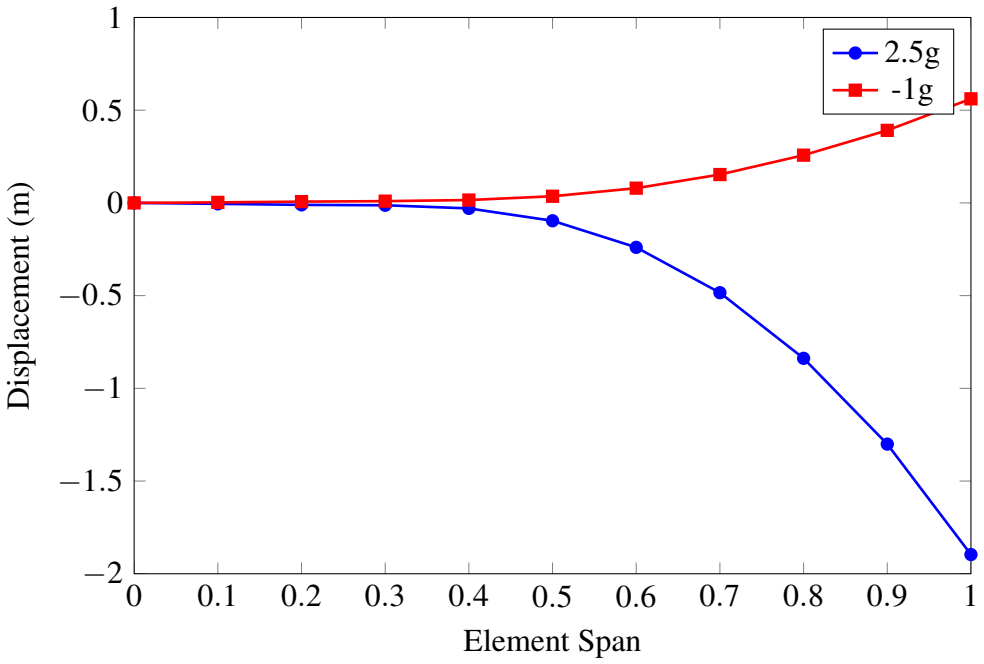

Figure A.12. Displacements ($\eta = 0.51$)

A.4 $\eta = 0.57$

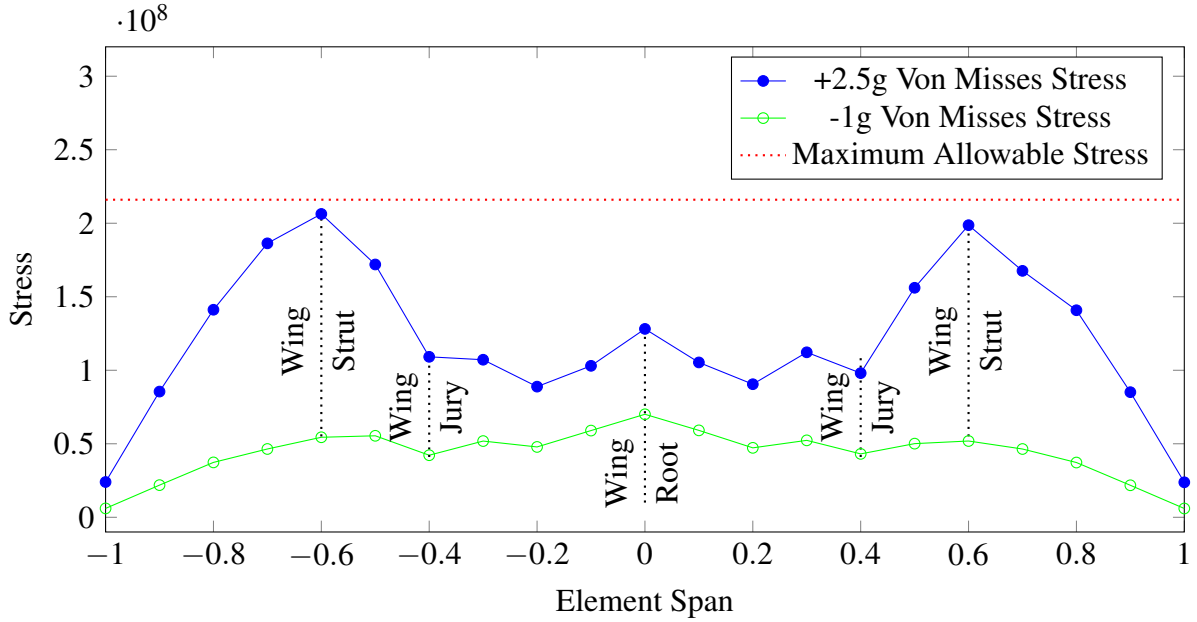

Figure A.13. Stress vs Element Span for $\eta = 0.57$.

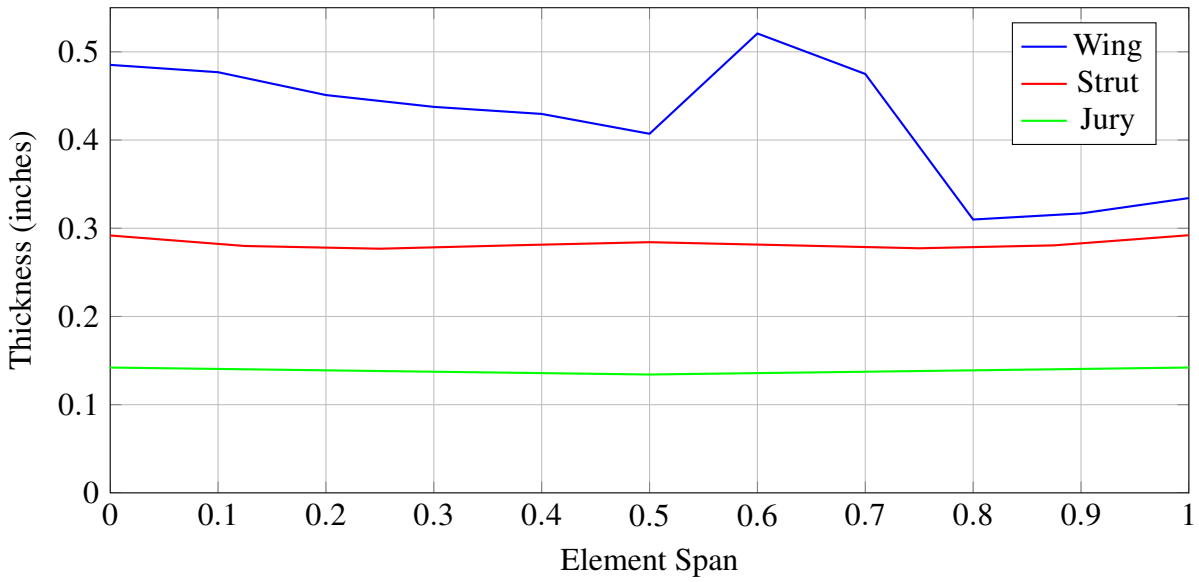

Figure A.14. Sized Spar Thickness ($\eta = 0.57$).

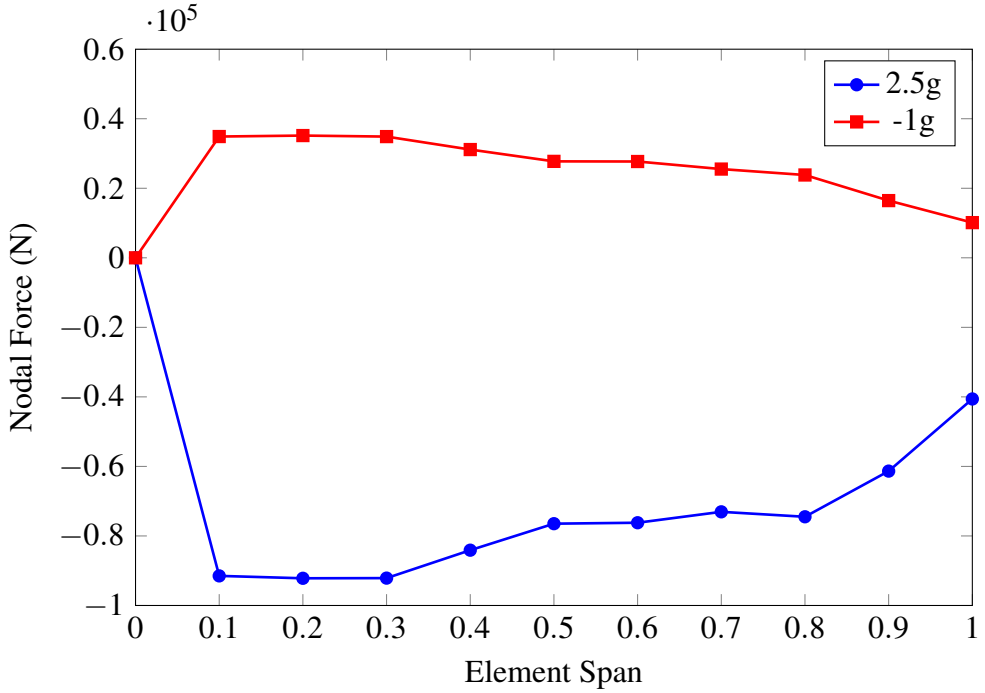

Figure A.15. Nodal Forces ($\eta = 0.57$).

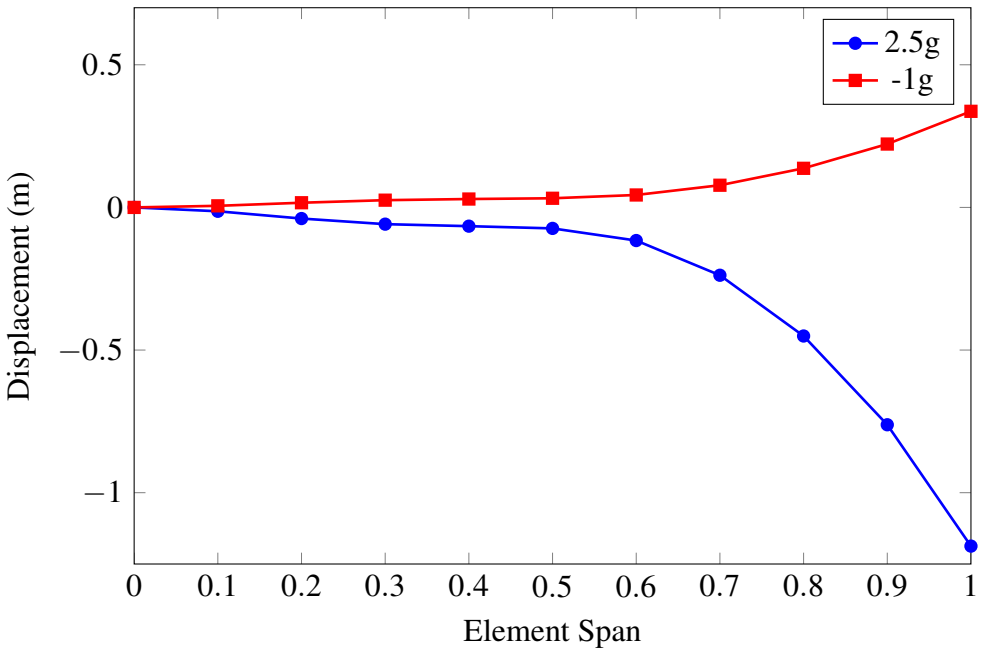

Figure A.16. Displacements ($\eta = 0.57$).

A.5 $\eta = 0.63$

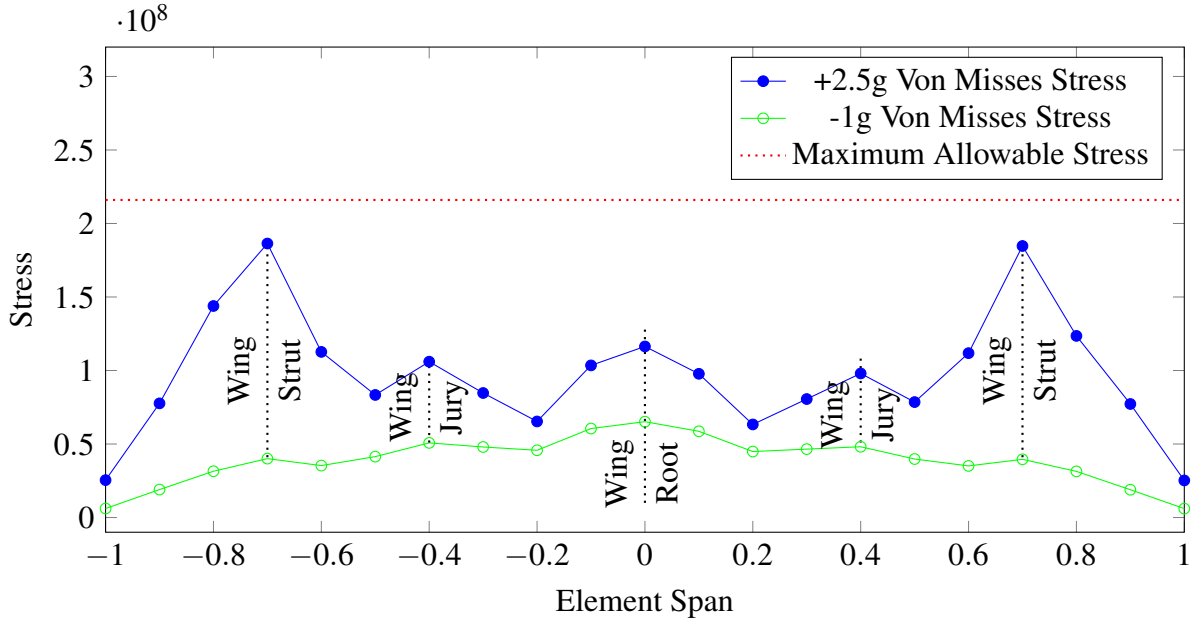

Figure A.17. Stress vs Element Span for $\eta = 0.63$.

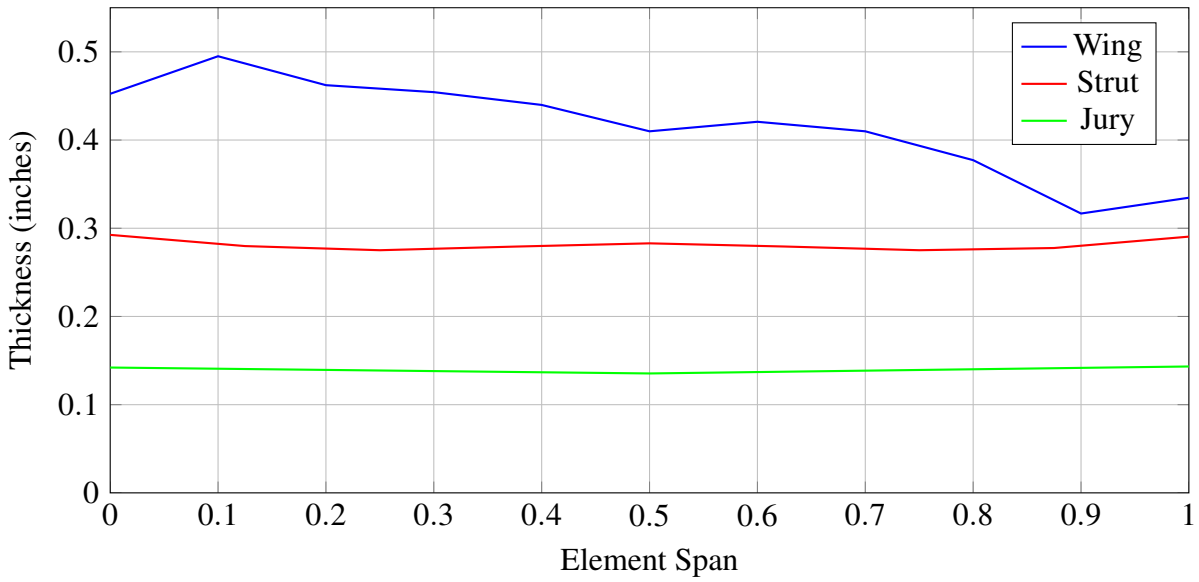

Figure A.18. Sized Spar Thickness ($\eta = 0.63$).

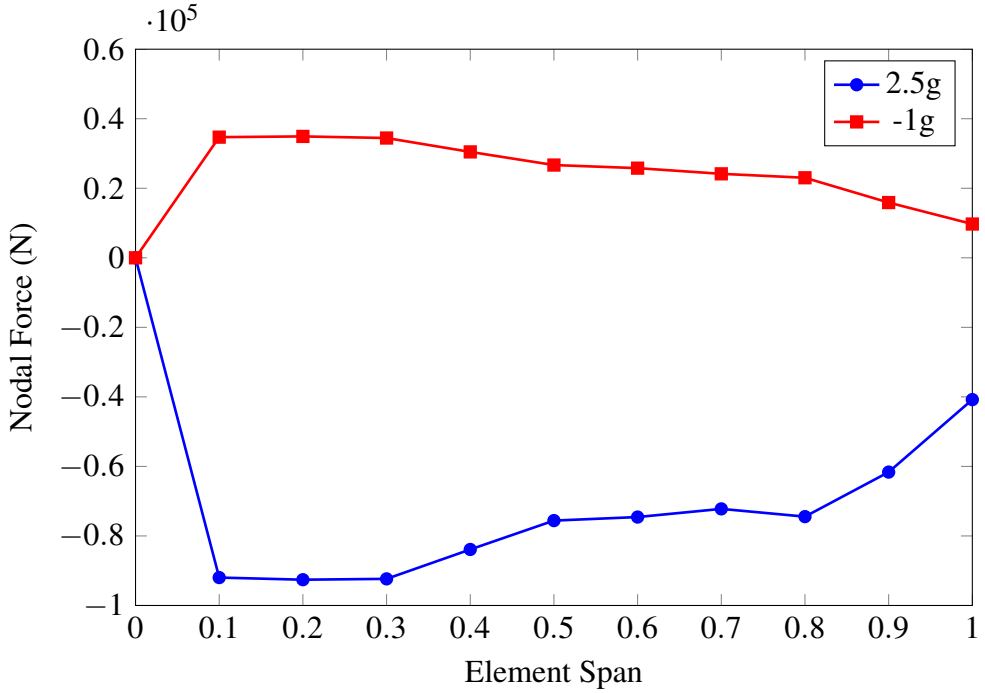

Figure A.19. Nodal Forces ($\eta = 0.63$).

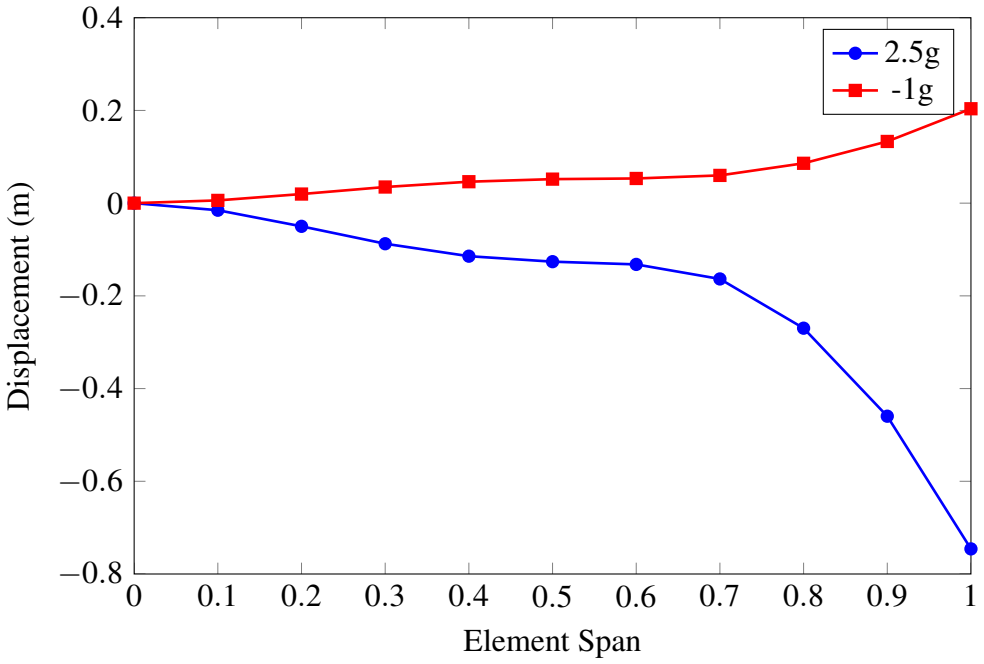

Figure A.20. Displacements ($\eta = 0.63$).

A.6 $\eta = 0.69$

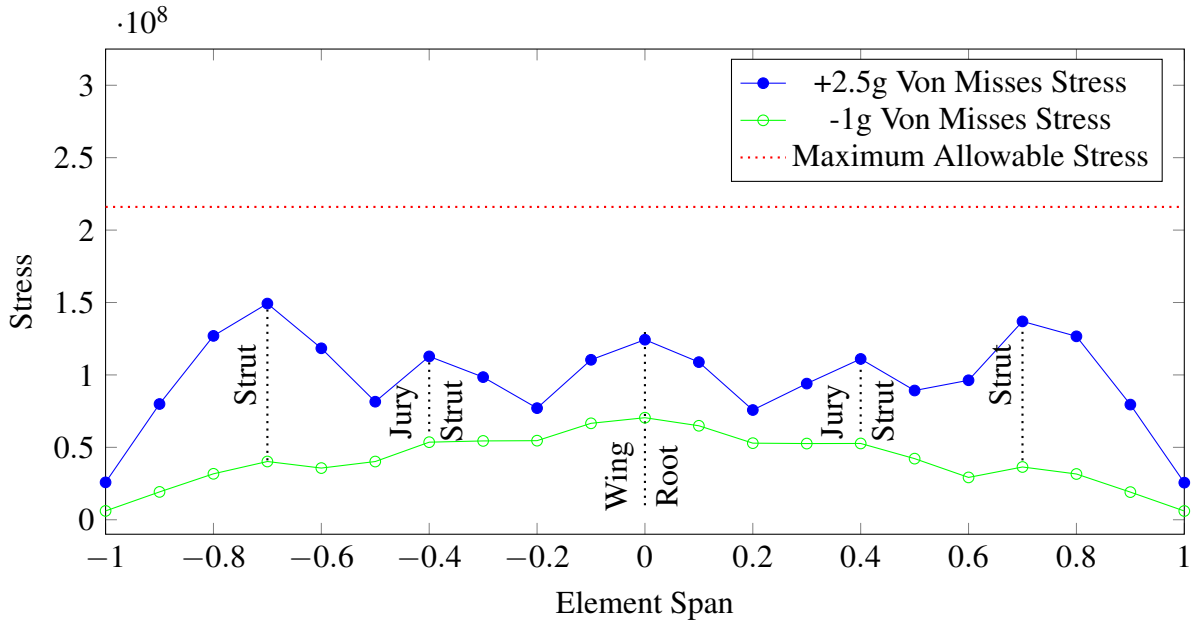

Figure A.21. Stress vs Element Span for $\eta = 0.69$.

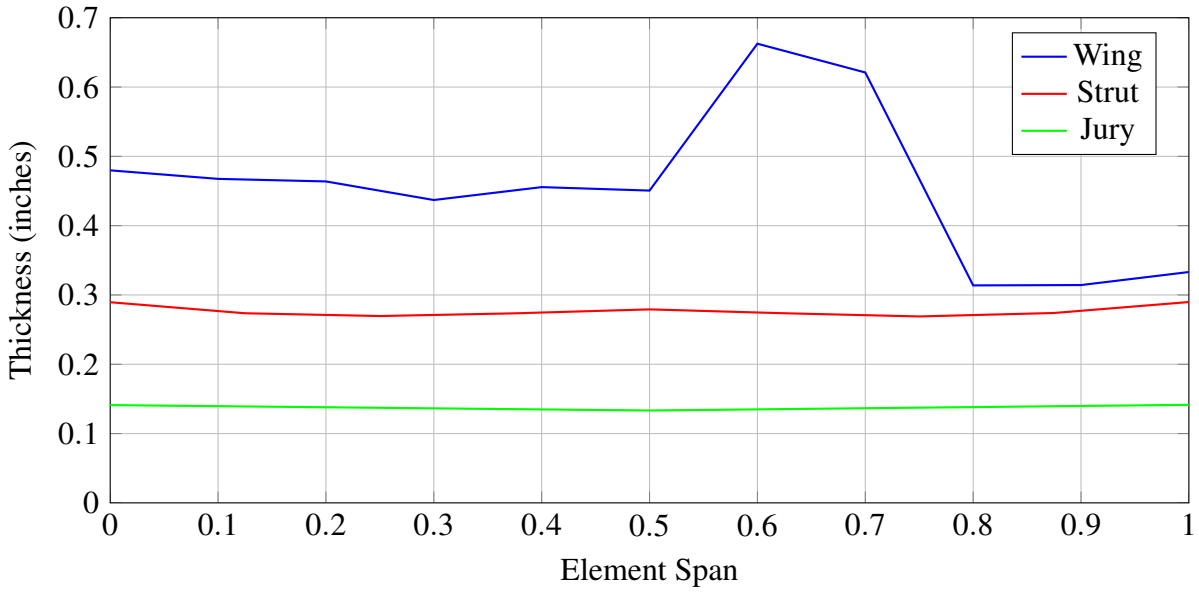

Figure A.22. Sized Spar Thickness ($\eta = 0.69$).

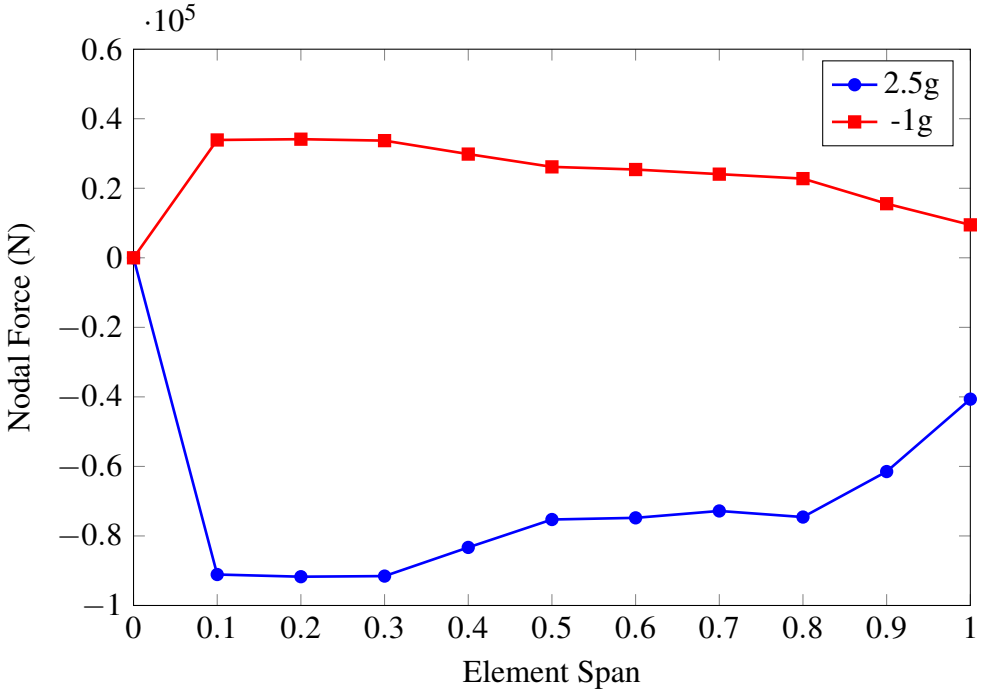

Figure A.23. Nodal Forces ($\eta = 0.69$).

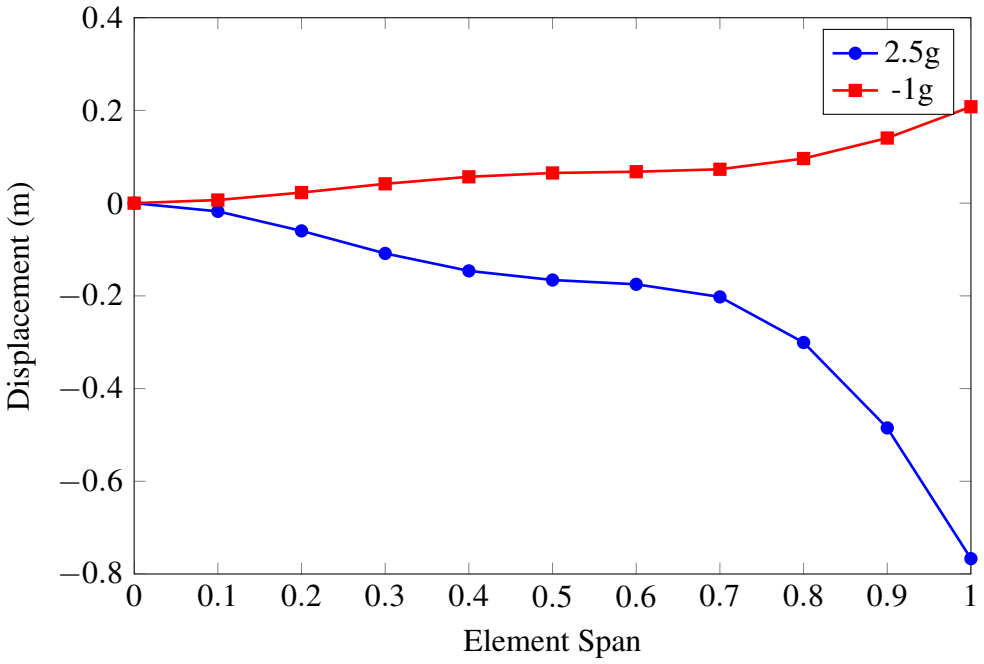

Figure A.24. Displacements (η = 0.69).

A.7 η = 0.76

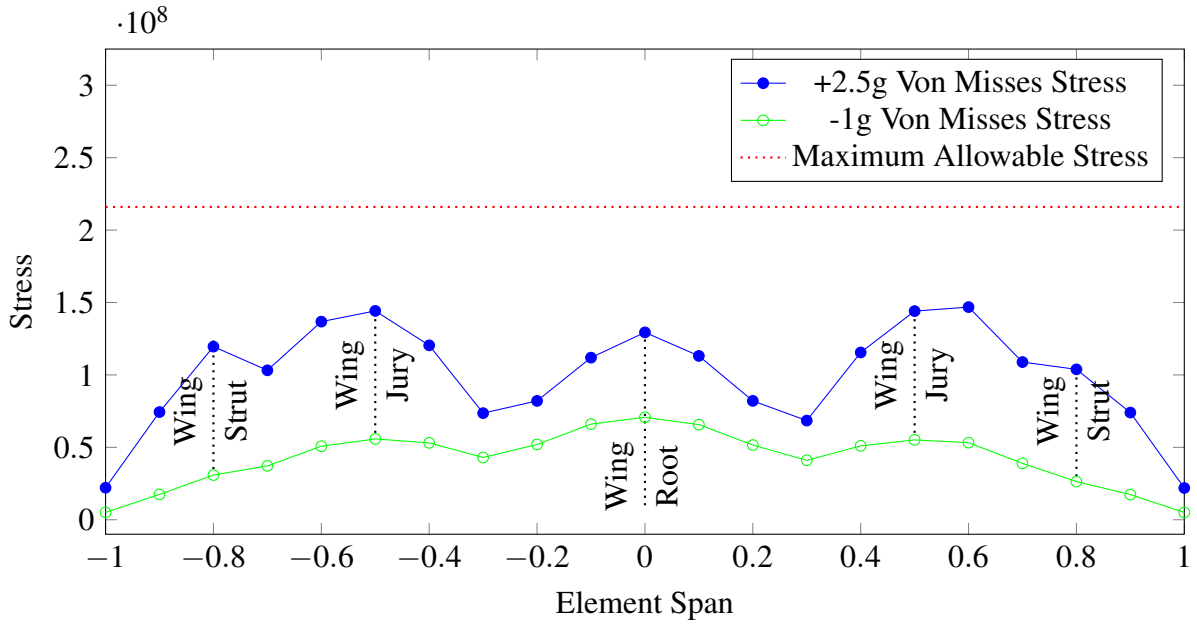

Figure A.25. Stress vs Element Span for η = 0.76.

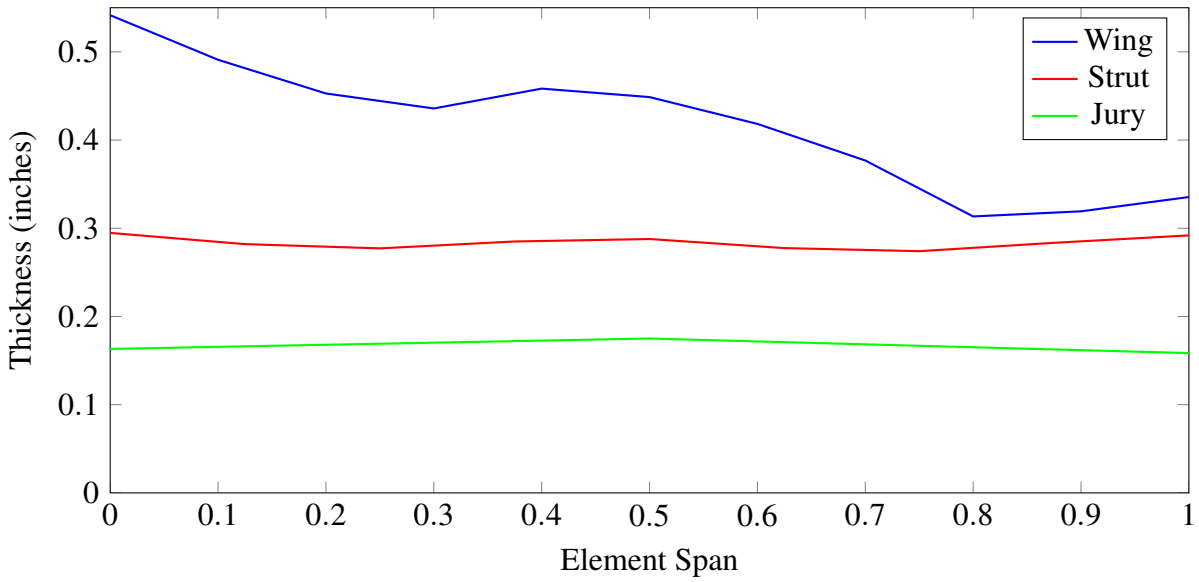

Figure A.26. Sized Spar Thickness ($\eta = 0.76$).

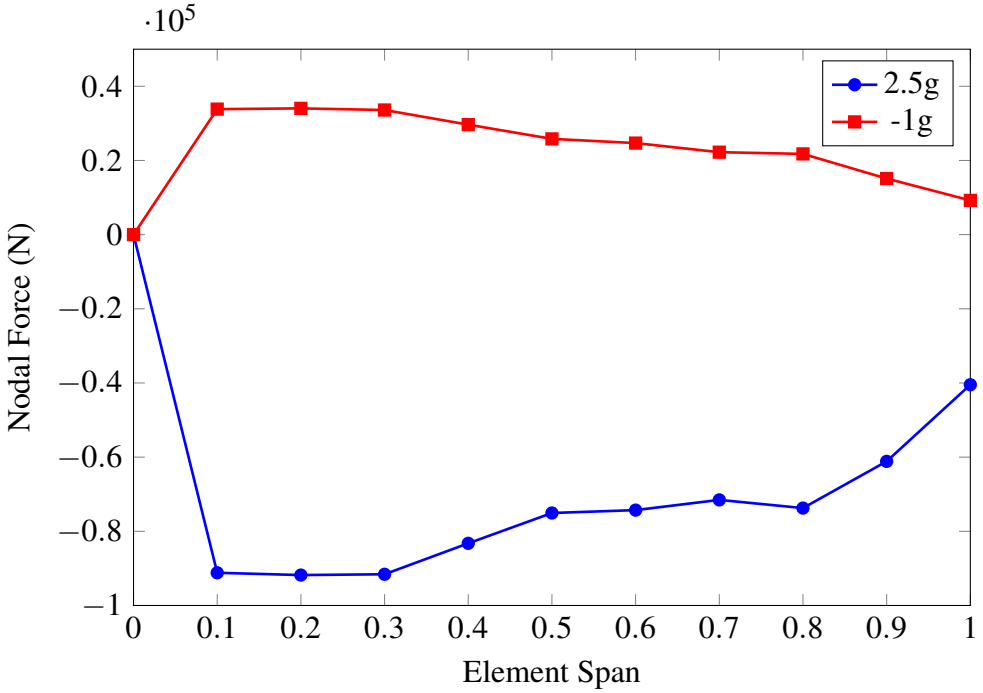

Figure A.27. Nodal Forces ($\eta = 0.76$).

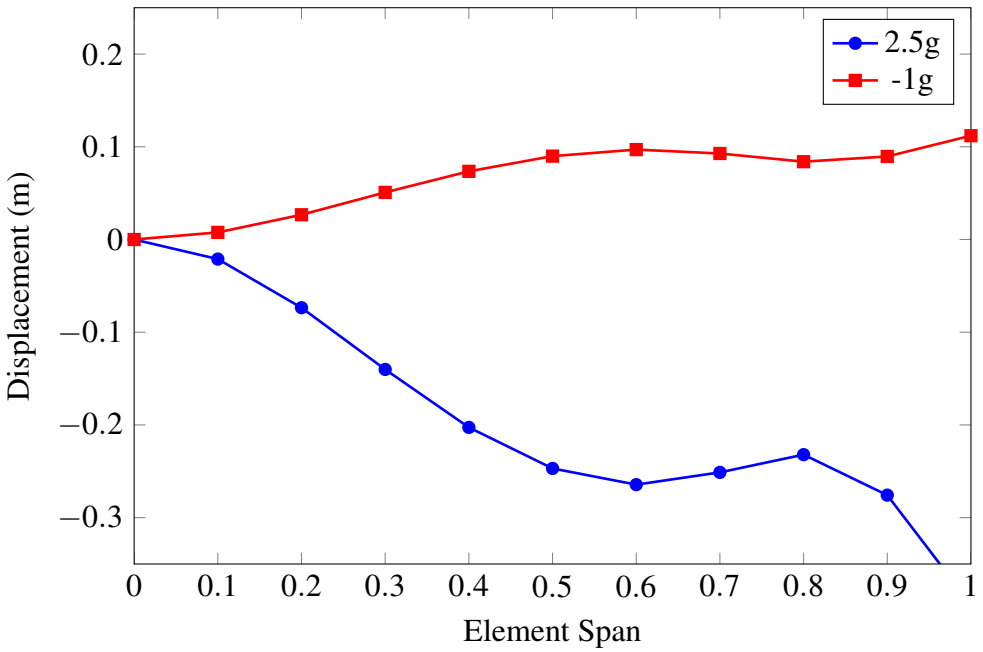

Figure A.28. Displacements ($\eta = 0.76$).

A.8 $\eta = 0.80$

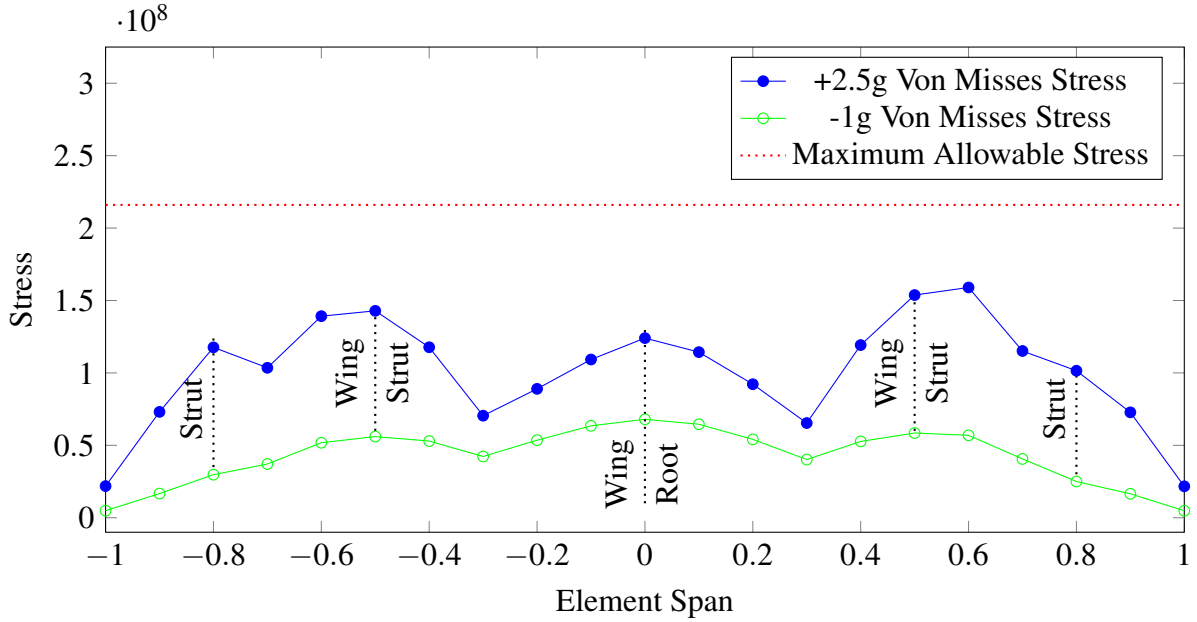

Figure A.29. Stress vs Element Span for $\eta = 0.80$.

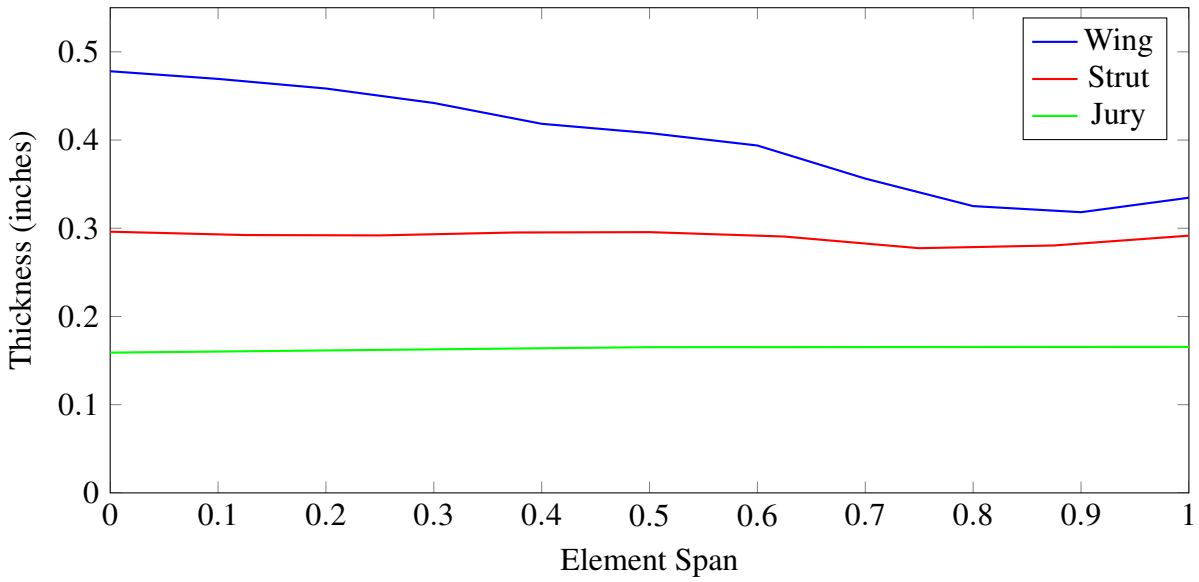

Figure A.30. Sized Spar Thickness ($\eta = 0.80$).

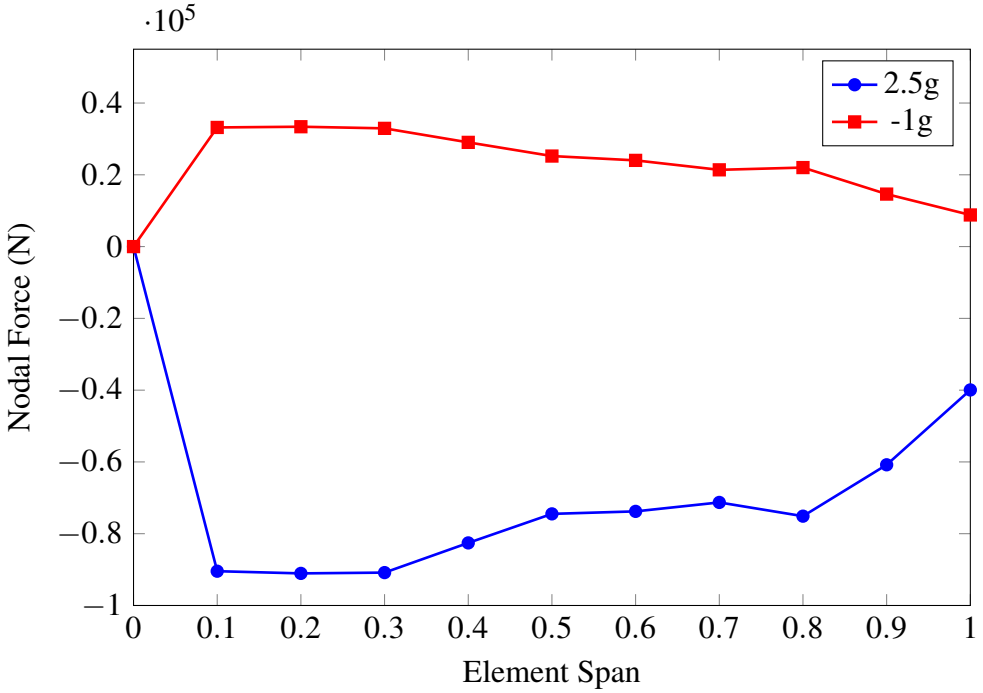

Figure A.31. Nodal Forces ($\eta = 0.80$).

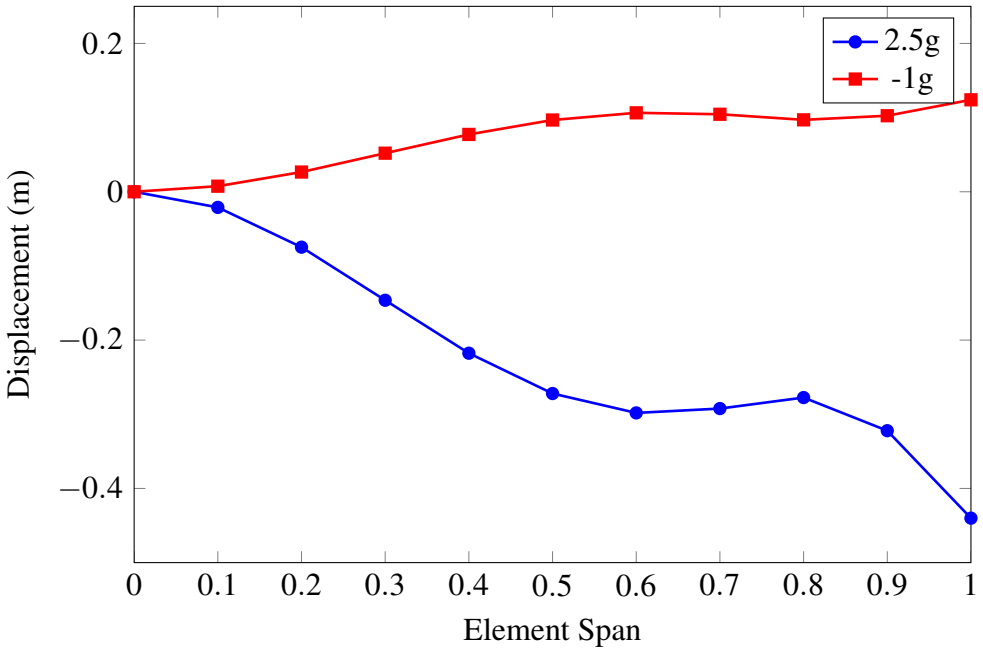

Figure A.32. Displacements ($\eta = 0.80$).

Appendix B

Full-Scale MDO

B.1 Estimating Span for different η

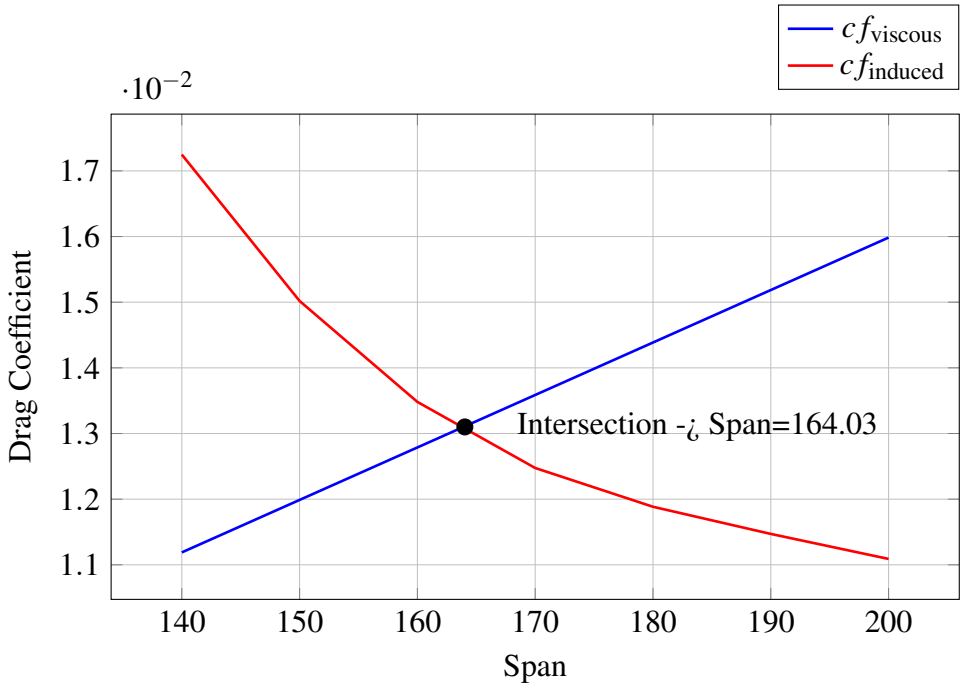

Figure B.1. Plot of viscous and induced drag coefficients against span (η = 0.40).

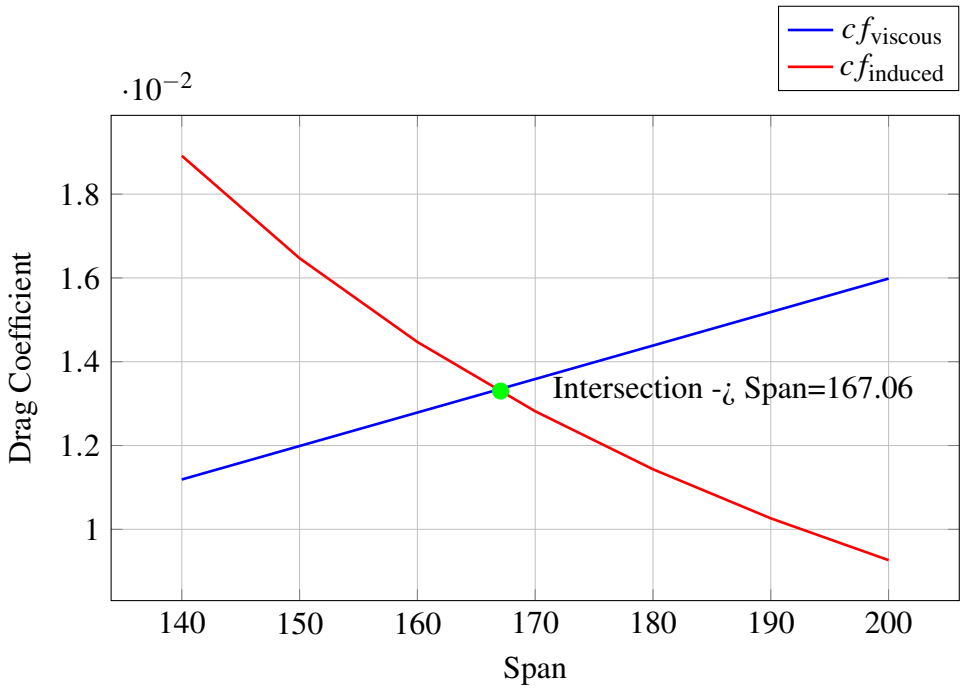

Figure B.2. Plot of viscous and induced drag coefficients against span ($\eta = 0.45$).

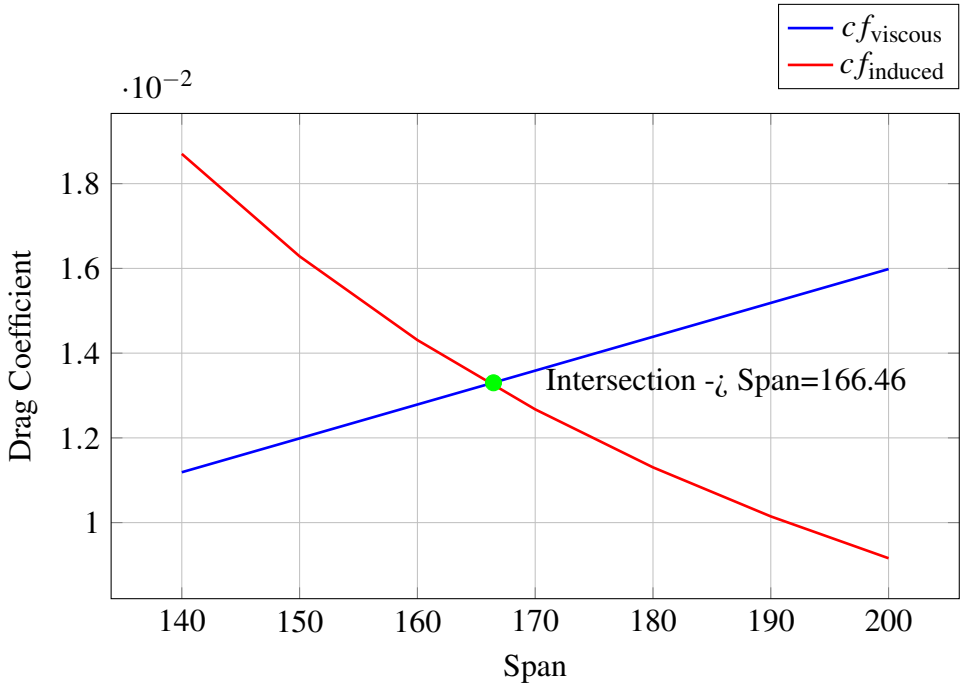

Figure B.3. Plot of viscous and induced drag coefficients against span ($\eta = 0.51$).

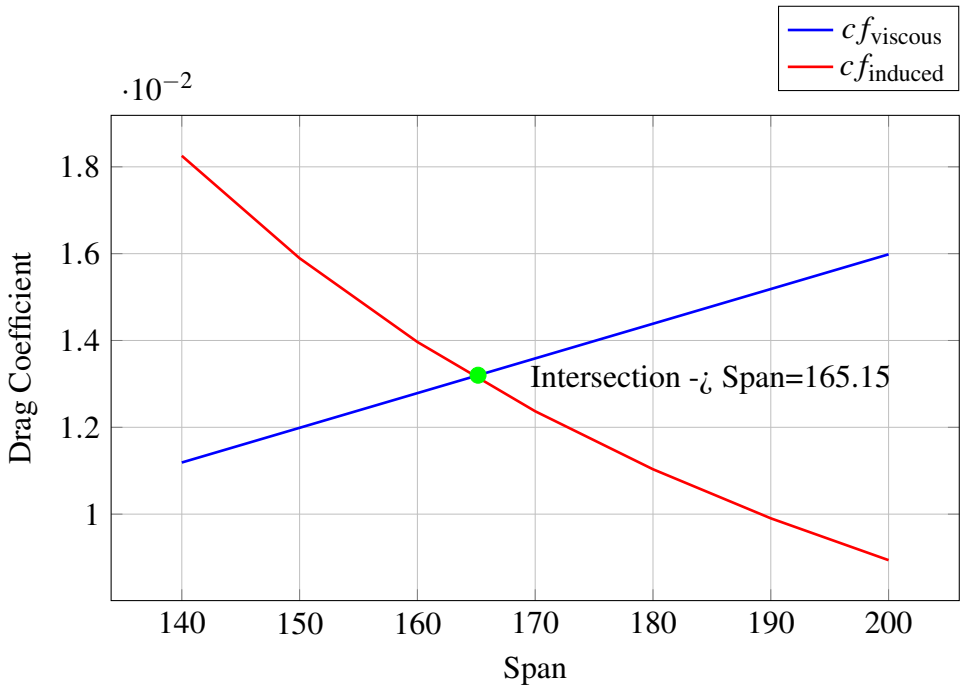

Figure B.4. Plot of viscous and induced drag coefficients against span ($\eta = 0.63$).

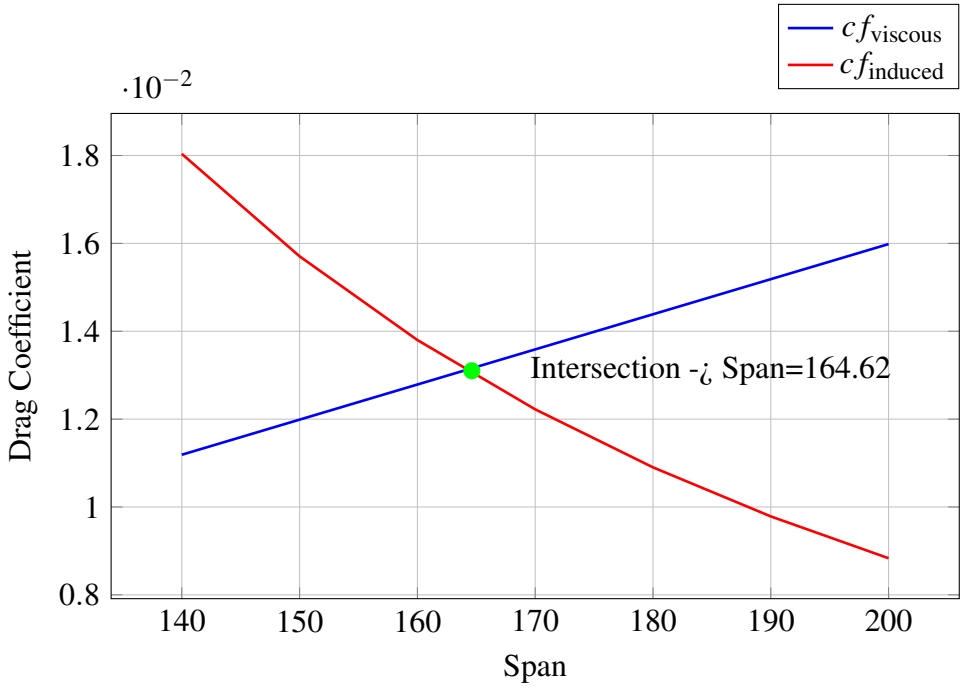

Figure B.5. Plot of viscous and induced drag coefficients against span ($\eta = 0.69$).

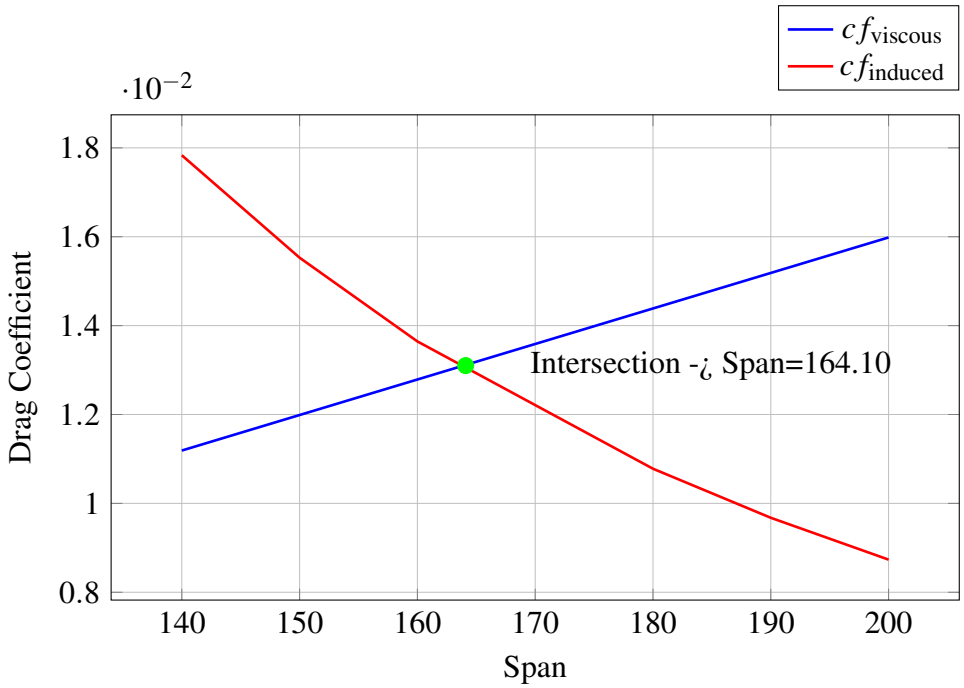

Figure B.6. Plot of viscous and induced drag coefficients against span ($\eta = 0.76$).

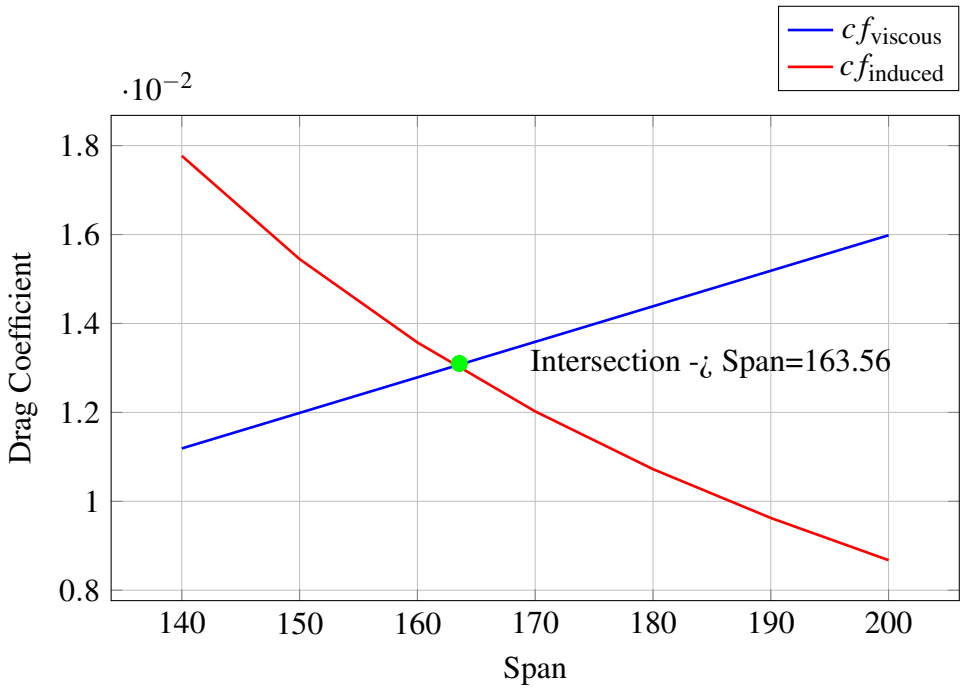

Figure B.7. Plot of viscous and induced drag coefficients against span ($\eta = 0.80$).

B.2 Fuel Burn for different η

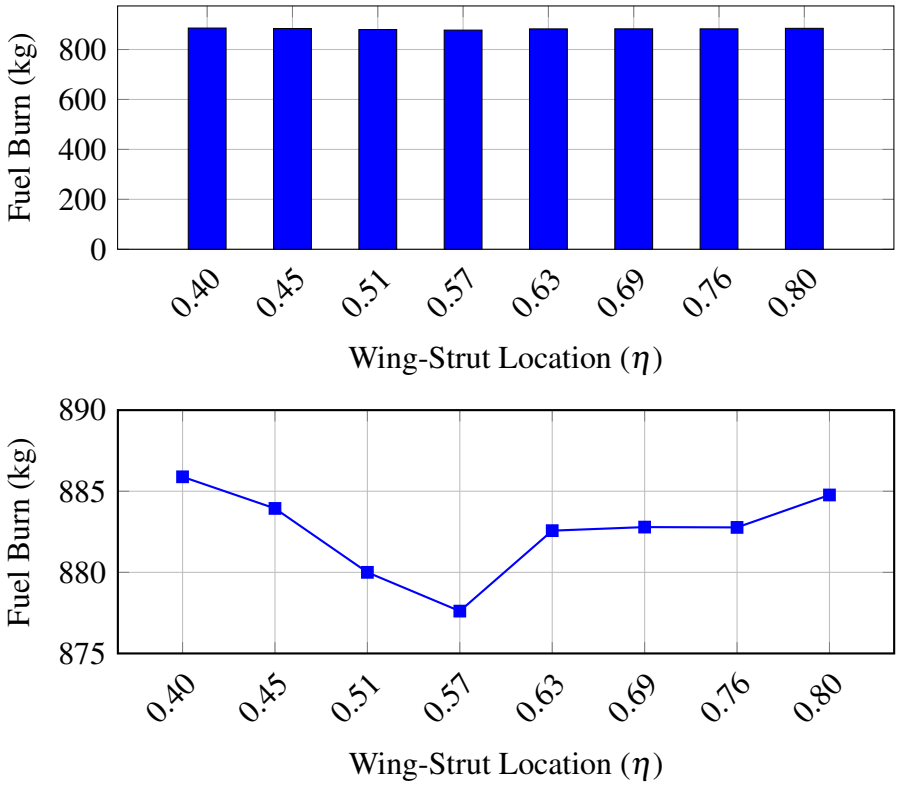

Figure B.8. Fuel Burnt during climb for different Wing-Strut Locations(η).

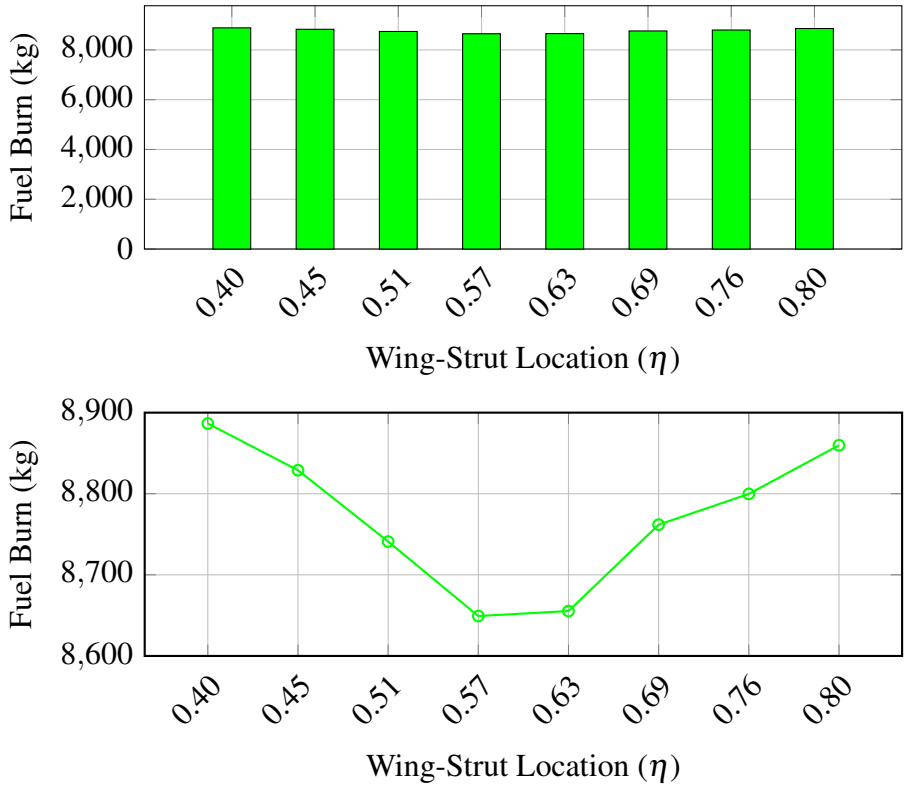

Figure B.9. Fuel Burnt during cruise for different Wing-Strut Locations(η).

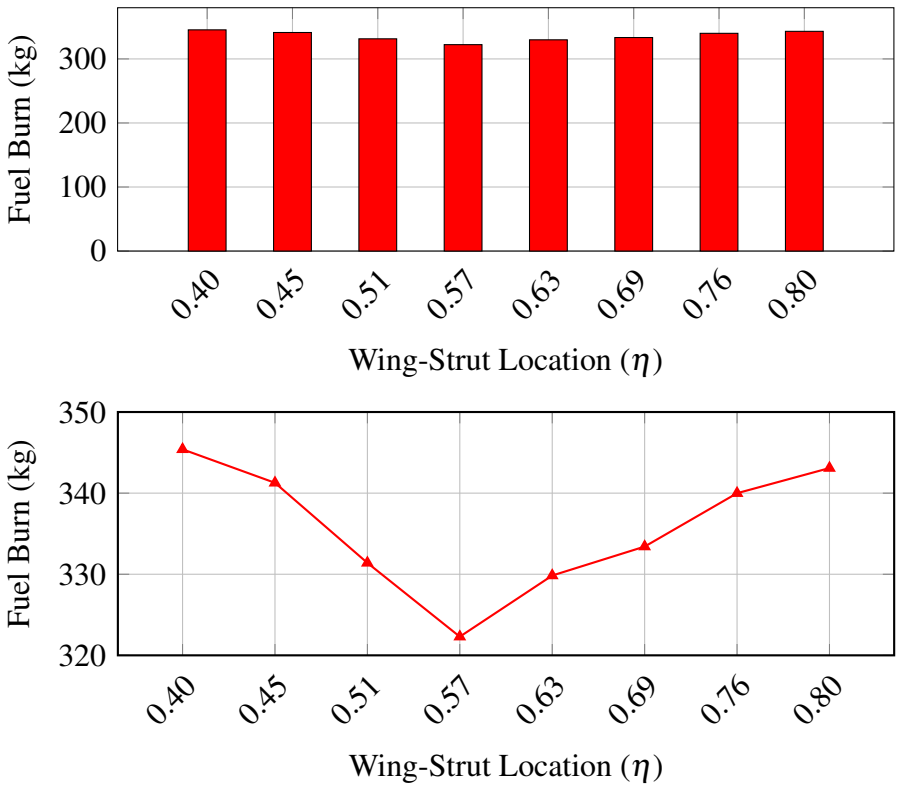

Figure B.10. Fuel Burnt during descent for different Wing-Strut Locations(η).

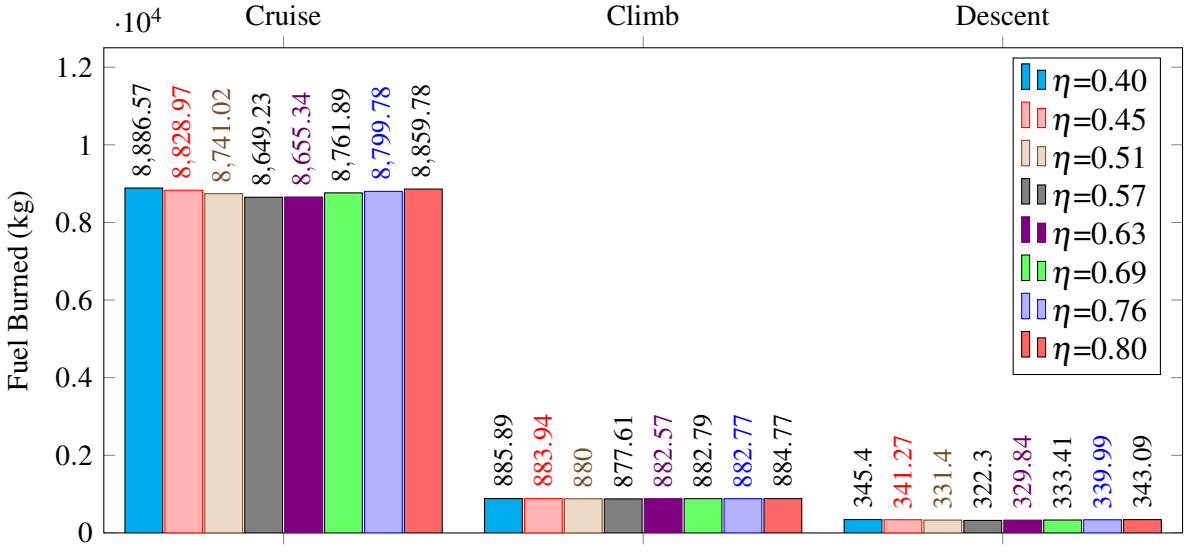

Figure B.12. Fuel Burnt (kg) during Cruise, Climb and Descent.

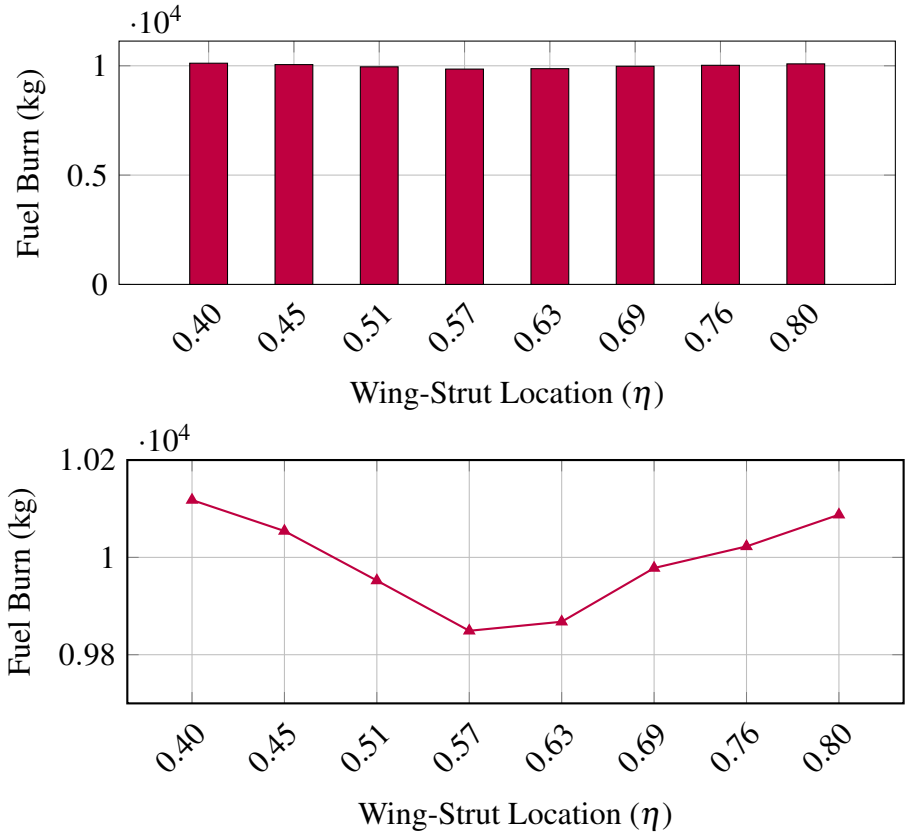

Figure B.11. Total Fuel Burnt during Cruise, Climb & Descent for different Wing-Strut Locations(η).

B.3 Weight Breakdown for different η

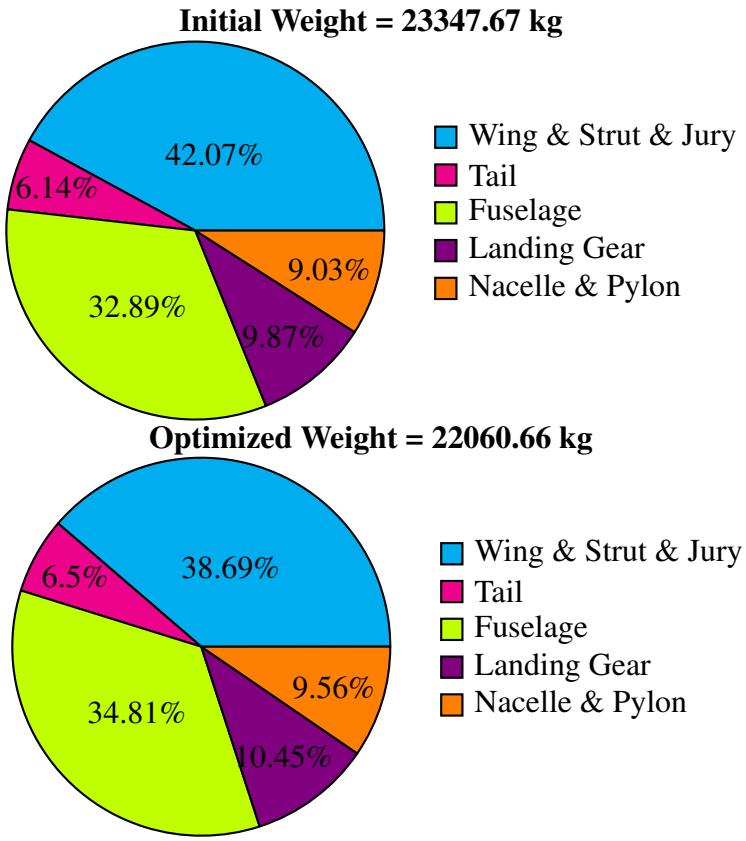

Figure B.13. Weight Breakdown before & after Optimization (η=0.40)

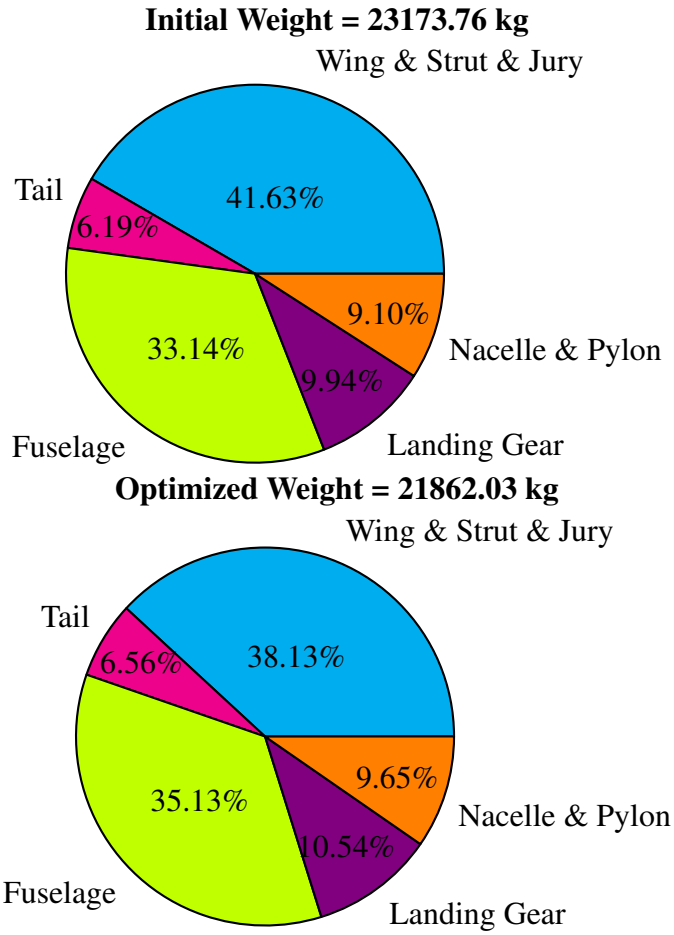

Figure B.14. Weight Breakdown before & after Optimization (η=0.45)

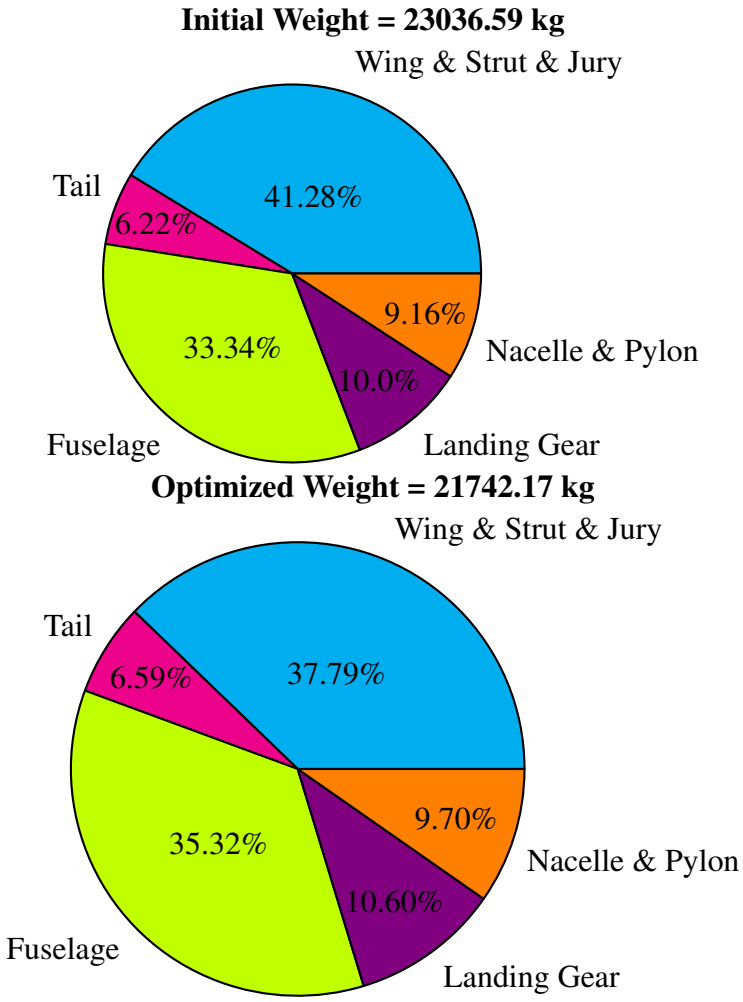

Figure B.15. Weight Breakdown before & after Optimization (η=0.51)

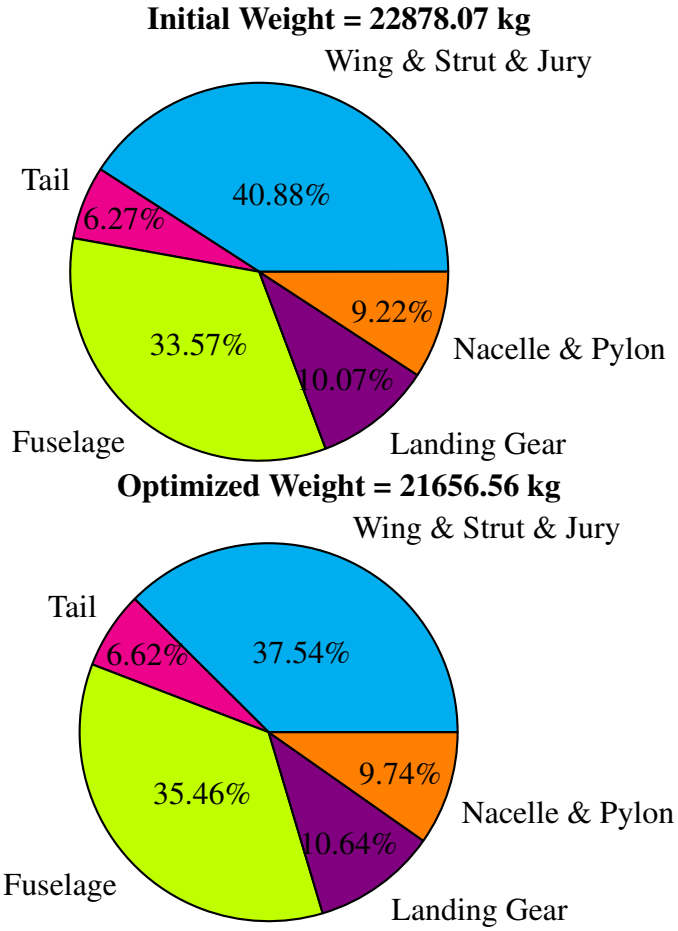

Figure B.16. Weight Breakdown before & after Optimization (η=0.63)

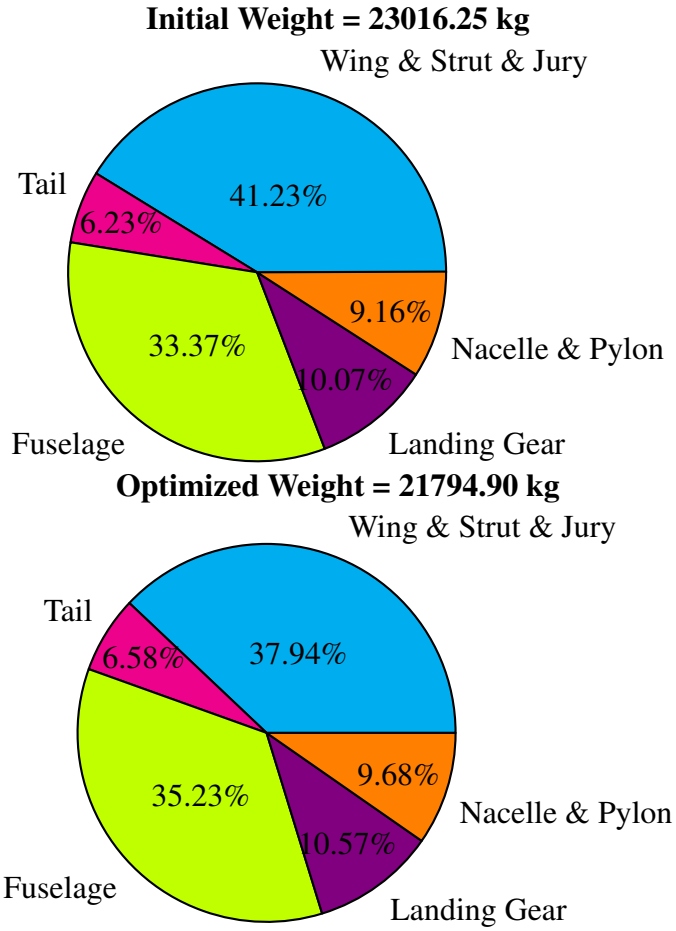

Figure B.17. Weight Breakdown before & after Optimization (η=0.69)

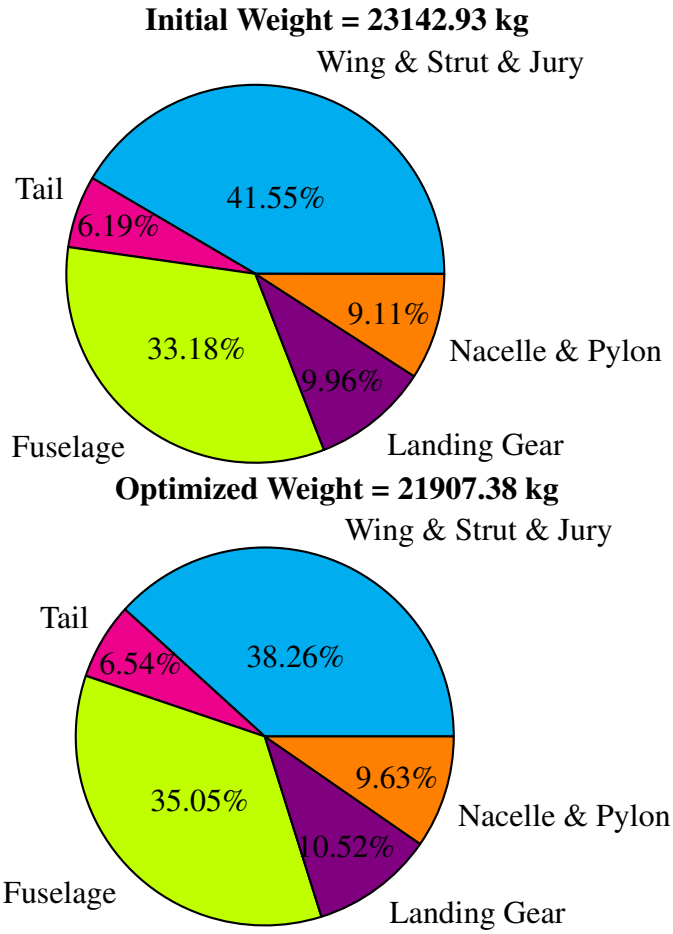

Figure B.18. Weight Breakdown before & after Optimization (η=0.76)

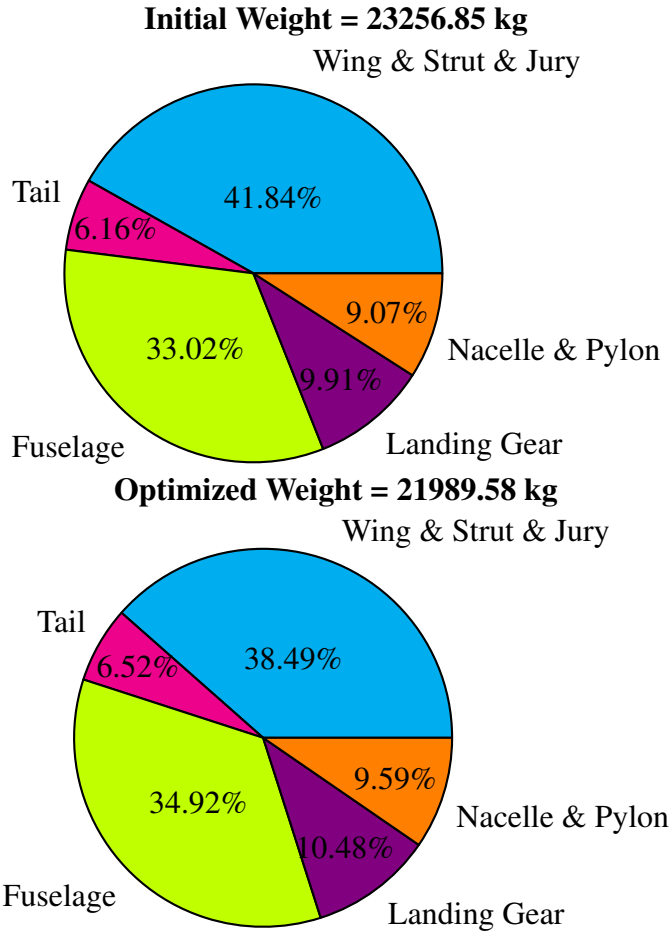

Figure B.19. Weight Breakdown before & after Optimization (η=0.80)

Bibliography

[1] Ira H. Abbott and Albert E. Von Doenhoff. *Theory of Wing Sections*. Dover Publications, Inc., New York, 1959.

[2] Frederico Afonso, José Vale, Éder Oliveira, Fernando Lau, and Afzal Suleman. A review on non-linear aeroelasticity of high aspect-ratio wings. *Progress in Aerospace Sciences*, 89:40–57, 2017.

[3] Timothy Allen, Bradley Sexton, and Matthew J Scott. Sugar truss braced wing full scale aeroelastic analysis and dynamically scaled wind tunnel model development. In *56th AIAA/ASCE/AHS/ASC Structures, Structural Dynamics, and Materials Conference*, page 1171, 2015.

[4] J.-H. An, D.-Y. Kwon, K.-S. Jeon, M. Tyan, and J.-W. Lee. Advanced sizing methodology for a multi-mode evtol uav powered by a hydrogen fuel cell and battery. *Aerospace*, 9(2):71, 2022.

[5] John D. Anderson. *Fundamentals of Aerodynamics*. McGraw-Hill Education, 2017.

[6] John David Anderson Jr. *Fundamentals of aerodynamics*. Tata McGraw-Hill Education, 2010.

[7] Akshay Basavaraj. Estimation of wave drag of non-transonic airfoils using korn equation. *Int J Innovative Research in Science, Engineering and Technology*, 4:2119–2126, 2015.

[8] Manav Bhatia, Rakesh Kapania, Maarten van Hoek, and Raphael Haftka. Structural design of a truss braced wing: potential and challenges. In *50th AIAA/ASME/ASCE/AHS/ASC Structures, Structural Dynamics, and Materials Conference 17th AIAA/ASME/AHS Adaptive Structures Conference 11th AIAA No*, page 2147, 2009.

[9] Manav Bhatia, Rakesh K Kapania, and Raphael T Haftka. Structural and aeroelastic characteristics of truss-braced wings: A parametric study. *Journal of Aircraft*, 49(1):302–310, 2012.

[10] Marty K Bradley, Timothy J Allen, and Christopher Droney. Subsonic ultra green aircraft

research: Phase ii-volume iii-truss braced wing aeroelastic test report. Technical report, 2014.

[11] Marty K Bradley and Christopher K Droney. Subsonic ultra green aircraft research phase ii: N+ 4 advanced concept development. Technical report, 2012.

[12] Marty K Bradley and Christopher K Droney. Subsonic ultra green aircraft research: Phase 2. Technical report, 2015.

[13] Marty K Bradley and Christopher K Droney. Subsonic ultra green aircraft research: phase ii–volume ii–hybrid electric design exploration. *NASA CR-218704*, page 378, 2015.

[14] Vincent Braibant and Claude Fleury. Shape optimal design using b-splines. *Computer methods in applied mechanics and engineering*, 44(3):247–267, 1984.

[15] Timothy R Brooks, Joaquim RRA Martins, and Graeme J Kennedy. Aerostructural tradeoffs for tow-steered composite wings. *Journal of Aircraft*, 57(5):787–799, 2020.

[16] Gerald Carrier, Olivier Atinault, Sylvie Dequand, Jean Luc Hantrais-Gervois, Cédric Liauzun, Bernard Paluch, Anne Marie Rodde, and Clement Toussaint. Investigation of a strut-braced wing configuration for future commercial transport. In *28th Congress of the International Council of the Aeronautical Sciences*, pages 2012–1. ICAS Bonn, 2012.

[17] Gerald G Carrier, Guillaume Arnoult, Nicolo Fabbiane, Jean-Sebastien Schotte, Christophe David, Sébastien Defoort, Emmanuel Benard, and Martin Delavenne. Multidisciplinary analysis and design of strut-braced wing concept for medium range aircraft. In *AIAA SCITECH 2022 Forum*, page 0726, 2022.

[18] Mustafa Cavcar. Bréguet range equation? *Journal of aircraft*, 43(5):1542–1544, 2006.

[19] Tuncer Cebeci and Peter Bradshaw. Momentum transfer in boundary layers. *Washington*, 1977.

[20] I. Chakraborty, A. A. Mishra, N. S. Miller, D. v. Dommelen, and W. A. Anemaat. Design and sizing of a dual-purpose hybrid-electric ducted fan lift-plus-cruise aircraft. In *AIAA SCITECH 2022 Forum*, page 1516, 2022.

[21] Imon Chakraborty, Taewoo Nam, Jonathan R Gross, Dimitri N Mavris, Joseph A Schetz, and Rakesh K Kapania. Comparative assessment of strut-braced and truss-braced wing configurations using multidisciplinary design optimization. *Journal of Aircraft*, 52(6):2009–2020, 2015.

[22] Daniel Chaparro, Gustavo E Fujiwara, Eric Ting, and Nhan T Nguyen. Transonic and viscous potential flow method applied to flexible wing transport aircraft. In *35th AIAA*

Applied Aerodynamics Conference, page 4221, 2017.

[23] Shamsheer S Chauhan and Joaquim RRA Martins. Low-fidelity aerostructural optimization of aircraft wings with a simplified wingbox model using openaerostruct. In *EngOpt 2018 Proceedings of the 6th International Conference on Engineering Optimization*, pages 418–431. Springer, 2019.

[24] M Coelho, F Afonso, F Lau, and A Suleman. Nonlinear aeroelastic scaling studies on high aspect ratio wings. In *Proceedings of the 6th EASN International Conference on Innovation in European Aeronautics Research, Porto, Portugal*, pages 18–21, 2016.

[25] AR Collar. A closed formula for the drag of a flat plate with transition in the absence of a pressure gradient. *The Aeronautical Journal*, 64(589):38–39, 1960.

[26] Evin J Cramer, John E Dennis, Jr, Paul D Frank, Robert Michael Lewis, and Gregory R Shubin. Problem formulation for multidisciplinary optimization. *SIAM Journal on Optimization*, 4(4):754–776, 1994.

[27] Agostino De Marco, Eugene Duke, and Jon Berndt. A general solution to the aircraft trim problem. In *AIAA Modeling and Simulation Technologies Conference and Exhibit*, page 6703, 2007.

[28] R Del Rosario, G Follen, R Wahls, and N Madavan. Subsonic fixed wing project overview of technical challenges for energy efficient, environmentally compatible subsonic transport aircraft. In *50th AIAA Aerospace Science Meeting, Nashville, TN, Jan*, pages 9–12, 2012.

[29] M Delavenne, E Benard, S Defoort, C David, N Fabbiane, JS Schotte, G Arnoult, and G Carrier. Multi-fidelity weight analyses for high aspect ratio strut-braced wings preliminary design. In *IOP Conference Series: Materials Science and Engineering*, volume 1226, page 012009. IOP Publishing, 2022.

[30] Matthias Eck and Hugues Hoppe. Automatic reconstruction of b-spline surfaces of arbitrary topological type. In *Proceedings of the 23rd annual conference on Computer graphics and interactive techniques*, pages 325–334, 1996.

[31] Jason Fugate, Nhan T Nguyen, and Juntao Xiong. Aero-structural modeling of the truss-braced wing aircraft using potential method with correction methods for transonic viscous flow and wing-strut interference aerodynamics. In *AIAA Aviation 2019 Forum*, page 3028, 2019.

[32] Victor Gandarillas. *Enhancing Multidisciplinary Design Optimization Through Automated Computational Model Construction and Sensitivity Analysis*. University of California, San Diego, 2023.

[33] Victor Gandarillas, Anugrah Jo Joshy, Mark Z Sperry, Alexander K Ivanov, and John T Hwang. A graph-based methodology for constructing computational models that automates adjoint-based sensitivity analysis. *Structural and Multidisciplinary Optimization*, 67(5):76, 2024.

[34] Frank H Gern, Amir H Naghshineh-Pour, Erwin Sulaeman, Rakesh K Kapania, and Raphael T Haftka. Structural wing sizing for multidisciplinary design optimization of a strut-braced wing. *Journal of aircraft*, 38(1):154–163, 2001.

[35] Philip E Gill, Walter Murray, and Michael A Saunders. Snopt: An sqp algorithm for large-scale constrained optimization. *SIAM review*, 47(1):99–131, 2005.

[36] Joel Grasmeyer. *Truss-Braced Wing Code Description and User's Manual*. PhD thesis, Virginia Polytechnic Institute and State University, 1852.

[37] Joel Grasmeyer and WH Mason. A discrete vortex method for calculating the minimum induced drag and optimum load distribution for aircraft configurations with noncoplanar surfaces. *VPIAOE-242, AOE Department, VPI & SU, Blacksburg, Virginia*, 24061, 1997.

[38] Joel M Grasmeyer III. *Multidisciplinary design optimization of a strut-braced wing aircraft*. PhD thesis, Virginia Tech, 1998.

[39] Justin S Gray, John T Hwang, Joaquim RRA Martins, Kenneth T Moore, and Bret A Naylor. Openmdao: An open-source framework for multidisciplinary design, analysis, and optimization. *Structural and Multidisciplinary Optimization*, 59:1075–1104, 2019.

[40] John F Gundlach IV, Philippe-Andre Tetrault, Frank H Gern, Amir H Nagshineh-Pour, Andy Ko, Joseph A Schetz, William H Mason, Rakesh K Kapania, William H Mason, Bernard Grossman, and Raphael T Haftka. Conceptual design studies of a strut-braced wing transonic transport. *Journal of aircraft*, 37(6):976–983, 2000.

[41] Ohad Gur, Manav Bhatia, William H Mason, Joseph A Schetz, Rakesh K Kapania, and Taewoo Nam. Development of a framework for truss-braced wing conceptual mdo. *Structural and Multidisciplinary optimization*, 44:277–298, 2011.

[42] Ohad Gur, Manav Bhatia, Joseph Schetz, William Mason, Rakesh Kapania, and Dimitri Mavris. Multidisciplinary design optimization of a truss braced wing aircraft. In *9th AIAA Aviation Technology, Integration, and Operations Conference (ATIO) and Aircraft Noise and Emissions Reduction Symposium (ANERS)*, page 7114, 2009.

[43] Ohad Gur, Manav Bhatia, Joseph A Schetz, William H Mason, Rakesh K Kapania, and Dimitri N Mavris. Design optimization of a truss-braced-wing transonic transport aircraft. *Journal of aircraft*, 47(6):1907–1917, 2010.

[44] Ian Halliwell and Karleine Justice. Fuel burn benefits of a variable-pitch geared fan engine. In *48th AIAA/ASME/SAE/ASEE Joint Propulsion Conference & Exhibit*, page 3912, 2012.

[45] H. W. Hilton. *High Speed Aerodynamics*. Longmans, Green and Co., London, 1951.

[46] S. F. Hoerner. *Fluid Dynamic Drag*. Hoerner Fluid Dynamics, Bakersfield, CA, 1965.

[47] Edward J Hopkins. Charts for predicting turbulent skin friction from the van driest method (2). Technical report, 1972.

[48] Edward J Hopkins and Mamoru Inouye. An evaluation of theories for predicting turbulent skin friction andheat transfer on flat plates at supersonic and hypersonic mach numbers. *AIAA Journal*, 9(6):993–1003, 1971.

[49] John T Hwang and Joaquim RRA Martins. A computational architecture for coupling heterogeneous numerical models and computing coupled derivatives. *ACM Transactions on Mathematical Software (TOMS)*, 44(4):1–39, 2018.

[50] John T Hwang and Andrew Ning. Large-scale multidisciplinary optimization of an electric aircraft for on-demand mobility. In *2018 AIAA/ASCE/AHS/ASC Structures, Structural Dynamics, and Materials Conference*, page 1384, 2018.

[51] GR Inger. Application of oswatitsch's theorem to supercritical airfoil drag calculation. *Journal of aircraft*, 30(3):415–416, 1993.

[52] C. E. Jobe. Prediction and verification of aerodynamic drag, part i: Prediction. In C. E. Eugene, editor, *Thrust and Drag: Its Prediction and Verification*, volume 98 of *Progress in Astronautics and Aeronautics*, chapter 4. AIAA, New York, 1985.

[53] W. Johnson and C. Silva. Nasa concept vehicles and the engineering of advanced air mobility aircraft. *The Aeronautical Journal*, 126(1295):59–91, 2022.

[54] Anugrah Jo Joshy and John T Hwang. modopt: A modular development environment and library for optimization algorithms. *arXiv preprint arXiv:2410.12942*, 2024.

[55] Byung-Soo Kang, GJ Park, and JS Arora. Optimization of flexible multibody dynamic systems using the equivalent static load method. *AIAA journal*, 43(4):846–852, 2005.

[56] Joseph Katz and Allen Plotkin. *Low-speed aerodynamics*, volume 13. Cambridge university press, 2001.

[57] Graeme J Kennedy and Joaquim RRA Martins. A parallel aerostructural optimization framework for aircraft design studies. *Structural and Multidisciplinary Optimization*, 50:1079–1101, 2014.

[58] Gaetan KW Kenway, Graeme J Kennedy, and Joaquim RRA Martins. Scalable parallel approach for high-fidelity steady-state aeroelastic analysis and adjoint derivative computations. *AIAA journal*, 52(5):935–951, 2014.

[59] Yong-Il Kim and Gyung-Jin Park. Nonlinear dynamic response structural optimization using equivalent static loads. *Computer Methods in Applied Mechanics and Engineering*, 199(9-12):660–676, 2010.

[60] Dieter Kraft. A software package for sequential quadratic programming. *DFVLR Obersfaffeuhofen Report SFB-88-28*, 28, 1988.

[61] Ilan Kroo. Nonplanar wing concepts for increased aircraft efficiency. *VKI lecture series on innovative configurations and advanced concepts for future civil aircraft*, pages 6–10, 2005.

[62] Sonia Lebofsky, Eric Ting, Khanh V Trinh, and Nhan T Nguyen. Optimization for load alleviation of truss-braced wing aircraft with variable camber continuous trailing edge flap. In *33rd AIAA Applied Aerodynamics Conference*, page 2723, 2015.

[63] CHANG-YU LIU. Drag of a flat plate with transition in the absence of pressure gradient. *Journal of Aircraft*, 9(7):509–510, 1972.

[64] D.L. Logan. *A First Course in the Finite Element Method, Enhanced Edition, SI Version*. CENGAGE Learning, 2022.

[65] T. W. Lukaczyk, A. D. Wendorff, M. Colonno, T. D. Economon, J. J. Alonso, T. H. Orra, and C. Ilario. Suave: An open-source environment for multi-fidelity conceptual vehicle design. In *16th AIAA/ISSMO Multidisciplinary Analysis and Optimization Conference*, page 3087, 2015.

[66] Yiyuan Ma, Stanislav Karpuk, and Ali Elham. Conceptual design and comparative study of strut-braced wing and twin-fuselage aircraft configurations with ultra-high aspect ratio wings. *Aerospace Science and Technology*, 121:107395, 2022.

[67] Brett Malone and William H Mason. Multidisciplinary optimization in aircraft design using analytic technology models. *Journal of Aircraft*, 32(2):431–438, 1995.

[68] James F Marchman. *Aerodynamics and aircraft performance*. James F. Marchman, 2004.

[69] James F Marchman III. The role of performance in aircraft design: Constraint analysis. *Aerodynamics and Aircraft Performance, 3rd edition*, 2021.

[70] Joaquim RRA Martins and Andrew B Lambe. Multidisciplinary design optimization: a survey of architectures. *AIAA journal*, 51(9):2049–2075, 2013.

[71] W Mason. Analytic models for technology integration in aircraft design. In *Aircraft design, systems and operations conference*, page 3262, 1990.

[72] L. McCullers. *Flight Optimization System, Release 8.11, User's Guide*. NASA Langley Research Center, Hampton, VA, Oct 2009.

[73] Robert A McDonald and James R Gloudemans. Open vehicle sketch pad: An open source parametric geometry and analysis tool for conceptual aircraft design. In *AIAA SciTech 2022 Forum*, page 0004, 2022.

[74] Nicholas A Meadows, Joseph A Schetz, Rakesh K Kapania, Manav Bhatia, and Guclu Seber. Multidisciplinary design optimization of medium-range transonic truss-braced wing transport aircraft. *Journal of Aircraft*, 49(6):1844–1856, 2012.

[75] Brandon Scott Newman. *A Comparison of Fuel Efficiencies Between DC-9-30 and B-737NG Aircraft for Delta Airlines at Atlanta Hartsfield Airport*. Doctoral dissertation, Embry-Riddle Aeronautical University, 2011.

[76] Nhan T Nguyen, Jason Fugate, Upender K Kaul, and Juntao Xiong. Flutter analysis of the transonic truss-braced wing aircraft using transonic correction. In *AIAA SciTech 2019 Forum*, page 0217, 2019.

[77] Nhan T Nguyen and Juntao Xiong. Transonic correction method for flight dynamic stability analysis of mach 0.745 transonic truss-braced wing. In *AIAA AVIATION 2021 FORUM*, page 2574, 2021.

[78] Nhan T Nguyen, Juntao Xiong, and Jason Fugate. Multi-point jig twist optimization of mach 0.745 transonic truss-braced wing aircraft and high-fidelity cfd validation. In *AIAA Scitech 2021 Forum*, page 0338, 2021.

[79] Melvin L. Nicolai. *Fundamentals of Aircraft Design*. METS, Inc., San Jose, CA, 1984.

[80] Mihaela Niţă and Dieter Scholz. *Estimating the Oswald factor from basic aircraft geometrical parameters*. Deutsche Gesellschaft für Luft-und Raumfahrt-Lilienthal-Oberth eV, 2012.

[81] Intergovernmental Panel on Climate Change. Climate change 2007: Synthesis report – summary for policy makers, November 2007.

[82] Nicholas C Orndorff, Bingran Wang, Marius L Ruh, Andrew Fletcher, and John T Hwang. Gradient-based sizing optimization of power-beaming-enabled aircraft. In *AIAA AVIATION 2023 Forum*, page 4019, 2023.

[83] W. Pfenninger. Laminar flow control laminarization. Report 654, AGARD, 1977. Special

Course on Concepts for Drag Reduction. Summarized from the report "Some thoughts on the design of large global range LFC transport airplanes," Jan., 1976.

[84] Ludwig Prandtl. Induced drag of multiplanes. Technical report, 1924.

[85] Daniella E Raveh, Yuval Levy, and Moti Karpel. Structural optimization using computational aerodynamics. *AIAA journal*, 38(10):1974–1982, 2000.

[86] Daniella E Raveh, Yuval Levy, and Moti Karpel. Efficient aeroelastic analysis using computational unsteady aerodynamics. *Journal of Aircraft*, 38(3):547–556, 2001.

[87] Daniel Raymer. *Aircraft Design: A Conceptual Approach*. American Institute of Aeronautics and Astronautics, Inc., 2012.

[88] Daniel Raymer. *Aircraft design: a conceptual approach*. American Institute of Aeronautics and Astronautics, Inc., 2012.

[89] Daniel P. Raymer. *Aircraft Design: A Conceptual Approach*. AIAA Education Series. AIAA, 2018.

[90] Emanuele Rizzo. *Optimization Methods Applied to the preliminary design of innovative non conventional aircraft configurations*. Emanuele Rizzo, 2009.

[91] Jan Roskam. *Airplane design*. DARcorporation, 1985.

[92] Marius L Ruh, Darshan Sarojini, Andrew Fletcher, Isaac Asher, and John T Hwang. Large-scale multidisciplinary design optimization of the nasa lift-plus-cruise concept using a novel aircraft design framework. *arXiv preprint arXiv:2304.14889*, 2023.

[93] Darshan Sarojini. Structural analysis and optimization of aircraft wings through dimensional reduction. 2021.

[94] Darshan Sarojini, Ruxandra Duca, Heriberto D Solano, Imon Chakraborty, Simon I Briceno, and Dimitri N Mavris. Framework to assess effects of structural flexibility on dynamic loads developed in maneuvering aircraft. In *2018 Aviation Technology, Integration, and Operations Conference*, page 4147, 2018.

[95] Darshan Sarojini, Evan Harrison, and Dimitri N Mavris. Dynamic environment for loads prediction and handling investigation (delphi). In *AIAA Scitech 2021 Forum*, page 0326, 2021.

[96] Darshan Sarojini and Dimitri Mavris. Structural analysis and optimization of wings subjected to dynamic loads. *AIAA Journal*, 60(2):1013–1023, 2022.

[97] Darshan Sarojini, Marius Ruh, Jiayao Yan, Luca Scotzniovsky, Nicholas C Orndorff, Ru Xiang, Han Zhao, Joshua Krokowski, Michael Warner, Sebastiaan van Schie, Ashley Cronk, Alexandre T Guibert, Jeffrey T Chambers, Lauren Wolfe, Rachel Doring, Robin Despins, Cibin Joseph, Ryan Anderson, Andrew Ning, Hyunjune Gill, Seongkyu Lee, Zeyu Cheng, Zhi Cao, Chris Mi, Ying Shirley Meng, Christopher Silva, Jiun-Shyan Chen, Alicia A Kim, and John T Hwang. Review of computational models for large-scale mdao of urban air mobility concepts. In *AIAA SciTech 2024 Forum*, page 0377, 2024.

[98] Darshan Sarojini, Marius L Ruh, Anugrah Jo Joshy, Jiayao Yan, Alexander K Ivanov, Luca Scotzniovsky, Andrew H Fletcher, Nicholas C Orndorff, Mark Sperry, and Victor E Gandarillas. Large-scale multidisciplinary design optimization of an evtol aircraft using comprehensive analysis. In *AIAA SCITECH 2023 Forum*, page 0146, 2023.

[99] Darshan Sarojini, Heriberto D Solano, Jason A Corman, and Dimitri N Mavris. Parametric wingbox structural weight estimation of the crm, pegasus and truss-braced wing concepts. In *AIAA AVIATION 2022 Forum*, page 4054, 2022.

[100] Daniel Schiktanz and Dieter Scholz. Box wing fundamentals–an aircraft design perspective. *DGLR Dtsch. Luft-und*, pages 601–615, 2011.

[101] Guclu Seber, Hongjun Ran, Taeqoo Nam, Joseph Schetz, and Dimitri Mavris. Multidisciplinary design optimization of a truss braced wing aircraft with upgraded aerodynamic analyses. In *29th AIAA Applied Aerodynamics Conference*, page 3179, 2011.

[102] Alessandro Sgueglia, Peter Schmollgruber, Emmanuel Benard, Nathalie Bartoli, and Joseph Morlier. Preliminary sizing of a medium range blended wing-body using a multidisciplinary design analysis approach. In *MATEC Web of Conferences*, volume 233, pages 1–9. EDP Sciences, 2018.

[103] Christopher M Shearer and Carlos ES Cesnik. Nonlinear flight dynamics of very flexible aircraft. *Journal of aircraft*, 44(5):1528–1545, 2007.

[104] Richard S. Shevell. *Fundamentals of Flight*. Prentice-Hall, Upper Saddle River, NJ, 1989.

[105] David Solano, Darshan Sarojini, Dushhyanth Rajaram, and Dimitri N Mavris. Adjoint-based analysis and optimization of beam-like structures subjected to dynamic loads. *Structural and Multidisciplinary Optimization*, 65(2):52, 2022.

[106] Heriberto D Solano, Darshan Sarojini, and Dimitri N Mavris. Computationally efficient analysis and sizing of the pegasus and truss-braced wing structures subjected to dynamic loads. In *AIAA AVIATION 2023 Forum*, page 3943, 2023.

[107] AA241 Stanford University. Body form factor. http://adg.stanford.edu/aa241/drag/BODYFORMFACTOR.HTML. Accessed: 2024-08-12.

[108] AA241 Stanford University. Lower surface form factor. http://adg.stanford.edu/aa241/drag/lsformfactor.html. Accessed: 2024-08-12.

[109] Douglas O. Stanley and Subbarao Surampudi. Fundamentals of space shuttle orbiter reentry and landing. Technical Report 20110011321, NASA, 2011. Retrieved from https://ntrs.nasa.gov/citations/20110011321.

[110] Afzal Suleman, Frederico Afonso, and Christian Spada. Aeroelastic analysis of high apect ratio wings. In *54th AIAA Aerospace Sciences Meeting*, page 0778, 2016.

[111] Rajashekar Swaminathan, Darshan Sarojini, and John T Hwang. Integrating mbse and mdo through an extended requirements-functional-logical-physical (rflp) framework. In *AIAA AVIATION 2023 Forum*, page 3908, 2023.

[112] Timothy T Takahashi and Tyler Lemonds. Transport category wing weight estimation using a optimizing beam-element structural formulation. In *53rd AIAA aerospace sciences meeting*, page 1898, 2015.

[113] Eric Ting, Kevin W Reynolds, Nhan T Nguyen, and Joseph Totah. Aerodynamic analysis of the truss-braced wing aircraft using vortex-lattice superposition approach. In *32nd AIAA Applied Aerodynamics Conference*, page 2597, 2014.

[114] Francesco Toffol and Sergio Ricci. Aeroelastic design and optimization of strut-braced high aspect ratio wings. *MATERIALS RESEARCH PROCEEDINGS*, 37:42–47, 2023.

[115] E. Torenbeek. *Synthesis of Subsonic Airplane Design: An Introduction to the Preliminary Design of Subsonic General Aviation and Transport Aircraft, with Emphasis on Layout, Aerodynamic Design, Propulsion and Performance*. Springer Science & Business Media, 2013.

[116] Egbert Torenbeek. *Synthesis of Subsonic Airplane Design*. Delft University Press, Delft, The Netherlands, 1982.

[117] Lance W Traub. Prediction of the oswald efficiency factor for cambered and swept wings. *Journal of Aircraft*, 61(1):317–322, 2024.

[118] US Department of Transportation; Research and Innovative Technology Administration; Bureau of Transportation Statistics. Airline data and statistics, 2008. Retrieved May 14, 2008 from http://www.bts.gov/programs/airline_information/.

[119] US Department of Transportation; Research and Innovative Technology Administration; Bureau of Transportation Statistics. Airline data and statistics, 2010. Retrieved March 09, 2010 from http://www.transtats.bts.gov/fuel.asp.

[120] SPC Van Schie, MAP Warner, AH Fletcher, and JT Hwang. Modular, consistent and conservative aeroelastic coupling for large-scale multidisciplinary design optimization. In *AIAA SciTech 2024 Forum*, 2024.

[121] Michael Warner, Andrew Fletcher, Sebastiaan P van Schie, and John T Hwang. A method for modular mdo model assembly via a solver independent field representation. In *AIAA SciTech 2024 Forum*, page 1802, 2024.

[122] J. R. Welstead, D. Caldwell, R. Condotta, and N. Monroe. An overview of the layered and extensible aircraft performance system (leaps) development. In *2018 AIAA Aerospace Sciences Meeting*, page 1754, 2018.

[123] FM White. 1974, viscous fluid flow. mcgraw-hill, new york.

[124] Ru Xiang, Sebastiaan PC van Schie, Luca Scotzniovsky, Jiayao Yan, David Kamensky, and John T Hwang. Automating adjoint sensitivity analysis for multidisciplinary models involving partial differential equations. 2024.

[125] Juntao Xiong, Robert E Bartels, and Nhan T Nguyen. Aerodynamic optimization of mach 0.745 transonic truss-bracedwing aircraft with variable-camber continuous trailing-edge flap. In *AIAA Scitech 2021 Forum*, page 0337, 2021.

[126] Juntao Xiong, Jason Fugate, and Nhan T Nguyen. Investigation of truss-braced wing aircraft transonic wing-strut interference effects using fun3d. In *AIAA Aviation 2019 Forum*, page 3026, 2019.

[127] Juntao Xiong, Nhan T Nguyen, and Robert E Bartels. Aerodynamic optimization of mach 0.8 transonic truss-braced wing aircraft using variable camber continuous trailing edge flap. In *AIAA SCITECH 2022 Forum*, page 0016, 2022.

[128] Juntao Xiong, Nhan T Nguyen, and Robert E Bartels. Aeroelastic analysis of mach 0.8 transonic truss-braced wing aircraft. In *AIAA SCITECH 2022 Forum*, page 0300, 2022.

[129] Juntao Xiong, Nhan T Nguyen, and Jason Fugate. Study of mach 0.8 transonic truss-braced wing aircraft wing-strut interference effects. In *AIAA Scitech 2021 Forum*, page 0336, 2021.

[130] K Zhang, Peng-Bo Ji, Abu Bakar, and Z Han. Multidisciplinary evaluation of truss-braced wing for future green aircraft. In *28th International Congress of the Aeronautical Sciences*, 2012.

[131] Wei Zhao, Rakesh K Kapania, Joseph A Schetz, and John M Coggin. Nonlinear aeroelastic analysis of sugar truss-braced wing (tbw) wind-tunnel model (wtm) under in-plane loads. In *56th AIAA/ASCE/AHS/ASC Structures, Structural Dynamics, and Materials Conference*,

page 1173, 2015.